

Air Force Institute of Technology

AFIT Scholar

Theses and Dissertations

Student Graduate Works

12-1995

Investigation of Aerodynamic Alterations for Improving the KC-135 Boom Performance during Aerial Refueling

Debra A. Nawrocki

Follow this and additional works at: <https://scholar.afit.edu/etd>



Part of the [Aerodynamics and Fluid Mechanics Commons](#)

Recommended Citation

Nawrocki, Debra A., "Investigation of Aerodynamic Alterations for Improving the KC-135 Boom Performance during Aerial Refueling" (1995). *Theses and Dissertations*. 6102.
<https://scholar.afit.edu/etd/6102>

This Thesis is brought to you for free and open access by the Student Graduate Works at AFIT Scholar. It has been accepted for inclusion in Theses and Dissertations by an authorized administrator of AFIT Scholar. For more information, please contact AFIT.ENWL.Repository@us.af.mil.



INVESTIGATION OF AERODYNAMIC ALTERATIONS
 FOR IMPROVING THE KC-135 BOOM PERFORMANCE
 DURING AERIAL REFUELING

THESIS

AFIT/GAE/ENY/95D-17

Debra A. Nawrocki
 Second Lieutenant USAF

DISTRIBUTION STATEMENT A
 Approved for public release.
 Distribution Unlimited

DEPARTMENT OF THE AIR FORCE
 AIR UNIVERSITY
AIR FORCE INSTITUTE OF TECHNOLOGY

Wright-Patterson Air Force Base, Ohio

DTIC QUALITY INSPECTED 1

AFIT/GAE/ENY/95D-17

INVESTIGATION OF AERODYNAMIC ALTERATIONS
FOR IMPROVING THE KC-135 BOOM PERFORMANCE
DURING AERIAL REFUELING

THESIS

AFIT/GAE/ENY/95D-17

Debra A. Nawrocki
Second Lieutenant USAF

Approved for public release; distribution unlimited.

19960402 079

INVESTIGATION OF AERODYNAMIC ALTERATIONS FOR
IMPROVING THE KC-135 BOOM PERFORMANCE DURING AERIAL REFUELING

THESIS

Presented to the Faculty of the School of Engineering
of the Air Force Institute of Technology

Air University

in Partial Fulfillment of the
Requirements for the Degree of
Master of Science

by

Debra A. Nawrocki
Second Lieutenant USAF

Graduate Aeronautical Engineering

December 1995

Approved for public release; distribution unlimited.

Acknowledgments

I am thankful for all my friends, who through their support, knowledge, and willingness to be there for me, made the completion of this thesis possible. To Brad Buxton, thanks for always answering my questions and even volunteering knowledge of possible pitfalls. To my thesis advisor, Dr. C. H. Spenny, for sponsoring my project. To Tinkerbell, for all of the unconditional love and perspective that she added to those long days and nights of working at home. To Shahnaz, Jon, Joel, Che, and Dave, for always being willing to lend a sympathetic ear and actually understanding what I'm talking about. To Rebecca, Chris, and Matt, for always allowing some social distractions that provided some relief from the possible onslaught of stress. To Mom, Dad, and Laura, for being so proud that it motivated me to actually keep working. May my work actually help someone else.

Debra A. Nawrocki

Contents

	Page
Acknowledgments	i
List of Figures	iv
List of Tables	vii
List of Symbols	viii
Abstract	x
Chapter	
I. Introduction	1
Background	1
Objective	8
II. System Description	12
KC-135 System	12
Computer Model	15
Refueling Envelope	23
III. Discussion	26
Curve Validation	26
Refueling Envelope	73
Oscillation Analysis	95
IV. Conclusions	99
V. Recommendations for Further Study	101
Bibliography	102
Appendices	
A. Input File for ENS3DAE	104
B. NACA0070 Coefficients of Lift and Drag vs. Time Plots	108

Appendices	Page
C. Blunt Fairing Coefficients of Lift and Drag vs. Time Plots	119
Vita	126

List of Figures

Figure		Page
1.	KC-135 Yawing Boom Pivot	2
2.	Upper Surface Plots of the NACA0070 and Blunt Fairing	4
3.	Hoerner's Test Data Lift Curve Plot	5
4.	NACA0070 Streamlines at AOA = 20°	6
5.	Lift and Drag Vector Definitions	7
6.	KC-135 Refueling Envelope Diagram	9
7.	Boom AOA Based on Yaw and Pitch Angles	10
8.	O-Grid Generation	17
9.	NACA0070 50x40 O-Grid	18
10.	Blunt Fairing O-Grid	18
11.	NACA0070 Initial Inviscid Solution - Coefficient of Lift vs. Iteration Number Plots.	26
12.	NACA0070 Initial Inviscid Solution - Mach Contour Plots	29
13.	NACA0070 Initial Inviscid Solution - Coefficient of Pressure Contour Plots.	31
14.	NACA0070 Initial Inviscid Solution - Convergence Histories	34
15.	NACA0070 Updated Inviscid Solution - Convergence History at AOA = 0 degrees	37
16.	NACA0070 Updated Inviscid Solution - Convergence Histories	38
17.	NACA0070 Updated Inviscid Solution - Mach Contour Plots	39

Figure		Page
18.	NACA0070 Updated Inviscid Solution - Coefficient of Pressure Contour Plots.	41
19.	NACA0070 Updated Inviscid Solution - Coefficient of Lift vs. Iteration Number Plots.	43
20.	NACA0070 Viscous Solution - Convergence Histories	46
21.	NACA0070 Viscous Solution - Mach Contour Plots	52
22.	NACA0070 Viscous Solution - Coefficient of Pressure Contour Plots.	58
23.	NACA0070 Viscous Solution - Coefficients of Lift & Drag vs. Iteration Number Plots	64
24.	NACA0070 Calculated vs. Test Results	70
25.	Relationship Between Conventional and Defined Lift and Drag Vectors	71
26.	NACA0070 Calculated vs. Test Results in Conventional Vector Frame	72
27.	Coefficient of Drag vs. Mach Number Plots	73
28.	NACA0070 & Circular Flyable Envelopes	74
29.	NACA0070 Flyable Envelope Plots	75
30.	Blunt Fairing - Convergence Histories	76
31.	Blunt Fairing - Mach Contour Plots	80
32.	Blunt Fairing - Coefficient of Pressure Contour Plots.	83

Figure		Page
33.	Blunt Fairing - Coefficients of Lift & Drag vs. Iteration Number Plots . . .	87
34.	Blunt Fairing Calculated Results	90
35.	Blunt Fairing Calculated Results in Conventional Vector Frame . . .	91
36.	Blunt Fairing & NACA0070 Flyable Envelope Plots	92
37.	Blunt Fairing Flyable Envelope Plots	93
38.	Oscillating Effects on the Flyable Envelopes	94

List of Tables

Table	Page
1. KC-135 Boom Design Measurements	12
2. Flowfield Conditions for the KC-135	15
3. NACA0070 Frequency and Amplitude Tabulation	96
4. Blunt Fairing Frequency and Amplitude Tabulation	97

List of Symbols

Symbol	Description
AOA	Angle of attack (degrees)
a_∞	Speed of sound (m/s)
c	Chord length (ft)
c_d	Coefficient of drag
c_ℓ	Coefficient of lift
c_m	Coefficient of moment
C_p	Coefficient of pressure
c_p	Coefficient of specific heat at constant pressure
E	Energy (J)
k/k_o	Thermal conductivity ratio
M	Local Mach number
M_∞	Freestream Mach number
p	Pressure (N/m^2)
Pr	Prandtl number
Re_c	Reynolds number based on chord
T	Freestream temperature (K)
t	Thickness ratio of an airfoil
V	Local velocity (m/s)
V_∞	Freestream velocity (m/s)
α	Angle of attack (degrees)

Symbol	Description
γ	Ratio of specific heats, c_p/c_v
μ_o/μ_∞	Viscosity ratio
θ	Pitch angle (degrees)
ρ	Density (kg/m^3)
ψ	Yaw angle (degrees)

Abstract

This study investigated the eligibility of the KC-135 air refueling boom for improved capabilities in the areas of control and performance. By using a thick airfoil cross-section for the boom tube, rather than the current circular cross-section, the ability to increase the lift characteristics was verified. Prior compiled test data was used for comparison against analytical computer solutions. The possibility and effects of control frequency oscillations were also examined due to the unstable nature of the flow at test conditions. Additionally, the effect of other cross-section shapes, such as the blunt fairing, on the size of the flyable envelope for the trailing aircraft was investigated by using FORTRAN coding. Results show that the KC-135 air refueling boom can be modified for better lift and refueling envelope capabilities.

INVESTIGATION OF AERODYNAMIC ALTERATIONS FOR IMPROVING THE KC-135 BOOM PERFORMANCE DURING AERIAL REFUELING

I. Introduction

Background

Aerial refueling is a process that was first successfully accomplished on June 25, 1923, through a 40 foot steel encased rubber hose (Ref. 12). The need for an aerial refueling system was first realized during World War I, when the pilots noted a loss of effectiveness on the front lines due to the short endurance of the aircraft. A method of refueling the airplanes without necessitating a long flight back to the home launching base needed to be developed. Hence, the concept of transferring fuel from one aircraft to another while in flight was conceived.

Initial attempts at aerial refueling consisted of long rubber hoses protected by metal wire. The dangers of flying in close formation and unsteady wind conditions became primary concerns, as well as the methods of cable disconnect. Therefore, the importance of the refueling envelope size was one of the first problems to be discovered. The larger the refueling envelope, the more motion a receiving aircraft was allowed before it must disconnect from the refueler, thus allowing for stronger wind gusts and pilot maneuvering error. As the cable disconnected from the receiving aircraft on these early models, fuel would spill on the pilot, thus causing considerable discomfort and safety concerns. Thus, an automatic shut-off valve was developed to prevent fuel from being

dispersed in any place other than the intended aircraft's fuel system. This automatic valve became incorporated in all subsequent designs, and is present in the KC-135 system, where it is activated when an automatic disconnect is employed.

The KC-135 air refueling system also uses a "flying boom" system, as pictured in Figure 1.

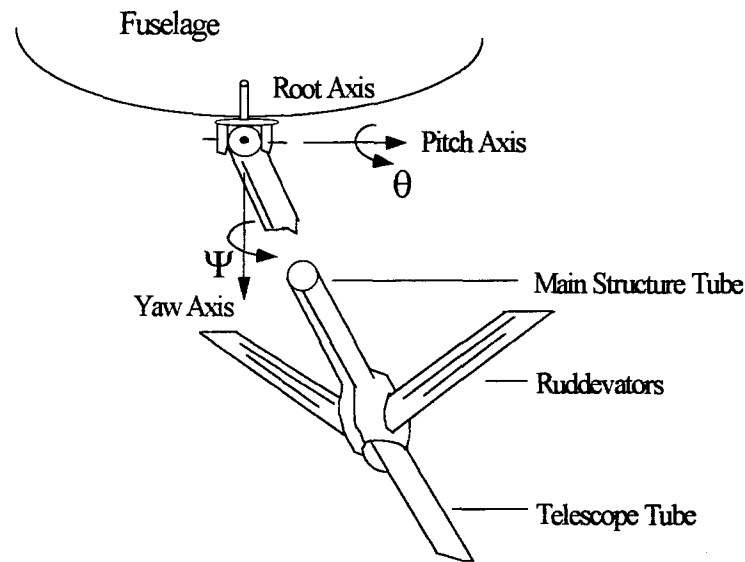


Figure 1. KC-135 Yawing Boom Pivot (Ref. 11)

The KC-135 has a telescoping rigid tube that extends from the lower aft section of the tanker aircraft. The tube is extended toward the refueling aircraft, and it is controlled by a boom operator through the use of ruddervators attached to its frame. This design, with its cylindrical cross-section, allows more fuel to flow to the receiving aircraft in a shorter period of time due to its shorter length and larger width compared to the earlier hose systems. Despite the improvements this model made compared to previous air refuelers, however, there are disadvantages to its use. Increased drag occurs due to the boom

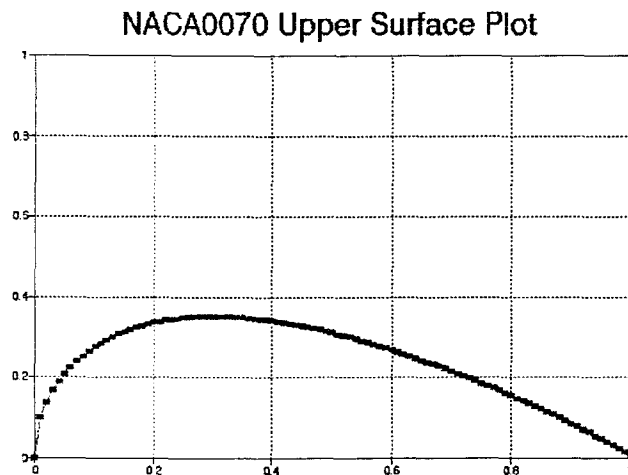
structure contacting freestream air, and a greater degree of pilot maneuverability skill is required due to the restrictive tube structure. Thus, the refueling envelope is smaller than desired, and disconnect can occur due to smaller airspeed fluctuations or pilot over-corrections to the refueling pattern.

This flying boom system is employed in the United States Air Force's two modern refueling aircraft, the KC-135 and the KC-10. However, there is a distinct advantage to the design of the KC-10 fleet. The KC-10 has a larger refueling envelope than the KC-135 partially due to a change in its root axis. The root axis is located where the boom connects to the tanker aircraft. The KC-135 employs a yawing boom pivot. This means that the telescoping tube first pivots about a yaw axis, through an angle Ψ , then about a pitch axis, through an angle θ , see Figure 1.

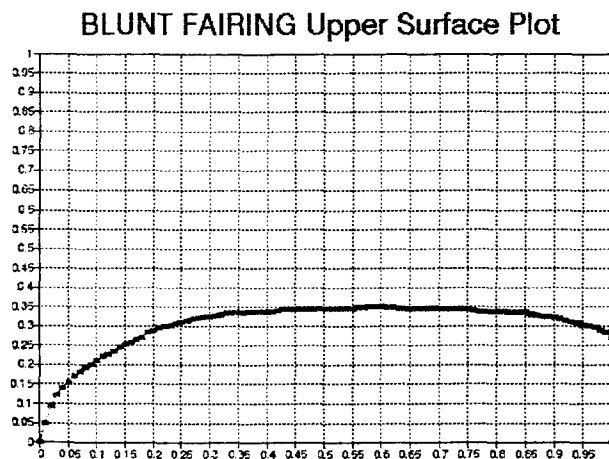
However, the KC-10 uses a different configuration, termed the rolling boom pivot. First, the boom is rotated about the roll axis, then about the pitch axis. This allows the same cross-section to always be facing the freestream wind, regardless of boom position. Thus, it is simple to find a boom shape that provides drag components that apply to all flight conditions and maximize the refueling envelope, thereby producing a larger range before disconnect occurs.

Since the KC-10 tanker became operational in 1981 (Ref. 15), options on improving the KC-135 to provide the same refueling capabilities have been suggested. An additional design factor stipulates that the modifications to the KC-135 need to be minimal in labor and cost, thus providing a constraint and presenting a more practical solution to the current problem. Previously, modifications to the boom's controlling ruddervators

have been studied, showing an increase in the size of the refueling envelope (Ref. 3). The use of alternative symmetric cross-sectional shapes for the main structure tube, i.e. a NACA0070 airfoil and the blunt fairing, is investigated in this study, including the aerodynamic and control effects from these variations. The upper surface of each of these cross-sectional shapes can be seen in Figure 2.



(a)



(b)

Figure 2. Upper Surface Plots of the (a) NACA0070 and (b) Blunt Fairing

The NACA0070 was chosen as a possible cross-sectional shape due to the negative lift this airfoil generates at low angles of attack, as shown by Hoerner's test data in Figure 3.

HOERNER TEST DATA (Ref. 9) Water Tunnel Test

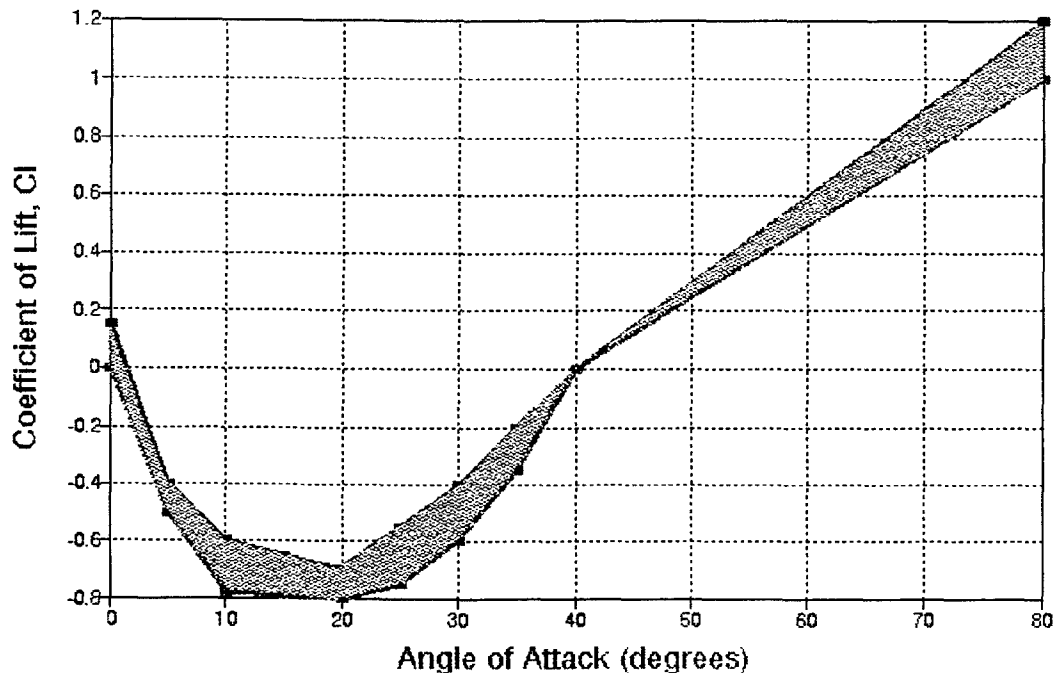


Figure 3. Hoerner's Test Data Lift Curve Plot (Ref. 9)

This negative lift below 40 degrees angle of attack, allows for better rudder authority and causes an increase in the maximum allowable movement of the boom (Ref. 16). The NACA0070 airfoil is 70% thick, which creates a separated flow along the upper surface when the cross-section is placed at a positive angle of attack. Figure 4 shows the surface streamlines over a NACA0070 cross-section at 20 degrees angle of attack.

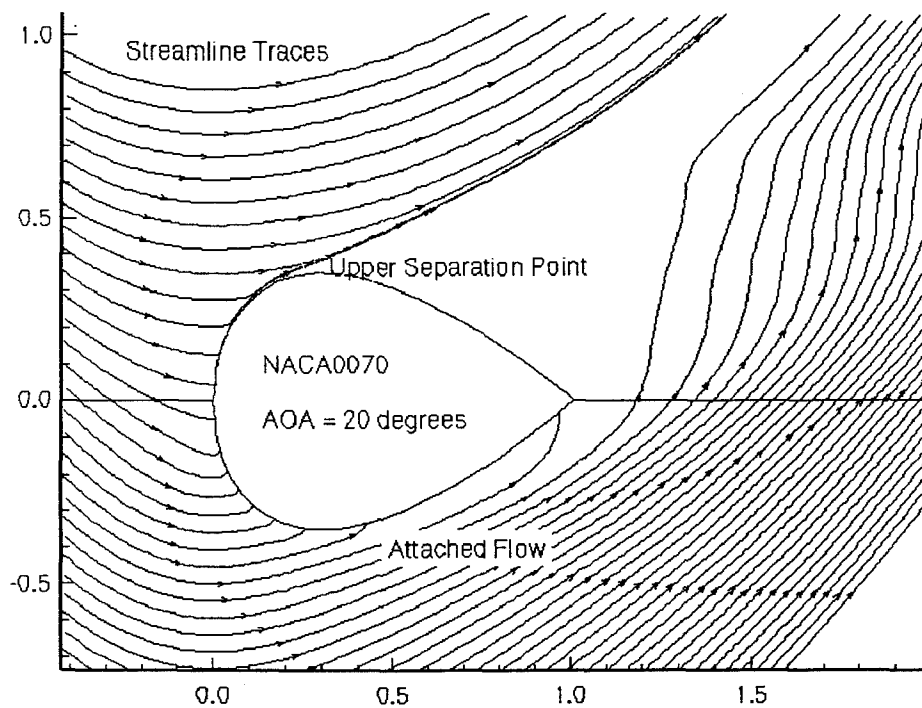


Figure 4. NACA0070 Streamlines at AOA=20°

It can be seen that the separation point on the upper surface occurs before the separation on the lower surface. The attached flow on the lower surface creates a strong negative pressure coefficient that essentially pulls the airfoil downward, and produces negative lift. This negative lift is caused by the thickness of the NACA0070 cross-section close to the leading edge. Therefore, other thick cross-sections may also give similar negative lift values, so the blunt fairing was also chosen as a possible improvement to the KC-135 boom cross-sectional shape.

Thus, with the lift and drag vectors as defined in Figure 5, without the common dependence on freestream direction, both negative lift and drag act to push the boom away from a zero line position. These special definitions of the lift and drag vectors, which do not change direction based on the angle of attack, were convenient due to the computer model simulation used and its method of calculating aerodynamic characteristics.

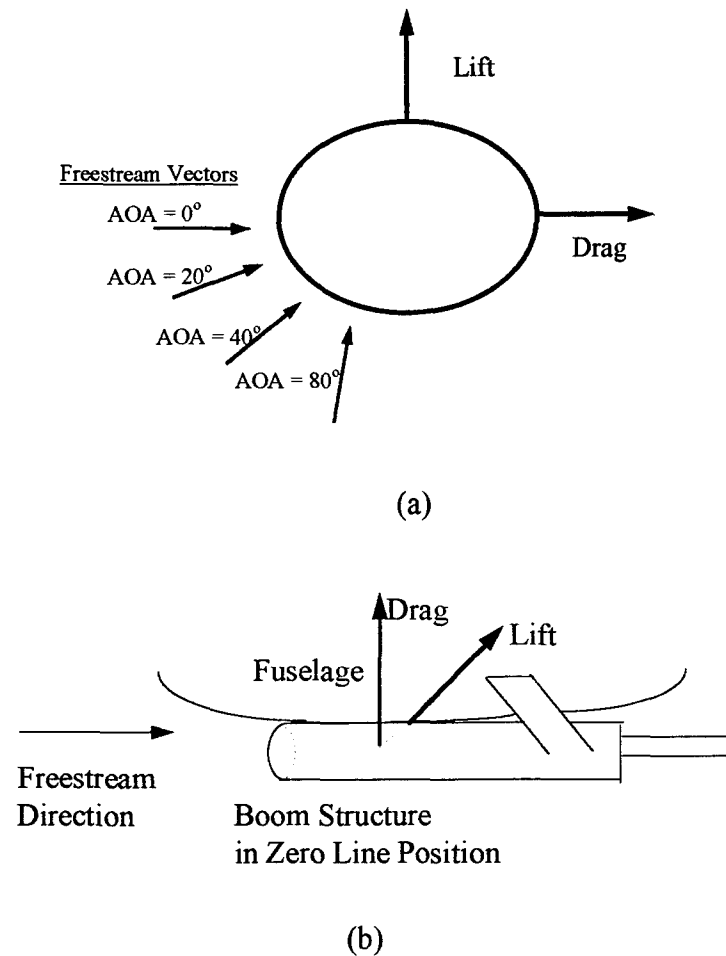


Figure 5. Lift and Drag Vector Definitions (a)Cross-Section (b)Boom Structure

Another aspect of Hoerner's lift curve, shown in Figure 3, is the temporal variation represented by the shaded band of c_l values. At each angle of attack, the lift can change

without any modification to the flight conditions. Therefore, this variation could be a factor in the boom operator's control if the boom cross-sectional shape is altered from circular to a NACA0070 airfoil.

Objective

When the NACA0070 airfoil, a teardrop contour, was chosen as a possible cross-sectional shape for the KC-135 boom structure, test data by Hoerner (Ref. 9) showed a fluctuating lift curve with respect to angle of attack, see Figure 3. The possibility of this oscillation had to be verified in order to find its effect on the boom operator, thus showing whether this thick airfoil could be controlled while in a refueling condition. Therefore, upon validation of the test data and its corresponding lift coefficient data fit, the frequency and oscillation of the boom needed to be calculated, consequently showing the effect on the boom operator's control stick.

The next step in the evaluation process was to increase the size of the KC-135's refueling envelope. The refueling envelope is a box that is defined as being the maximum angle limits that a boom can operate at without an automatic disconnect occurring. This refueling envelope is represented as the dotted lines in Figure 6. The current refueling envelope for the KC-135 is represented by $-40^\circ < \theta < -20^\circ$ for the pitch axis and $-10^\circ < \Psi < 10^\circ$ on the yaw axis. The flyable envelope, also shown on Figure 6, is the actual maximum position that the boom can attain due to its design limits. When the boom operator is flying the boom structure, the mechanical design creates limits on the motion of the refueling tube.

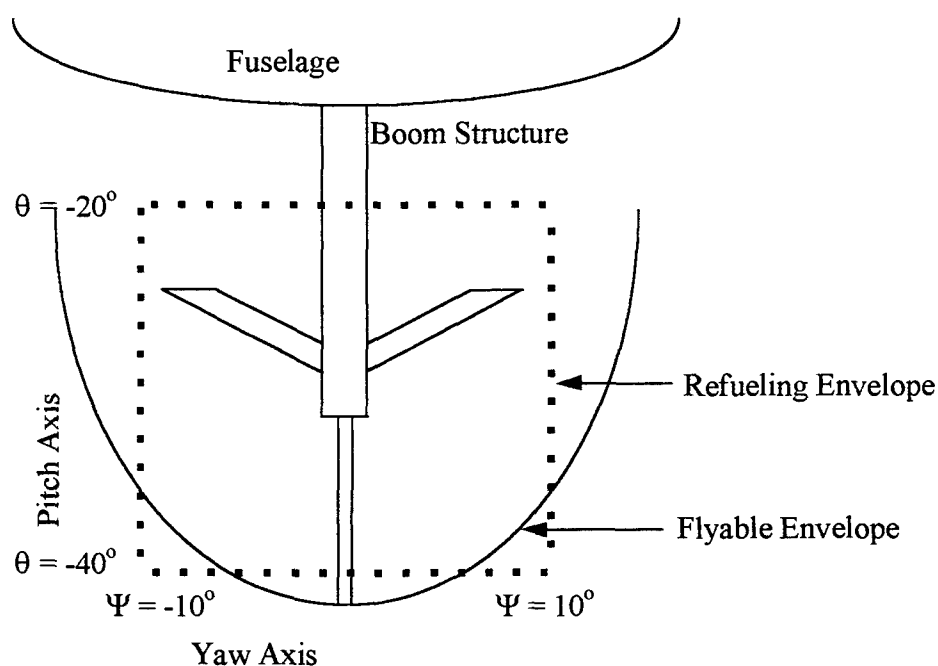


Figure 6. KC-135 Refueling Envelope Diagram

For the KC-135, part of the flyable envelope lies inside the refueling envelope. This means that during free flight the boom can not reach the angles that are defined in the lower corners of the refueling envelope. Therefore, the current refueling envelope size is larger than the boom can actually perform without a risk of nozzle binding occurring. Thus, it is desirable to enlarge the flyable envelope and set the limits for the refueling envelope within the flyable envelope's maximum angles. The goal is to increase the flyable envelope size so that the refueling envelope can also be enlarged. Since the KC-10 has a larger refueling envelope, this improvement will bring the KC-135 closer to the new developments made by the KC-10. Also, the Air Force has expressed an interest in increasing the refueling envelope size so that a receiving aircraft has a wider range of motion before automatic disconnect.

The negative lift predicted by Hoerner at angles of attack lower than 40 degrees, see Figure 3, would cause an increase in the flyable envelope due to the defined vector directions in Figure 5. This increase in the possible flight positions would only be seen where the combination of yaw and pitch angles cause the corresponding angle of attack on the boom structure. Due to the configuration of the yawing boom pivot used by the KC-135, see Figure 1, the angle of attack of the cross-section is dependent on the yaw angle, Ψ , and pitch angle, θ , of the boom, as shown in Figure 7.

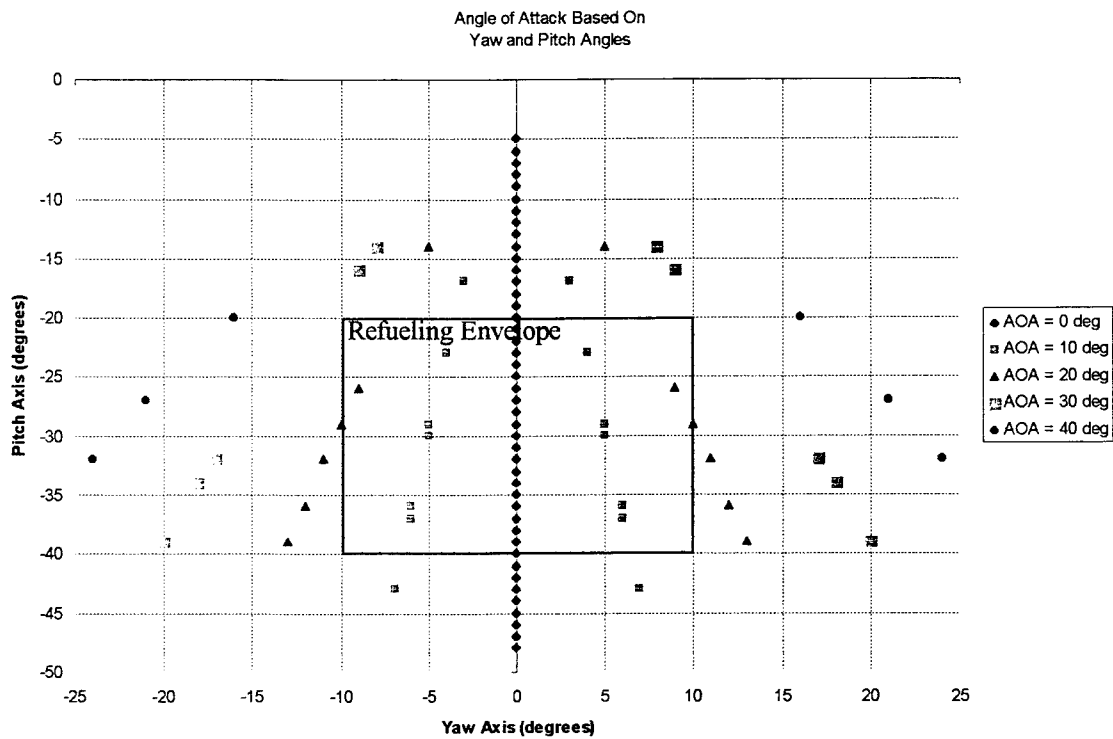


Figure 7. Boom AOA Based on Yaw & Pitch Angles

Thus, at angles of attack below 40 degrees, the flyable envelope could be improved, and since the current refueling envelope is within this limit, the negative lift is a favorable characteristic of changing the cross-section shape to a NACA0070 airfoil.

By using the NACA0070 and blunt fairing contours, the maximum possible yaw and pitch angles are found, thereby producing a map of the flyable envelope limits. Examining these findings with potential modifications to the boom operator's control stick and to the rudddevators produce the refueling envelope sizes. In addition, the effects of the boom oscillations on the refueling envelope are found in order to better represent the actual limits on the boom during a refueling exercise.

II. System Description

KC-135 System

Due to the KC-135 yawing boom pivot, the boom aerodynamics are affected by the angle of attack of its cross-section. However, it is possible to assume the boom stays in a fully extended position while refueling transpires, thereby calculating the maximum allowable flyable envelope sizes. This allows several characteristics of the boom assemblage to be stated. These values should be considered fixed and not variable due to various restrictions placed by the internal apparatus of the boom, such as the fuel tube, telescope drive assembly, surge boot, and fuel switches.

Length of telescope section (fully extended)	12.2 ft
Length of main structure tube	27.667 ft
Radius of main structure tube	0.458 ft
Radius of telescope tube	0.259 ft

Table 1. KC-135 Boom Design Measurements (Ref. 3)

The boom structure can be modified using other methods, however. By changing the cross-sectional shape, there is a change in the drag experienced by the boom. Also, the boom is modeled as having three limitations on its movements. These limits are classified as the restricting movement of the control stick, ruddervators, and angle of attack. The boom operator's control stick limit is simple to modify. Confining materials

consist of the surrounding pocket that protects and fastens the stick to the aircraft and boom assembly. By enlarging this container, or removing the rigid structure within the stick's vicinity, the controller will no longer encounter a limit on the stick movement. The size and configuration of the stick and boom do not change, hence not affecting the aerodynamics of the refueling system, and therefore not requiring any extensive retraining for the boom operator. Since the boom assembly is controlled by a hydraulic system, simply changing the gain amount between the operator's stick and the boom structure would consist of an extensive remodeling to the actual control system. Therefore, modifying the actual stick dimensions and holding case would be the easiest adjustment. The rudder limit is classified as the restrictive nature of boom motion due to the rudders' size, shape, and mounting location (Ref. 16). The easiest modification to this limit is to increase the planform area of the rudders. By examining previous studies (Ref. 3 & 16), an increase of 20% in the rudder size was investigated for this yawing boom configuration. The third limit, on rudder angle of attack, is caused by the maximum allowable angle that the rudders can deflect due to its structural design. Removing this limit necessitates considerable design changes in the boom and the attachment of the rudders. Thus, this is the most costly restriction to remove, although it is feasible.

In addition to the boom structure, the actual flight conditions of the KC-135 refueler need to be determined. The typical flight path of the tanker requires refueling operations to occur at approximately 32,000 feet and an airspeed of Mach 0.8 (Ref. 14). Setting these restrictions allowed the flowfield conditions to be calculated. From a U.S.

Standard Atmosphere Table at a geometric altitude of 32,000 ft. (Ref. 2), the freestream temperature, T , pressure, p , density, ρ , viscosity ratio, μ/μ_∞ , thermal conductivity ratio, k/k_∞ , and speed of sound, a_∞ , were found. By using the relation

$$V_\infty = \frac{Re_c \mu_\infty}{\rho_\infty c}$$

$$\text{and } M_\infty = \frac{V_\infty}{a_\infty}$$

with a Mach of 0.8, the Reynolds Number for the flow is 6.99×10^5 , which is higher than the critical Reynolds Number of 6×10^5 , as presented by Hoerner in his test data (Ref. 9). To find the Prandtl Number of the flow, a table of the heat capacity of air as a real gas at constant pressure was consulted. For the noted freestream temperature, the coefficient of specific heat at constant pressure, c_p , was found. This value was converted to the units Joules per a kilogram-Kelvin by using the relation

$$1 \text{ mole air} = 0.02896 \text{ kilograms.}$$

Then, the Prandtl number was found by using

$$Pr = \frac{c_p \mu}{k}$$

This gives the following values for the flight conditions of 32,000 ft. and Mach 0.8:

T	224.849 K
p	275,110 N/m ²
ρ	0.42624 kg/m ³
μ/μ _o	0.81945
μ _o	1.7894x10 ⁻⁵ N*s/m ²
μ _∞	1.4663x10 ⁻⁵ N*s/m ²
V _∞	240.48 m/s
Re _c	6.9905337x10 ⁵
k/k _o	0.7973034
k _o	2.5362x10 ⁻⁵ J/m*s*K
k	2.0221x10 ⁻⁵ J/m*s*K
c _p	29.421335 J/mol*K 1015.9301 J/kg*K
Pr	0.73668872

Table 2. Flowfield Conditions for KC-135

Computer Model

The first step to run the simulation of a modified cross-sectional shape of the KC-135 boom is to model upper and lower surfaces. A data file of the surface contour,

with x, y, and z positions is generated. For the NACA0070 cross-section, this was accomplished through the use of a symmetric airfoil equation dependent upon thickness ratio (Ref. 1). For the top surface of the airfoil,

$$y(x) = \frac{t}{0.2} * (0.29690\sqrt{x} - 0.12600x - 0.35160x^2 + 0.28430x^3 - 0.10150x^4)$$

where t is the thickness ratio, equal to 0.7 for the NACA0070 shape. This equation outputs an airfoil with a chord of one, thus allowing easier correlations to be made between apparatus of the same shape, but different sizes. For the blunt fairing, a chord of one was initialized, and a maximum height equal to that of the NACA0070 was set, as can be seen in Figure 2. The thickness ratio of this shape is 0.41, thus placing the maximum thickness further aft than on the NACA0070. However, the same symmetric airfoil equation does not apply, so the top surface was plotted without the use of a governing equation, and it was examined for continuous curvature using visual approximations.

These data files were then used to generate a two-dimensional grid about the cross-section using GRIDGEN2D. GRIDGEN2D is a computer program that uses an elliptical solver to create a grid surrounding a defined surface. The grid is used to produce node points that can later be used for the differentiation of pressure forces in the computer aerodynamic simulation model. A standard O-grid configuration was used, with the outer boundary of the O-grid ten chord lengths from the airfoil of interest. This full size O-grid and a magnified view of the NACA0070 airfoil in the grid field can be seen in Figure 8.

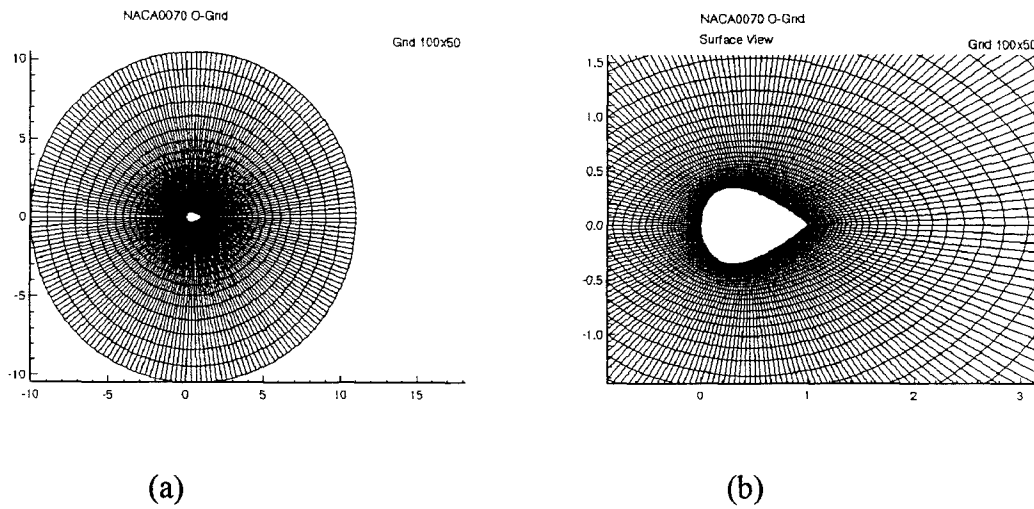


Figure 8. O-Grid Generation (a) Full Size (b) Magnified View of Surface

The grid was generated using an iteration method with an ideal grid block shape being a rectangle. The final grid configuration was accepted only when all grid blocks were within a maximum residual of 10^{-6} from being a rectangular shape. This process concluded after approximately 1000 iterations. Additionally, the coarseness of the grid could be specified in this procedure. Initially, a grid 100x50 was generated, with 100 data points along the top surface of the cross-section, and 50 points along the centerline from the surface of the cross-section to the outer boundary, as seen in Figure 7. The grid essentially has two zones. The top hemisphere is defined as zone 1, and the lower hemisphere is zone 2. Both top and lower surfaces are identical and symmetric, due to the shape definition and grid generation procedure. The grid data points were also compressed closer to the airfoil surface in order to better capture the changing flow characteristics at this boundary.

Due to some poor convergence results using the 100x50 grid, a 50x40 grid was used for the NACA0070 and blunt fairing. This increased the distance from the surface to the first node point, which allowed better data comparison between freestream and surface pressure forces when using a flow tangency boundary condition on the surface. The NACA0070 50x40 grid can be seen in Figure 9, and the blunt fairing grid is shown in Figure 10.

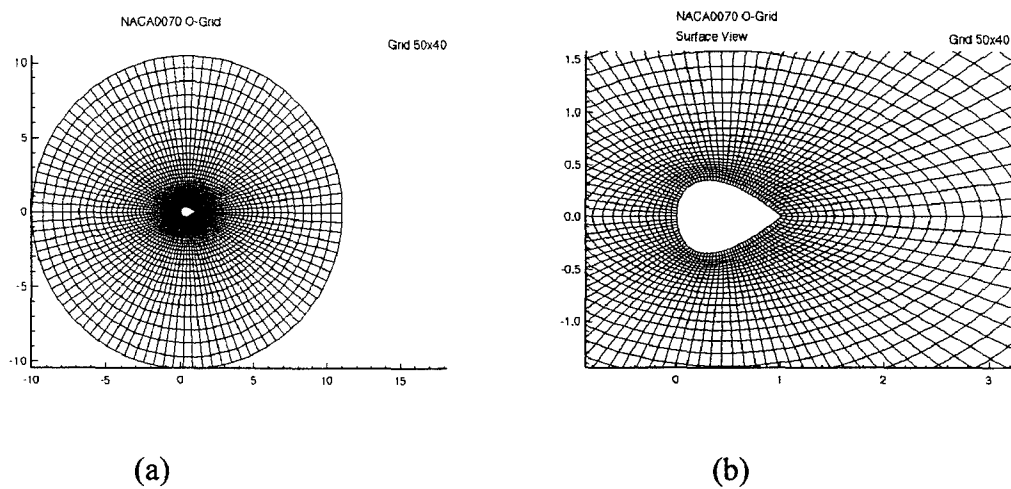


Figure 9. NACA0070 50x40 O-Grid (a) Full Size (b) Magnified View of Surface

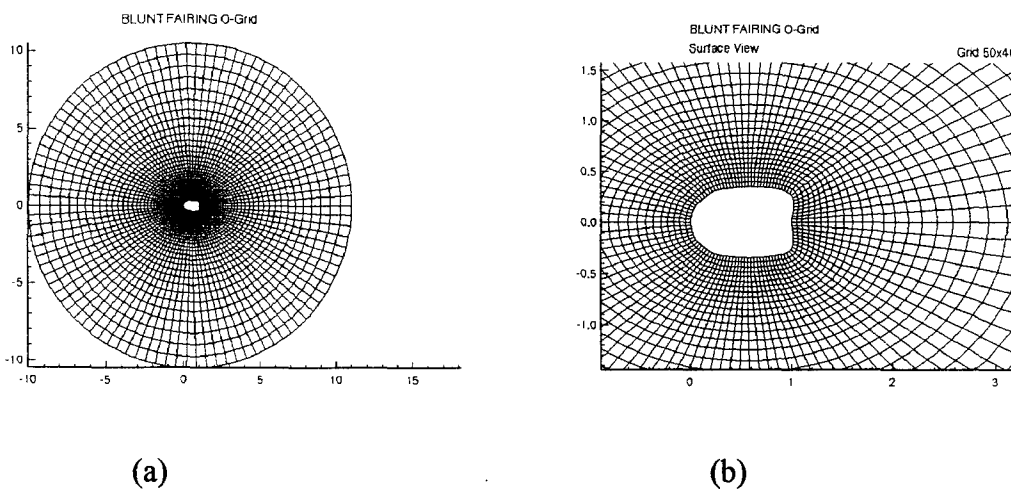


Figure 10. Blunt Fairing O-Grid (a) Full Size (b) Magnified View of Surface

Next, the generated grid was used with an input data file to calculate the local flowfield variables and overall aerodynamic coefficients. The computer code used for this simulation was the Euler/Navier-Stokes Aeroelastic Method (ENS3DAE) Version 2. This code has been validated for thin airfoils, such as a NACA0012, or the F-15 wing structure, and for a circular cross-section, thus showing definite applicability to the thick airfoils in question for this study. The ENS3DAE algorithm uses an explicit predictor-corrector scheme to integrate the equations of motion at each node point. Lumped pressure forces are calculated by aerodynamic analysis, and used to regulate the iteration scheme. For viscous calculations, the Navier-Stokes equations are integrated using an implicit finite difference method to form the aerodynamic analysis.

ENS3DAE allows the user to specify several input variables in order to define and control the flowfield calculations. See Appendix A for a complete listing of the input file. The flowfield conditions chosen for this study are those calculated in the previous section and presented in Table 2. The pitch, or angle of attack, is set as a variable, with values chosen between 0 and 80 degrees in order to simulate the boom structure as it moves within the refueling envelope. A value titled KVIS represents the type of solution to be calculated. A value of 0 denotes an Euler Equation solution in which the flow is modeled as inviscid, and the surface of the cross-section is defined as a solid boundary with flow tangency. A value of KVIS=2 denotes full Navier-Stokes calculations and the airfoil surface is defined as a solid boundary with a no-slip condition, and a viscous solution is obtained.

The next section of the data input file contains numerical conditions for ENS3DAE. The number of total iterations, ITTOTAL, is set to 8000. This means that

each grid point will be iterated 8000 times. However, if there is a discrepancy in the pressure force values between two subsequent iterations at a grid point, the code will abort its run. This premature end to the calculations is controlled by the residual calculations. The residual is based on the equations used for aerodynamic analysis and is the square root of the sum of the squares of the residuals for each grid point. Next, the number of time steps to be taken per an iteration is set to 1 in order to obtain a real-time representation of the output. The term CFL represents a multiplier for the time step and acts as a damping term for non-linear oscillations inherent in the numerical approximation of the differential equations. By decreasing this value, the overshoot of pressure calculations at a shock wave can be controlled. For this study, CFL is set at 1.0, in order to better investigate the propagation of unsteady flow as angle of attack is changed. To stabilize the solutions and to try to eliminate early termination of the program (before the total number of iterations is reached), this term should be decreased. Also in this numerical conditions section are the settings for the amount of dissipation to be added. EI regulates the amount of implicit dissipation, or the amount of damping to be applied to the left-hand-side of the finite difference equations. The implicit finite difference equation is

$$\frac{f_{i,j}^{n+1} - f_{i,j}^n}{\Delta t} = c_2 \left[\frac{f_{i+1,j}^{n+1} - 2f_{i,j}^{n+1} + f_{i-1,j}^{n+1}}{(\Delta x)^2} + \frac{f_{i,j+1}^{n+1} - 2f_{i,j}^{n+1} + f_{i,j-1}^{n+1}}{(\Delta y)^2} \right] + O[\Delta t, (\Delta x)^2, (\Delta y)^2]$$

(Ref. 10), where c_2 is a constant. This implicit formulation reveals that it has five unknowns. Thus, since changing the value of EI affects several grid points, it is the last value to be modified when finding a convergent solution, and EI is usually increased in order to further damp numerical oscillations. The explicit dissipation is applied using XK2

and XK4, second and fourth order respectively. When the pressures increase rapidly around a shock, the second order damping, XK2, should be increased. When decoupling occurs between adjacent grid points, causing sawtooth patterns in the pressure distribution, XK4 is increased.

Following the numerical conditions data list is the numerical options listing. Within this category, the value KTSTEP=2 specifies a variable time step option in which each grid point is advanced at its local speed, thus forming a steady-state mode. The next significant variable is KSPEC. This term represents the type of spectral radius computed for dissipation. With the thick, blunt bodies at $M=0.8$ used for this study, the flow is transonic with a strong shock, thus indicating that the spectral radius should be calculated for all directions rather than individually based on dissipation direction (Ref. 7).

The next list in the input data set is the printing options. For this study, the convergence file (a listing of the maximum residual for each iteration), and solution file (containing lift, drag, and moment coefficients) were output for each iteration. Additionally, the solution file (consisting of x, y, and z coordinates, u, v, and w velocity components, Mach number, energy, and coefficient of pressure for each grid point) is output every iteration or every 100 iterations depending on the probability of early program termination due to unsteady flow characteristics. These values are found by using the relations

$$p = (\gamma - 1) \left(E - \frac{1}{2} \rho V^2 \right)$$

$$C_p = \frac{2(p - p_\infty)}{M_\infty^2} \quad (\text{Ref. 7}).$$

$$M = \frac{|V|}{\left(\frac{\gamma p}{\rho} \right)^{1/2}}$$

In order to obtain the best results from ENS3DAE, the optimal values for all of the input data had to be found. Initially, all of the default values from a previous run using the F-15 wing were examined. These values then were tailored to the flow conditions and desired output for this study. The dissipation terms were modified by examining the various outputs and attempting to obtain a convergence to a steady-state condition for an inviscid solution at zero degree angle of attack. In order to best capture the total flowfield effects, the two-dimensional cross-section was modeled as a wing with constant cross-section and a span of five cross-sections. Then, the third, or middle, cross-section's properties were extracted for the solution file. Boundary conditions were modeled using the i, or x, face as the surface of the cross-section, the j, or y, face as the centerline starting from the trailing edge of the cross-section to the outer boundary of the O-grid, and the k, or z, face as the span of the five cross-sections. The cross-section is defined as being statically rigid, and there is no turbulence modeling. Therefore, the output is based on a solid, stationary airfoil at constant angle of attack.

Once a set of data values produced an inviscid output solution for an indeterminate number of iterations, at least more than 8000, several angles of attack were examined in order to verify the predicted output of negative lift for $0^\circ < \alpha < 40^\circ$ on the NACA0070.

Then, the boundary conditions are changed to provide a viscous flowfield solution using the Navier-Stokes equations. Next, a grid was generated for the blunt fairing and used to run ENS3DAE. The same input file allowed this cross-section to converge at $\alpha=0^\circ$ while using a viscous structure.

Refueling envelope

Once the aerodynamic characteristics of the cross-section were known, the affect on the boom refueling envelope could be calculated. By using FORTRAN coding that outputted the limiting values of the flyable envelope and was developed in a previous thesis by Campbell, et. al. (Ref. 3), slight modifications could adapt the existing algorithm to this study. The code is an aerodynamic model of the KC-135 boom. It is a static model of the air refueling configuration using the measurements stated in Table 1. The airspeed, density, and speed of sound were inputted using the values in Table 2. The program then iterated from $\psi = 0^\circ$ to 50° by 1° for each value of $\theta = -10^\circ$ to -50° with $\psi = 0^\circ$ being a boom structure that is aligned with the centerline of the fuselage and $\theta = 0^\circ$ defines the position where the boom structure is parallel to and flush against the fuselage (see Figure 5(b) for a schematic drawing). When using a symmetric cross-section, the flyable envelope is mirrored across the middle of the envelope, the $\psi = 0^\circ$ line. Therefore, only half of the flyable envelope is calculated, then the negative yaw angle values have maximum pitch angles equal to the same pitch angle limit as the one found for absolute value of the yaw angle:

$$\theta_{\max} \text{ for positive } \psi = \theta_{\max} \text{ for negative } \psi.$$

The coding allows for various options to be selected for optimizing the refueling envelope, including changing the yawing boom pivot to a rolling boom pivot, increasing the rudder area, and adjusting the control stick gain ratio. None of these options were selected for use in this study, since the effect of changing boom cross-sectional shape was the point of interest.

In order to account for the effect of changing the structure and telescope tube shapes, the change in drag had to be indicated. Initially, this change in drag could be found by examining a c_d versus Mach chart for the cross-sectional shape at $\alpha=0^\circ$. Since the FORTRAN code transforms the freestream velocity vector for each iteration to a vector normal to the leading edge stagnation point at zero angle of attack, the drag at zero angle of attack is the only necessary data. The program then outputs the maximum allowable θ and ψ angles for the compiled configuration.

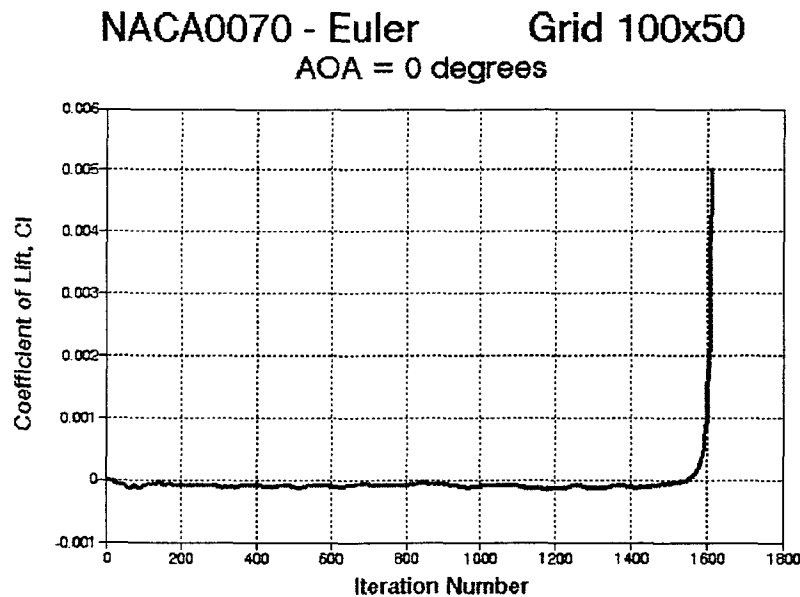
By removing certain lines of code that deal with the restrictions on the boom movement, modifications to the boom limitations can be made. The effect of removing the restrictions on movements due to 1) the boom operator's control stick, 2) rudder, 3) angle of attack, or any combination thereof can consequently be made. The output file also contains the discriminating limit which set each maximum allowable angle, so each limit can be removed in succession of significance. Once the output data file was produced, the resulting envelope restrictions could be plotted. The goal was to obtain maximum angles that occurred outside of the refueling envelope, thus preventing automatic disconnect within the envelope.

Presently, the KC-135 operates with a refueling envelope within $-10^\circ < \psi < 10^\circ$ and $-40^\circ < \theta < -20^\circ$. It is desirable to increase the size of this envelope in order to compete with the capabilities of the KC-10 tanker aircraft. However, due to the oscillations predicted by Hoerner for a thick airfoil (Ref. 9), the refueling envelope size could be time dependent. The ENS3DAE output could be used to obtain a minimum and maximum drag coefficient to input into the FORTRAN coding. Then, a refueling envelope band could be produced. Subsequently, the significance of the stick, rudder, and angle of attack limits could be examined on this oscillating envelope size.

III. Discussion

Curve Validation

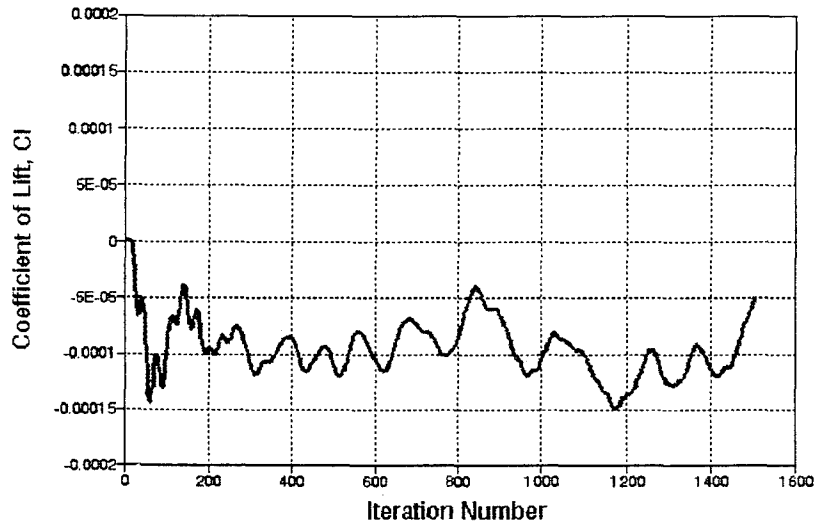
Initial attempts at converging a solution over the NACA0070 cross-section, using a 100x50 grid, resulted in solutions that only continued for a maximum of 1600 iterations. In order to have valid results, the solution should be able to complete an infinite number of iterations, but an average number of 4000 iterations is usually required before the solution converges (Ref. 7). By plotting the coefficient of lift versus the iteration number for inviscid conditions, the lift was seen to perform the expected oscillating trend. However, the c_l did not stay steady about any particular average value. See Figure 11 for plots at low angles of attack.



(a)

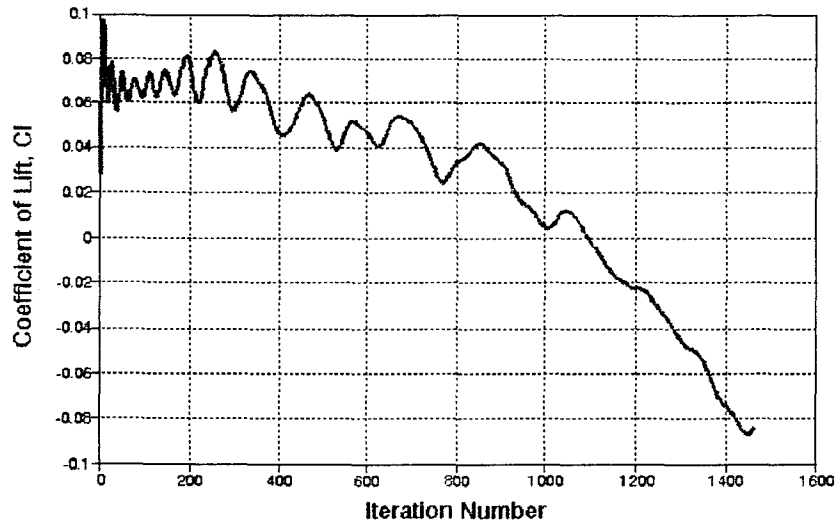
Figure 11. NACA0070 Initial Inviscid Solutions - Coefficient of Lift vs. Iteration Number
(a) AOA = 0°

NACA0070 - Euler Grid 100x50
AOA = 2 degrees



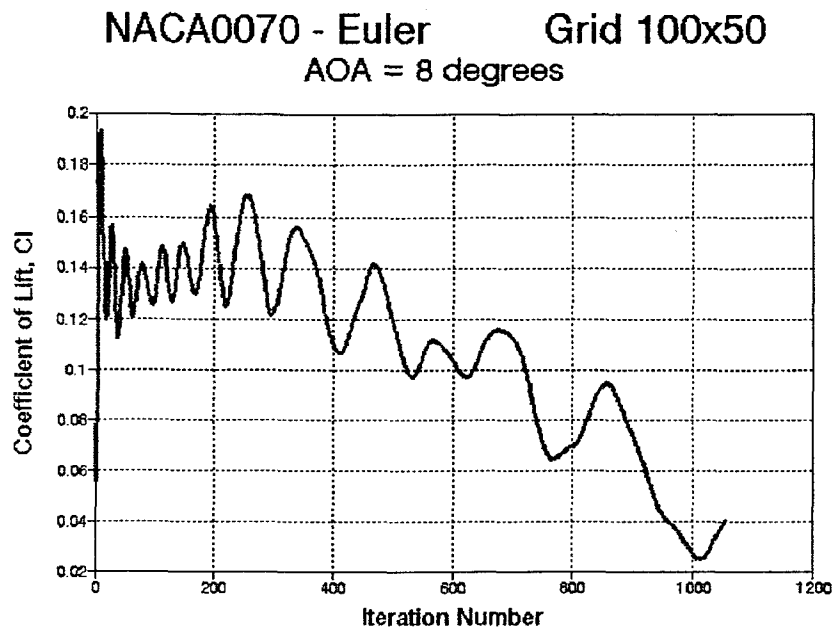
(b)

NACA0070 - Euler Grid 100x50
AOA = 4 degrees



(c)

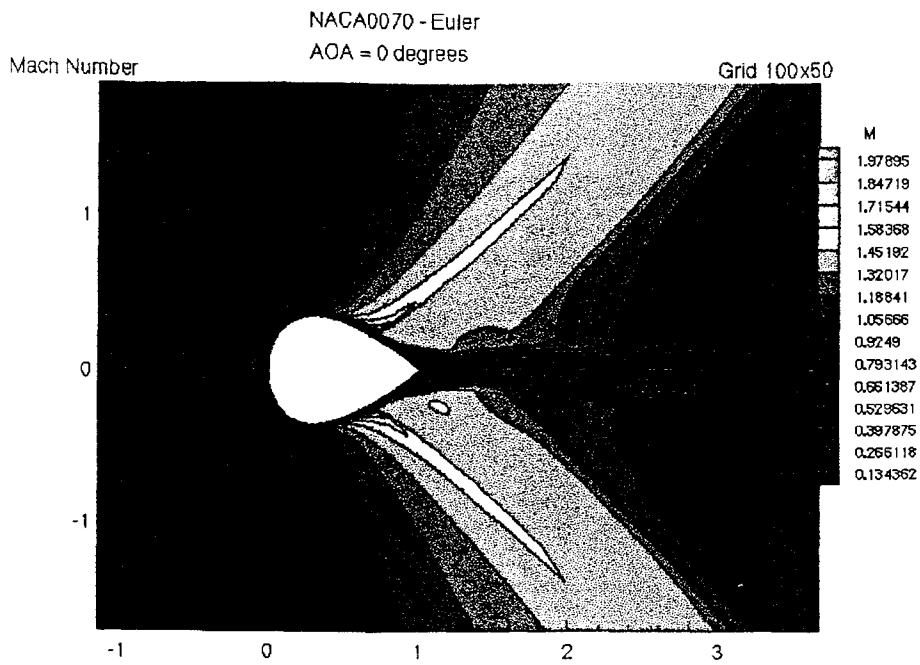
Figure 11 (continued). NACA0070 Initial Inviscid Solutions -
Coefficient of Lift vs. Iteration Number (b) AOA=2° (c) AOA = 4°



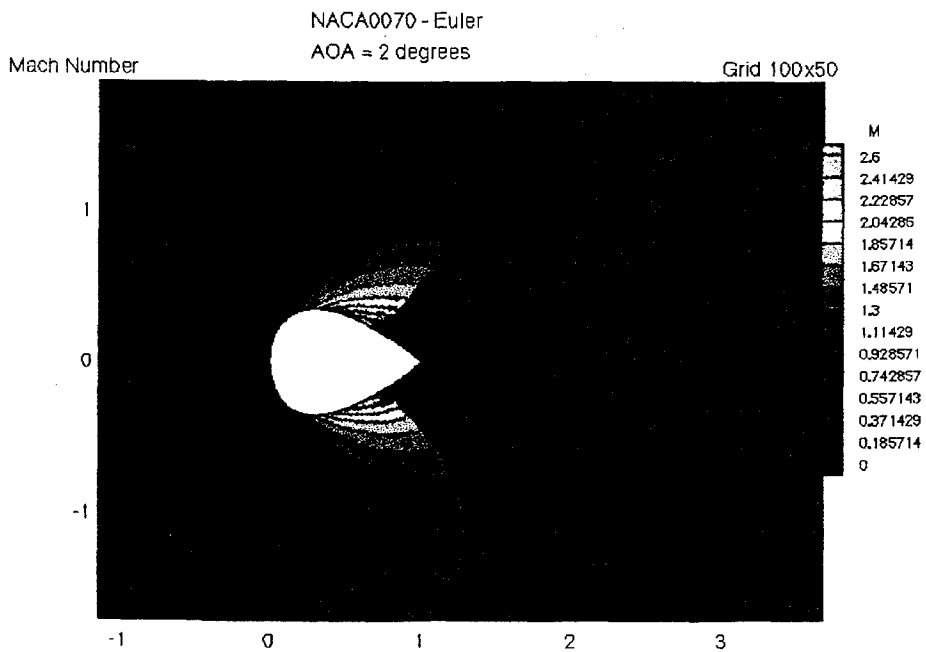
(d)

Figure 11 (continued). NACA0070 Initial Inviscid Solution -
Coefficient of Lift vs. Iteration Number (d) AOA = 8°

Indeed, upon examination of some flow visualization plots, using TECPLOT, the freestream conditions can be seen as not being fully developed. This means that each grid node point is not feeling the effect of the surrounding grid points, as should be the case when using the finite difference method as a governing equation. Through analysis of the Mach number contour plots shown in Figure 12, it is seen that the shock wave produced by transonic flow past the blunt body is visible, but the magnitude of the mach numbers are larger than expected for a Mach 0.8 freestream flow.

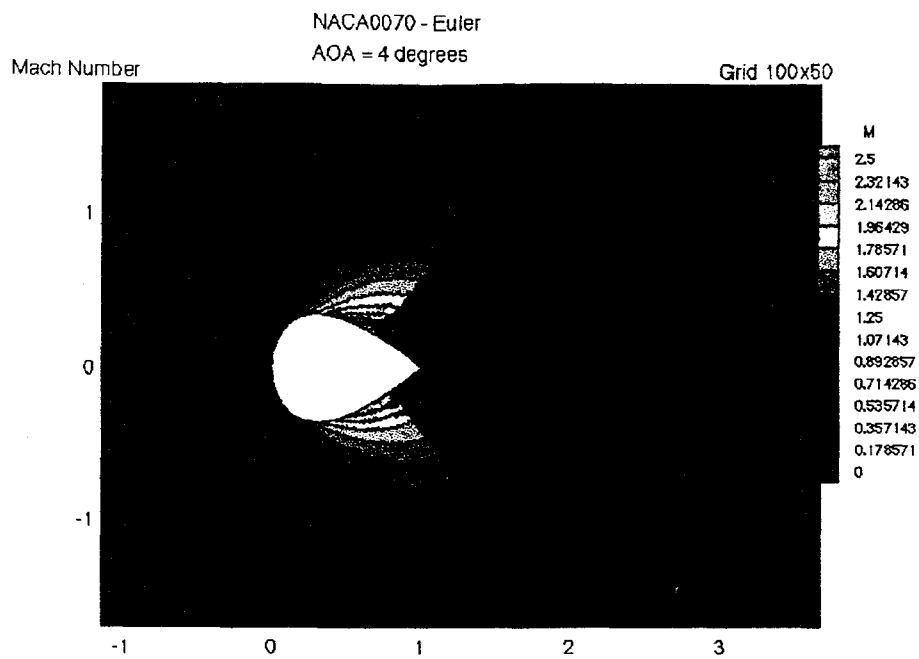


(a)

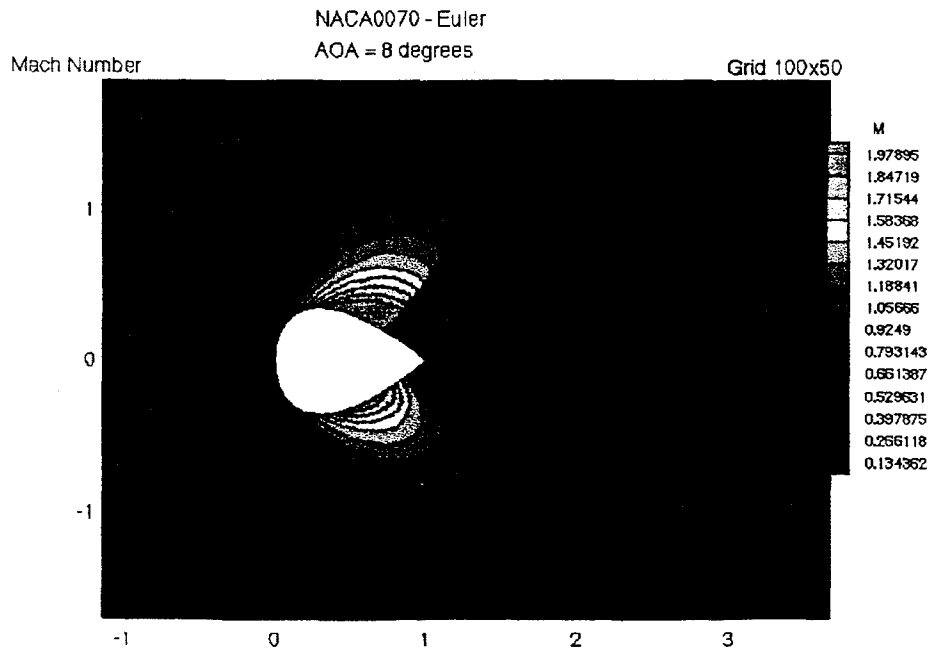


(b)

Figure 12. NACA0070 Initial Inviscid Solution - Mach Contour Plots
(a) AOA = 0° (b) AOA=2°



(c)



(d)

Figure 12 (continued). NACA0070 Initial Inviscid Solution - Mach Contour Plots
(c) AOA = 4° (d) AOA = 8°

Analyses of the pressure coefficient contour plots , as shown in Figure 13, also exhibit a discontinuity between grid points. The high differences between adjacent grid points' pressure coefficient magnitudes produce a sawtooth pattern. This sawtooth pattern is easily seen at the trailing edge on the contour plots in Figure 13. The jagged lines caused by discontinuities in the finite difference solution can be eliminated by using methods that were mentioned in the "Computer Model" section of Chapter II.

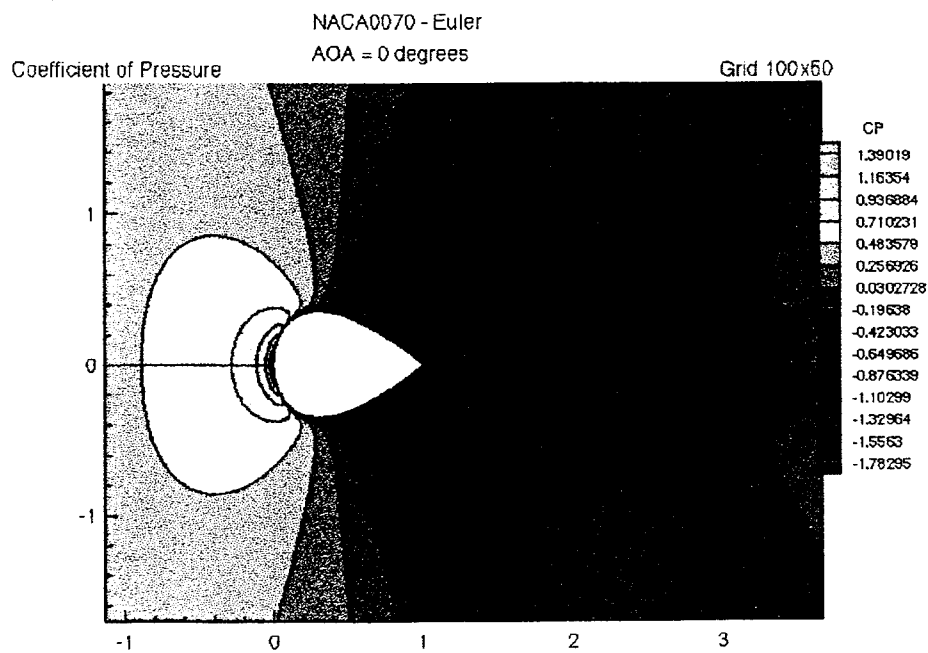
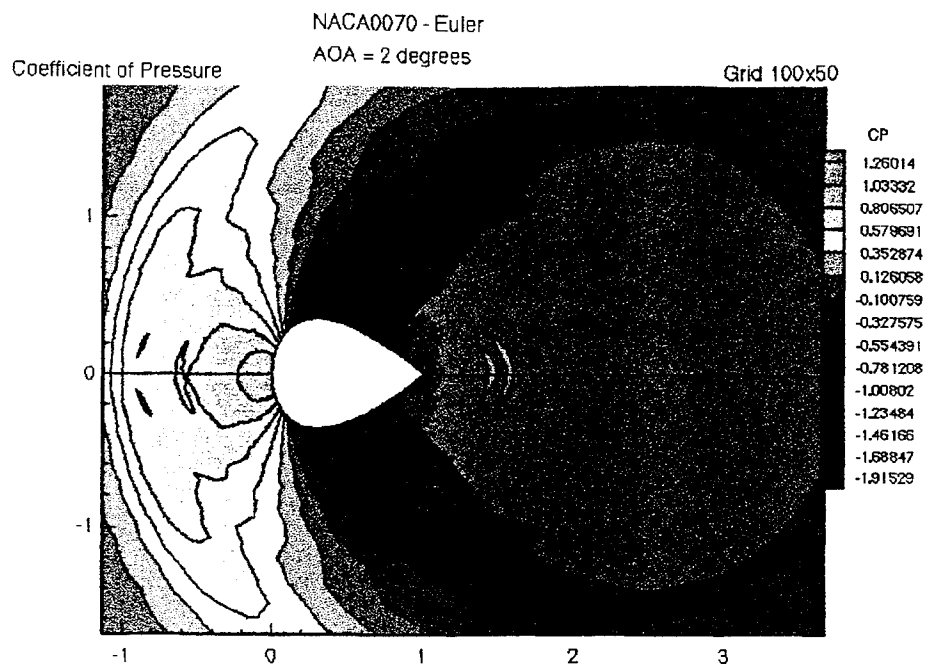
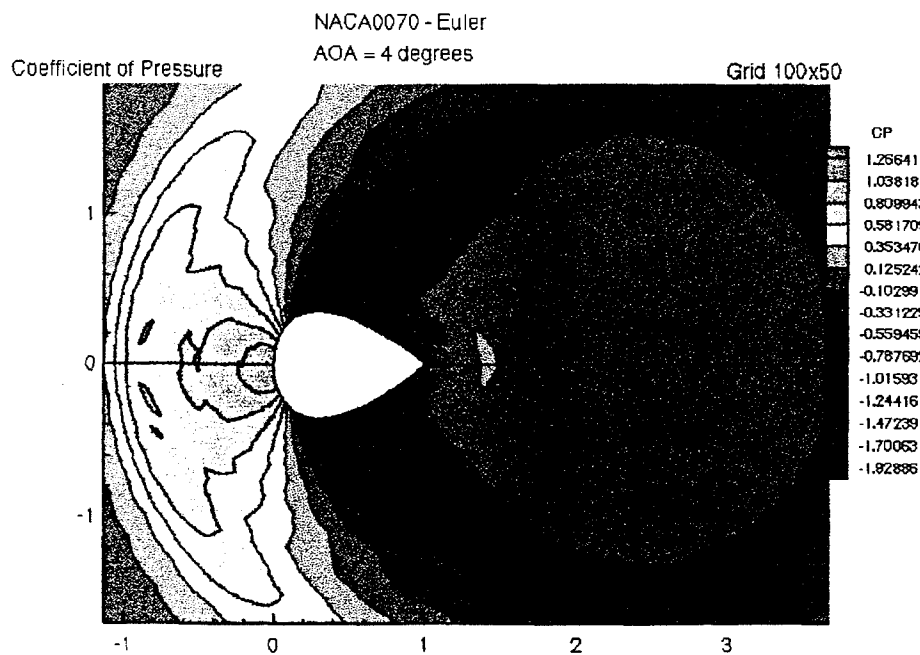


Figure 13. NACA0070 Initial Inviscid Solution - Coefficient of Pressure Contour Plots
(a) AOA = 0°

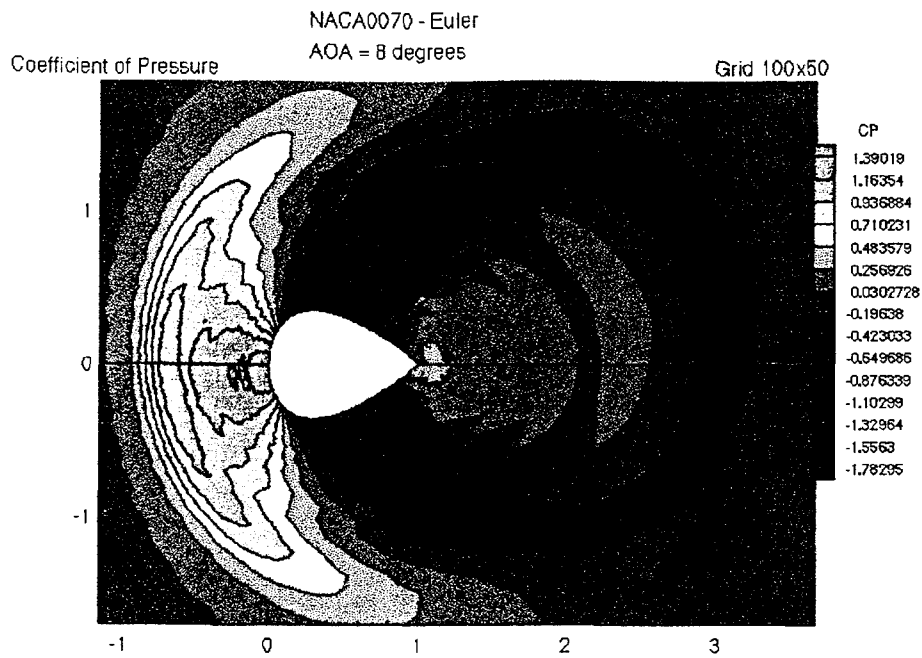


(b)



(c)

Figure 13 (continued). NACA0070 Initial Inviscid Solution -
Coefficient of Pressure Contour Plots (b) AOA=2° (c) AOA = 4°

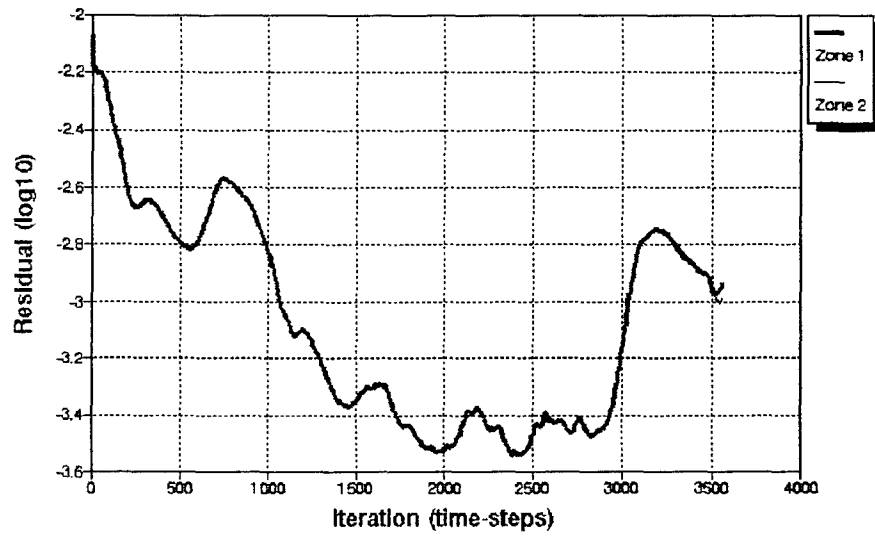


(d)

Figure 13 (continued). NACA0070 Initial Inviscid Solution -
Coefficient of Pressure Contour Plots (d) AOA = 8°

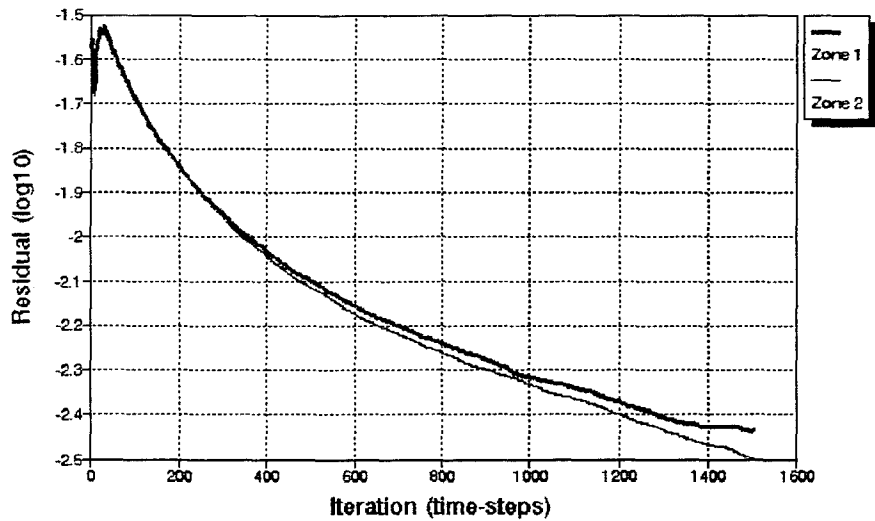
However, upon printout of the convergence histories, see Figure 14, a promising trend toward converging to a steady-state solution is visible, i.e., a decrease in the log of the residual as the iteration number increases.

Convergence History for NACA0070
Euler, AOA = 0 deg., Grid 100x50



(a)

Convergence History for NACA0070
Euler, AOA = 2 deg., Grid 100x50

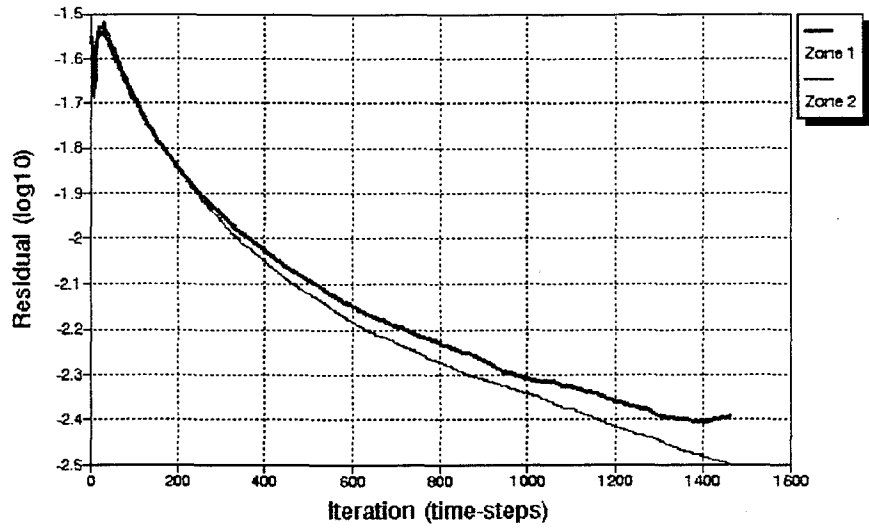


(b)

Figure 14. NACA0070 Initial Inviscid Solution - Convergence Histories
(a) AOA = 0° (b) AOA=2°

Convergence History for NACA0070

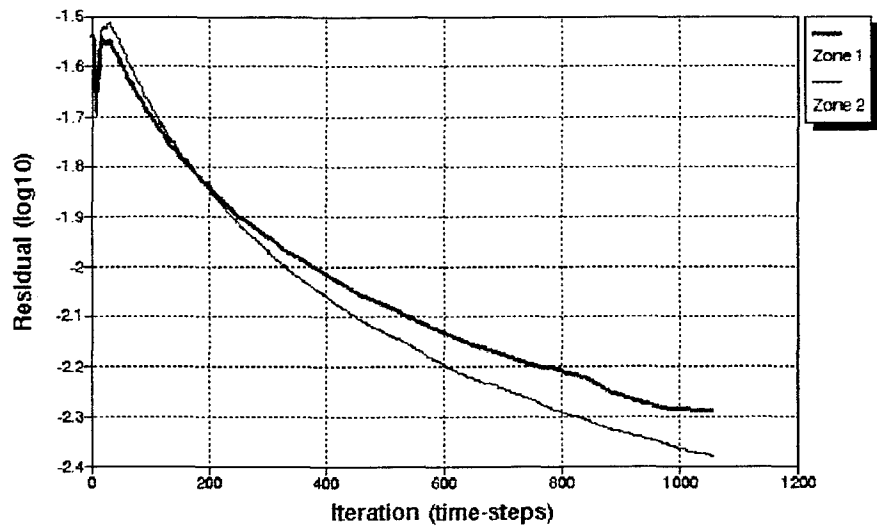
Euler, AOA = 4 deg., Grid 100x50



(c)

Convergence History for NACA0070

Euler, AOA = 8 deg., Grid 100x50



(d)

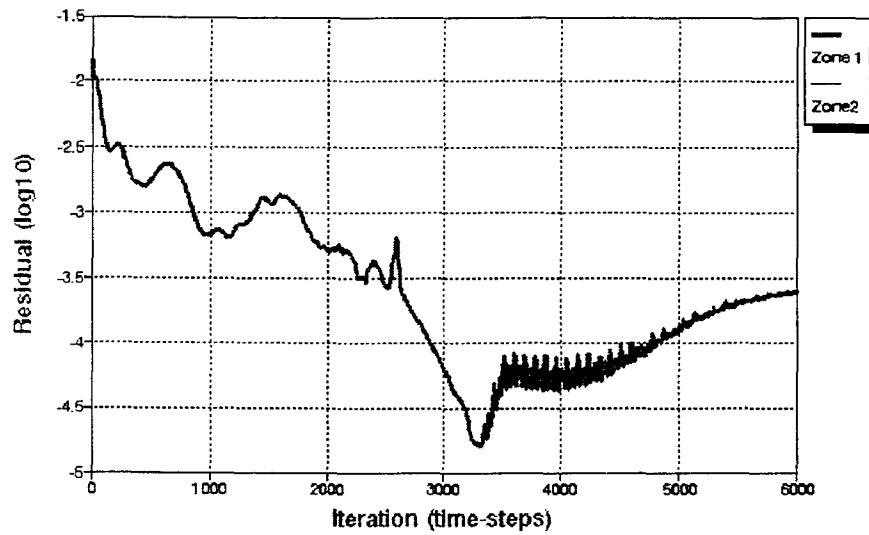
Figure 14 (continued). NACA0070 Initial Inviscid Solution - Convergence Histories

(c) AOA = 4° (d) AOA = 8°

It should be noted that a steady-state solution, or a perfectly converged result, is not expected in this case. Typically, a convergence history chart is expected to reach a value of -5 (or a residual value of 10^{-6}), but due to the predicted unsteady and oscillatory, time dependent nature of the flow over the selected cross-sections, this convergence value will not be attained for this study.

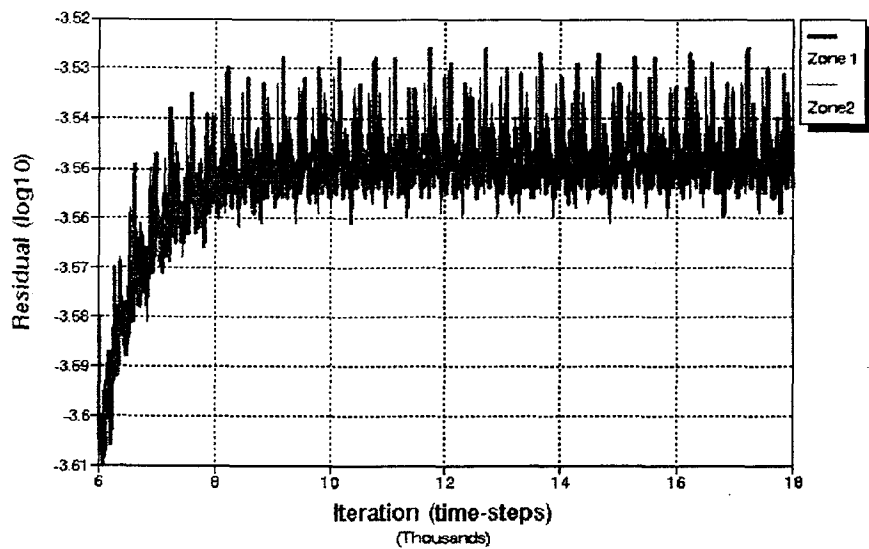
To correct for the numerous trends noted in the initial inviscid solution, the guidelines mentioned in chapter 2 of this thesis were followed. By increasing the second order explicit dissipation, XK2, the large values of flow properties at the shock were reduced. At this point, the sawtooth pattern of the pressure coefficient became markedly visible on the trailing edge surface of the cross-section, so the fourth order explicit damping term, XK4, was increased. The solution continued to have difficulty reaching a significant number of iterations, so the initial O-grid configuration was examined. Upon comparison to other input grids of thin airfoils which resulted in steady-state solutions, it was noted that the 100x50 grid was a much finer composition. Therefore, a new grid was generated that consisted of a 50x40 schematic. This caused the gridlines to be spaced farther away from the surface of the airfoil. The new spacing allowed ENS3DAE more scope in its calculations since the pressure differential had a larger distance over which to vary, thus allowing the residual between two grid points to be greater before the program terminated prematurely. The updated inviscid result for $\alpha=0^\circ$ allowed a better converged solution, thus more valid results were obtained. Upon viewing the convergence history, an average steady value of -3.55 is reached, or a residual of order 10^{-4} . Figure 15 shows the convergence history at 0° angle of attack by using a 50x40 grid.

Convergence History for NACA0070 Euler, AOA = 0 deg., Grid 50x40



(a)

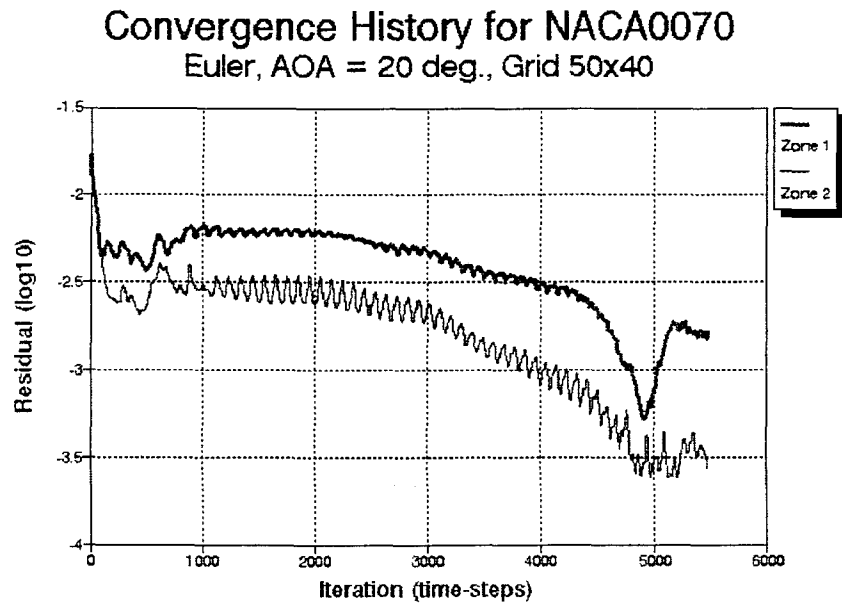
Convergence History for NACA0070 Euler, AOA = 0 deg., Grid 50x40



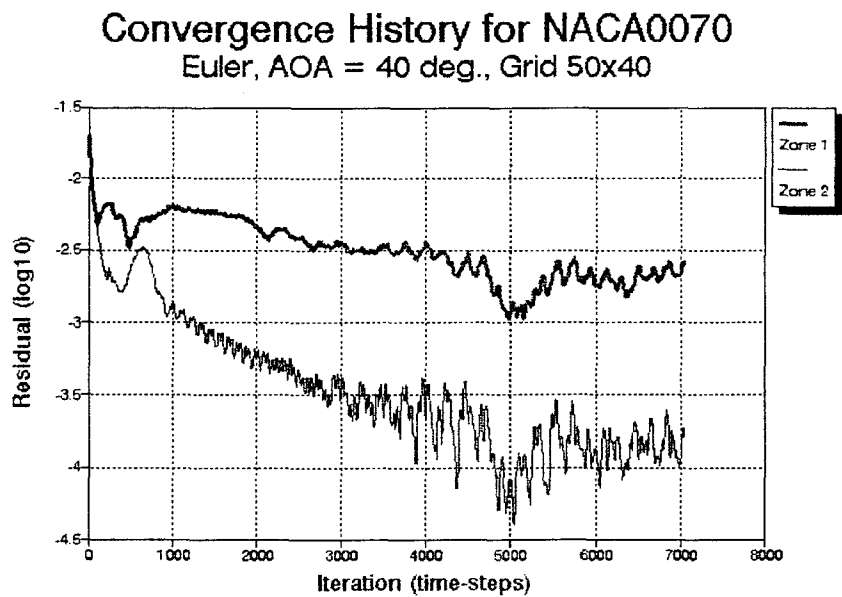
(b)

Figure 15. NACA0070 Updated Inviscid Solution - Convergence History at AOA = 0 degrees (a) 0-6000 Iterations (b) 6000-18,000 Iterations

This inviscid solution is also repeated for values $\alpha=20^\circ$ and $\alpha=40^\circ$, shown in Figure 16.



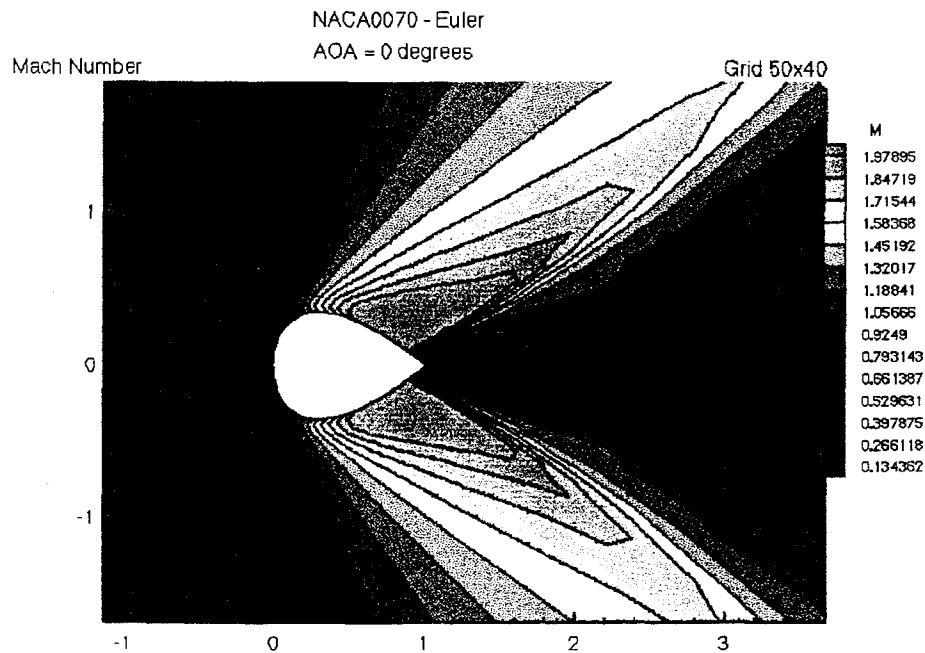
(a)



(b)

Figure 16. NACA0070 Updated Inviscid Solution - Convergence Histories
(a) AOA = 20° (b) AOA = 40°

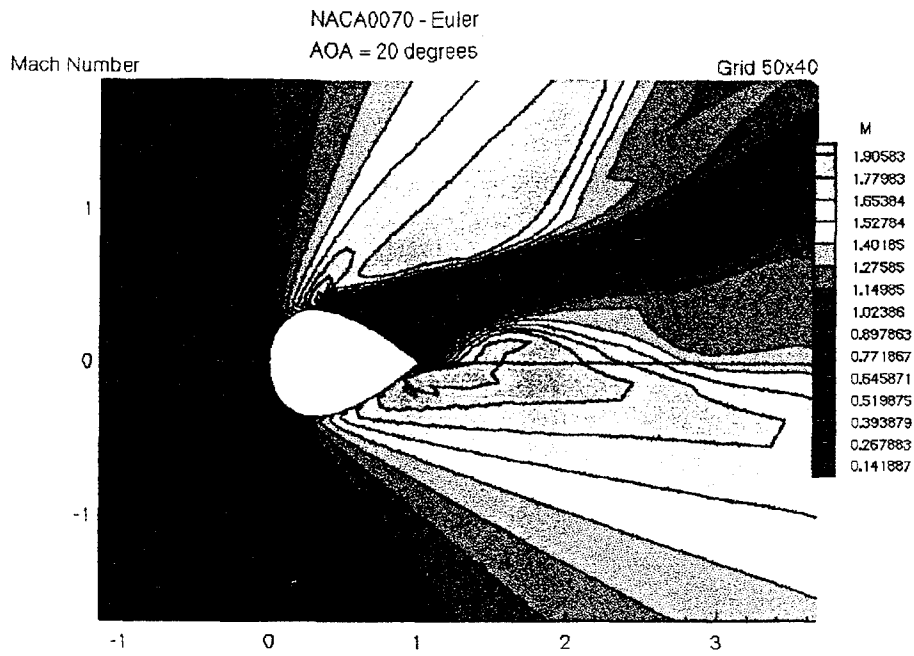
The convergence histories for these two cases also show an oscillating value, which can be explained by the nature of the unsteady flowfield. As the flow sheds itself first from one surface then from the other, the pressure alternates between high and low values. The maximum residual is plotted, so it is most likely this maximum residual occurs at a grid point near the trailing edge of the cross-section where the alternating flowfield is strongest. By examining the time-captured Mach contour plots, see Figure 17, the unsteady flow can best be visualized.



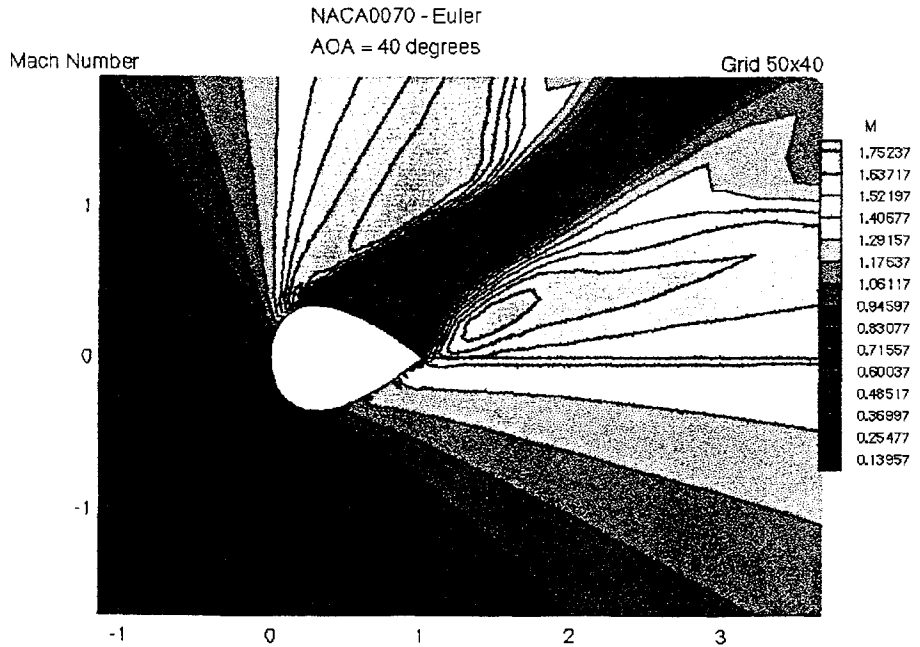
(a)

Figure 17. NACA0070 Updated Inviscid Solution - Mach Contour Plots

(a) AOA = 0°



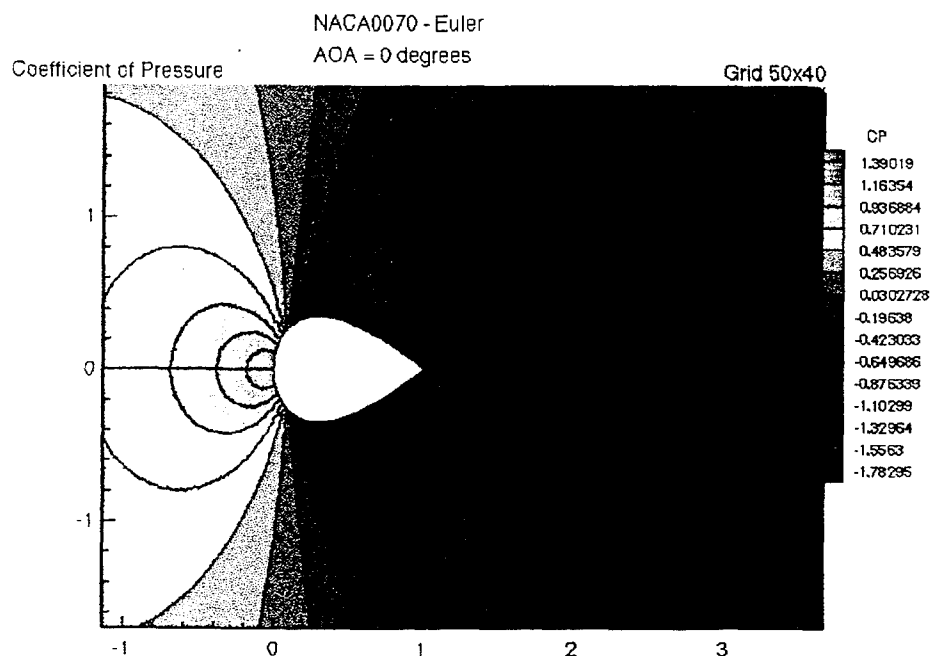
(b)



(c)

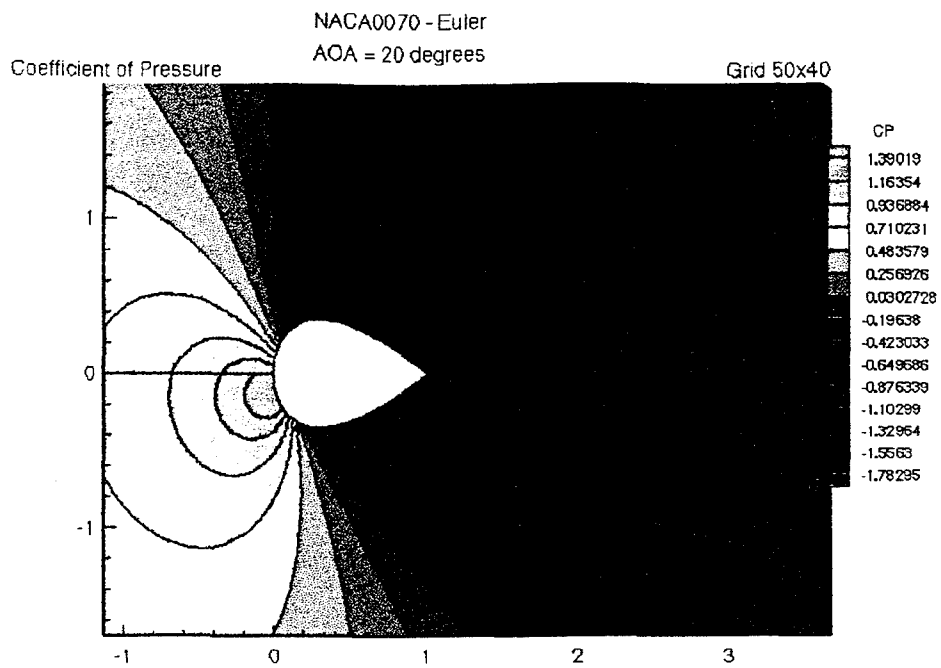
Figure 17 (continued). NACA0070 Updated Inviscid Solution - Mach Contour Plots
(b) AOA = 20° (c) AOA = 40°

The wake generated by the blunt body produces swirling vortex flow behind the shock wave. Consequently, this vortex flow yields low pressure coefficients in the wake region, as can be seen in Figure 18.

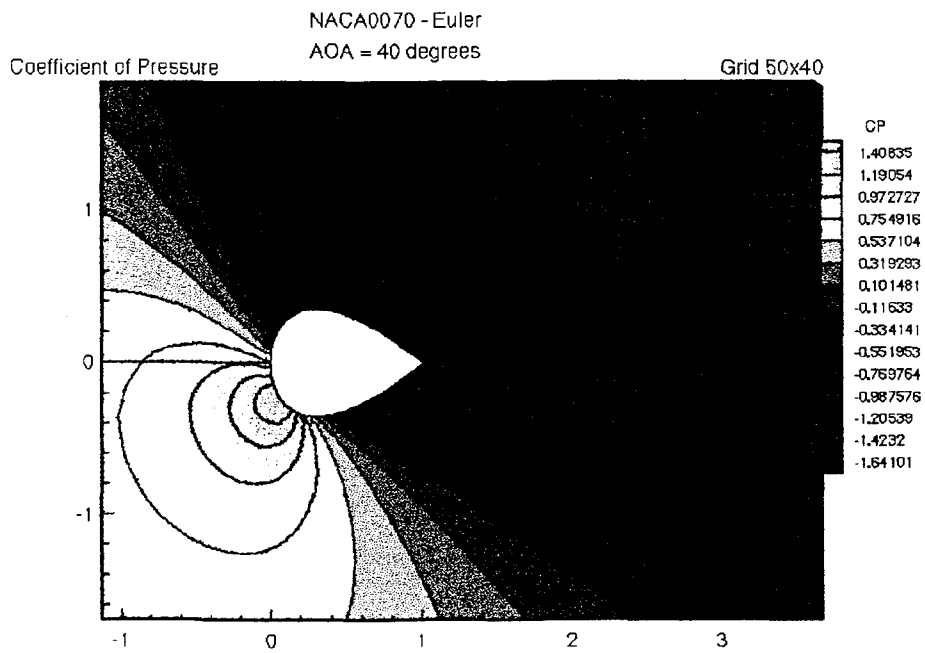


(a)

Figure 18. NACA0070 Updated Inviscid Solution - Coefficient of Pressure Contour Plots
(a) AOA = 0°



(b)



(c)

Figure 18 (continued). NACA0070 Updated Inviscid Solution -
Coefficient of Pressure Contour Plots (b) AOA = 20° (c) AOA = 40°

Next, the lift coefficients for this inviscid case were plotted in Figure 19.

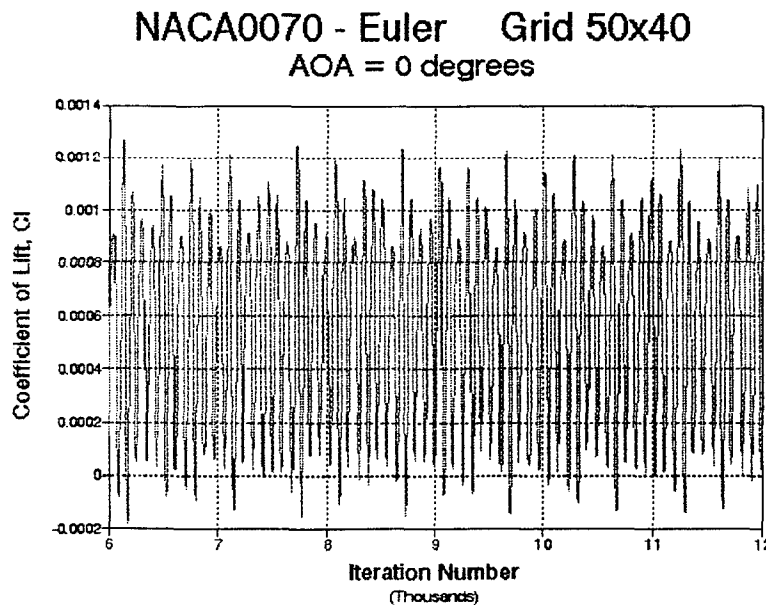
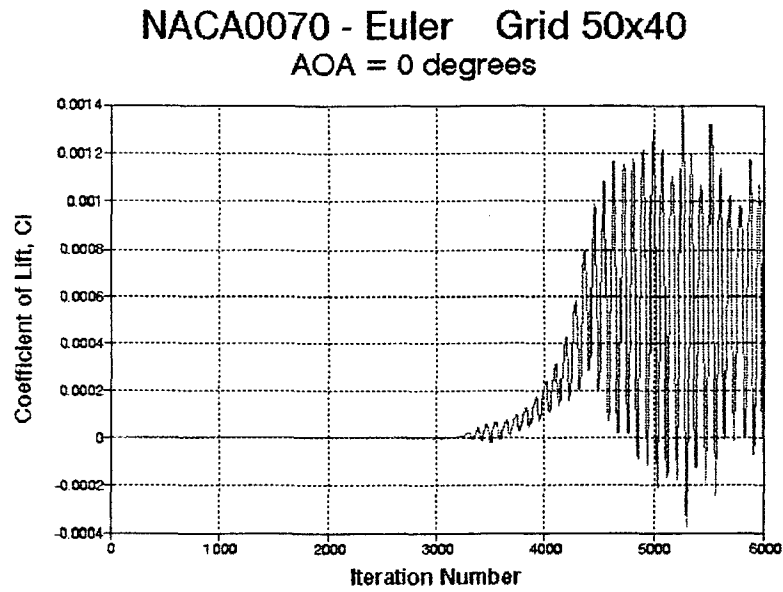
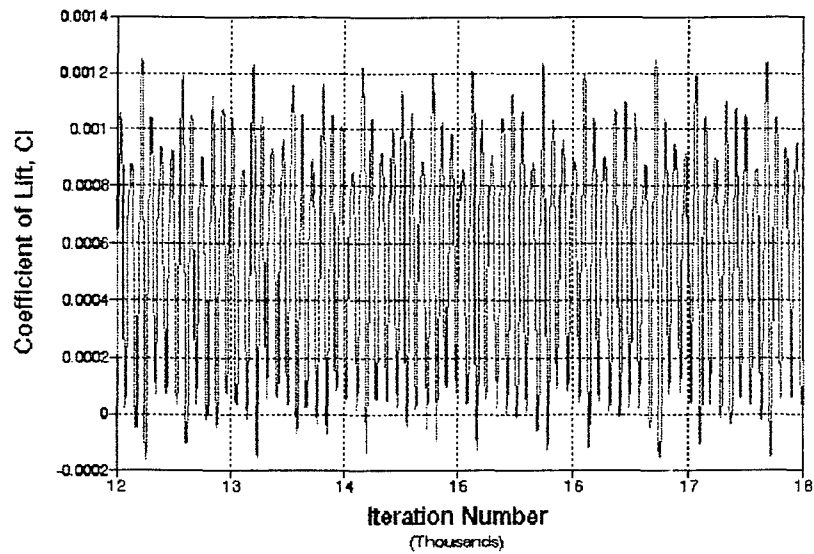


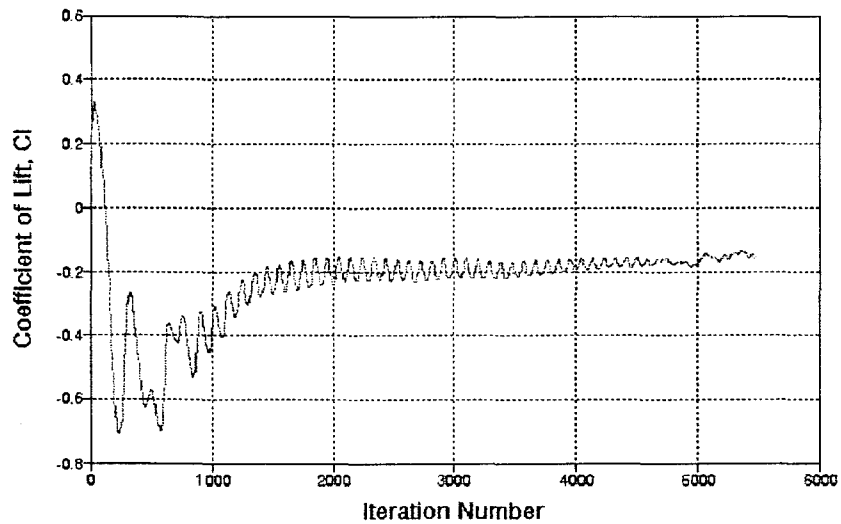
Figure 19. NACA0070 Updated Inviscid Solution -
Coefficient of Lift vs. Iteration Number Plots
(a) AOA = 0°, 0-6000 Iterations (b) AOA = 0°, 6000-12,000 Iterations

NACA0070 - Euler Grid 50x40
AOA = 0 degrees



(c)

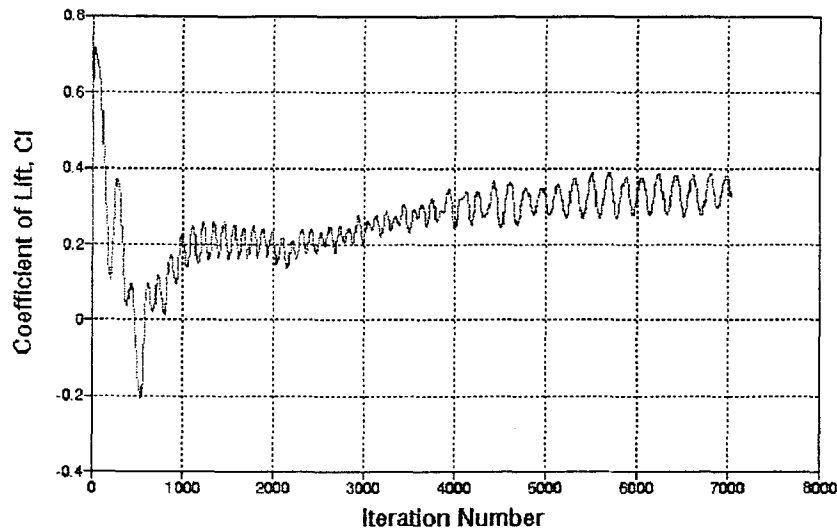
NACA0070 - Euler Grid 50x40
AOA = 20 degrees



(d)

Figure 19 (continued). NACA0070 Updated Inviscid Solution -
Coefficient of Lift vs. Iteration Number Plots
(c) AOA = 0°, 12,000-18,000 Iterations (d) AOA = 20°

NACA0070 - Euler Grid 50x40
AOA = 40 degrees

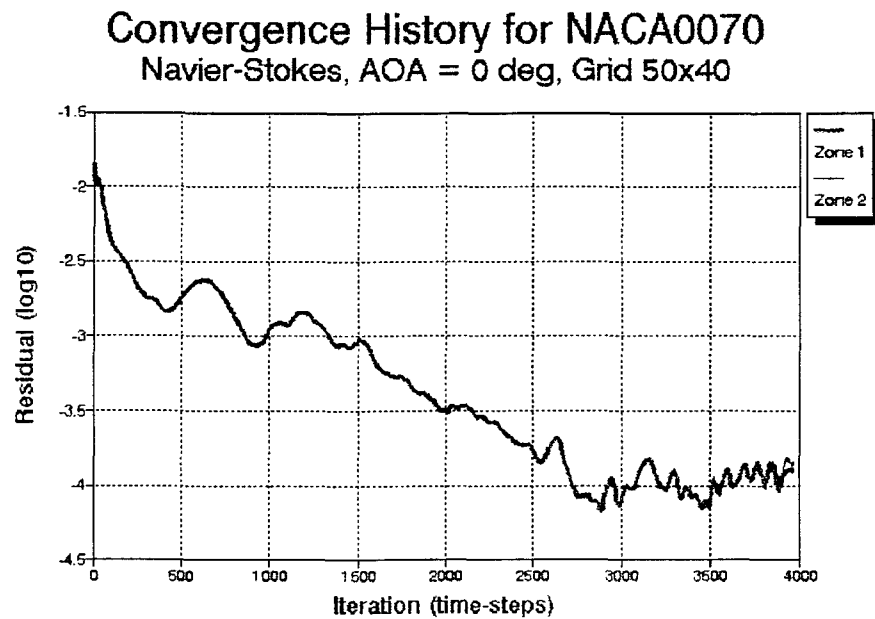


(e)

Figure 19 (continued). NACA0070 Updated Inviscid Solution -
Coefficient of Lift vs. Iteration Number Plots
(e) AOA = 40°

For $\alpha=0^\circ$, after 4500 iterations, c_l is seen to oscillate about an average value of 0.0005, or approximately zero. This is close to the predictions made by Hoerner's test data (Ref. 9). The oscillation is sinusoidal in nature and is a repeating pattern dependent upon time. The c_l trend at $\alpha=20^\circ$ is also as predicted. At positive angle of attack, the thick NACA0070 airfoil provides negative lift, thus producing a greater yaw angle due to the configuration of the boom pivot. This is an advantageous property since a negative lift boom allows for an increase in the allowable ψ on the KC-135 refueling envelope. At $\alpha=40^\circ$, however, the c_l is positive. The predicted trend also shows that for high angles of attack the lift becomes positive.

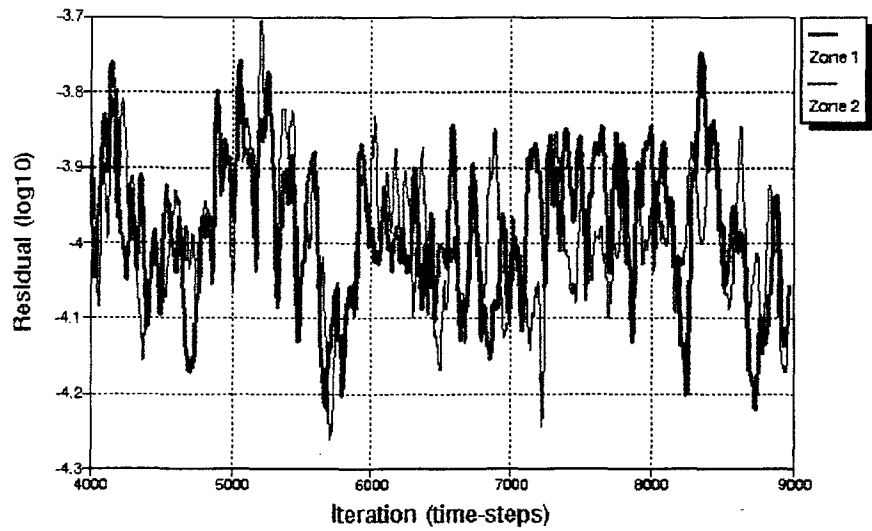
Since these updated inviscid solutions match the predicted trends and showed expected flow conditions, the boundary conditions of the model were changed to reflect a viscous flow quality. Runs were made for values of $\alpha=0^\circ$ to 40° by increments of 5° and for $\alpha=80^\circ$. Viewing the convergence history plots in Figure 20, the same observations as the inviscid cases are made.



(a)

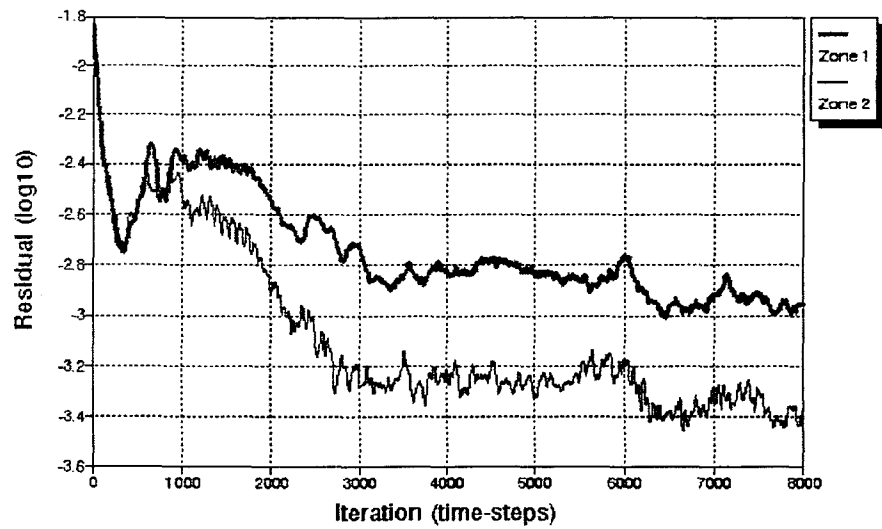
Figure 20. NACA0070 Viscous Solution - Convergence Histories
(a) AOA = 0° , 0-4000 Iterations

Convergence History for NACA0070
Navier-Stokes, AOA = 0 deg, Grid 50x40



(b)

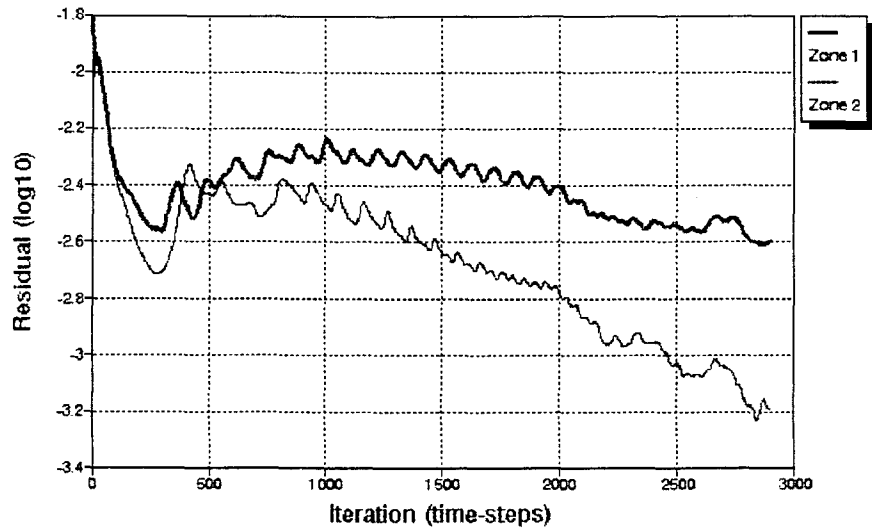
Convergence History for NACA0070
Navier-Stokes, AOA = 5 deg, Grid 50x40



(c)

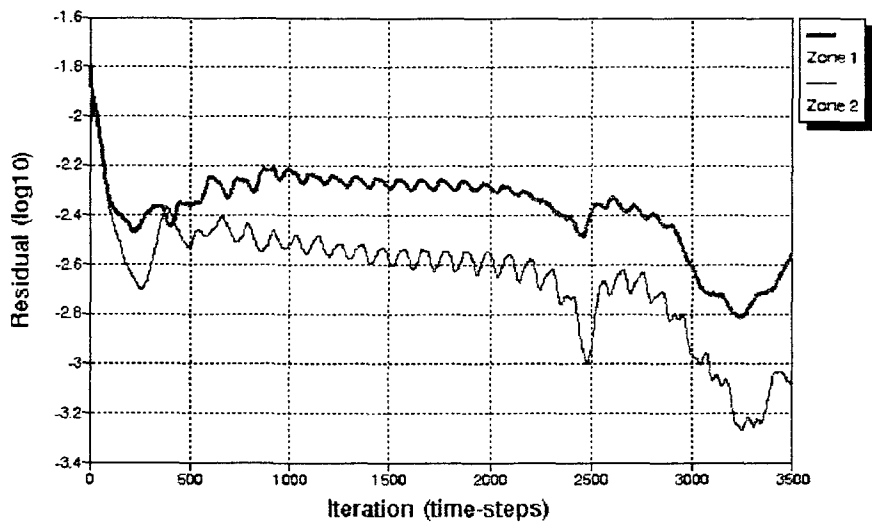
Figure 20 (continued). NACA0070 Viscous Solution - Convergence Histories
(b) AOA = 0°, 4000-9000 Iterations (c) AOA = 5°

Convergence History for NACA0070
Navier-Stokes, AOA = 10 deg, Grid 50x40



(d)

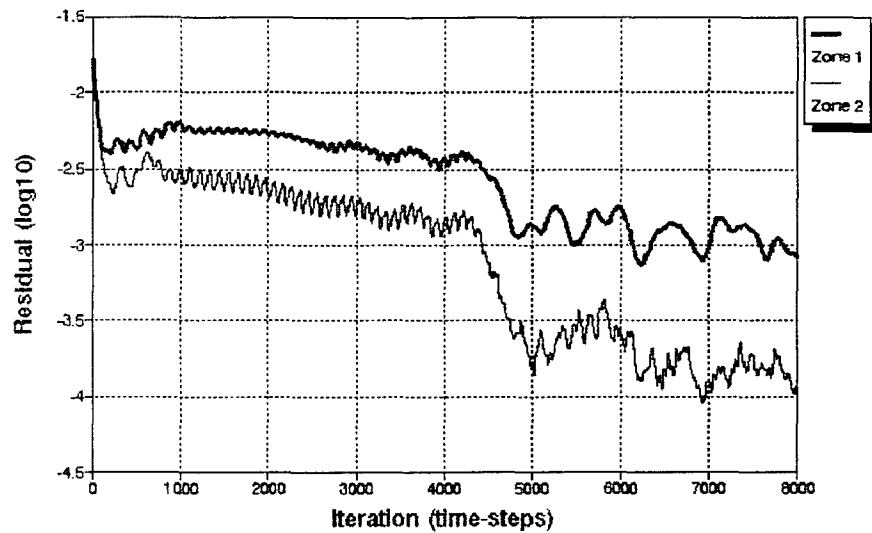
Convergence History for NACA0070
Navier-Stokes, AOA = 15 deg, Grid 50x40



(e)

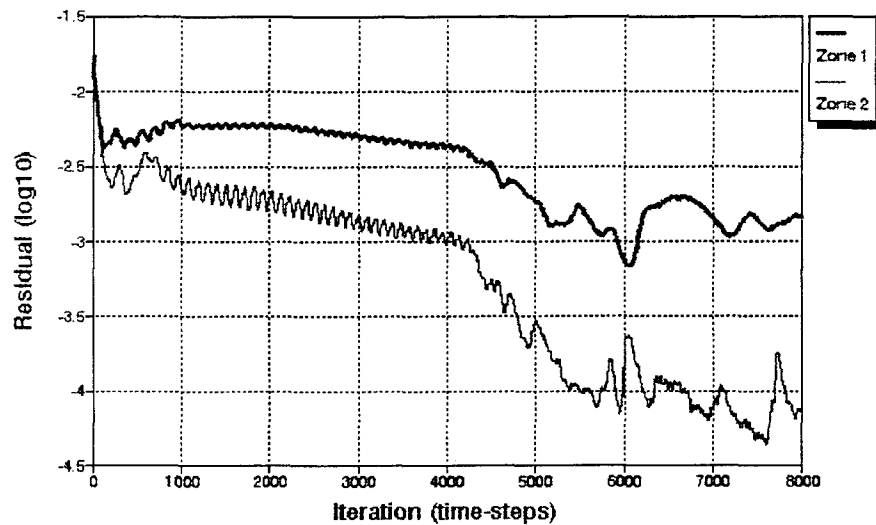
Figure 20 (continued). NACA0070 Viscous Solution - Convergence Histories
(d) AOA = 10° (e) AOA = 15°

Convergence History for NACA0070
Navier-Stokes, AOA = 20 deg, Grid 50x40



(f)

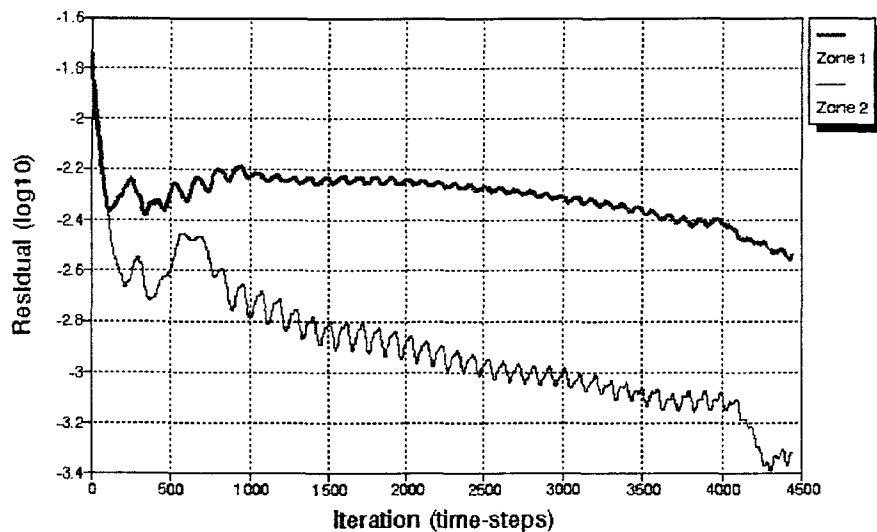
Convergence History for NACA0070
Navier-Stokes, AOA = 25 deg, Grid 50x40



(g)

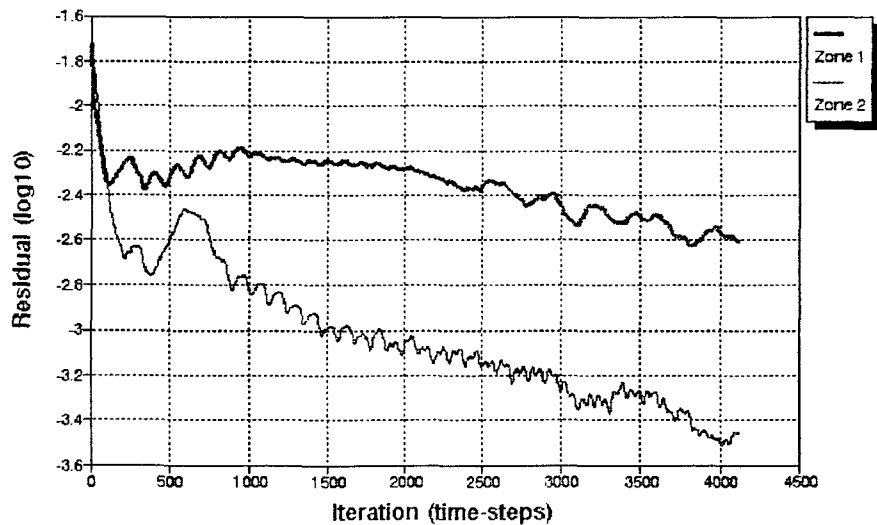
Figure 20 (continued). NACA0070 Viscous Solution - Convergence Histories
f) AOA = 20° (g) AOA = 25°

Convergence History for NACA0070
Navier-Stokes, AOA = 30 deg, Grid 50x40



(h)

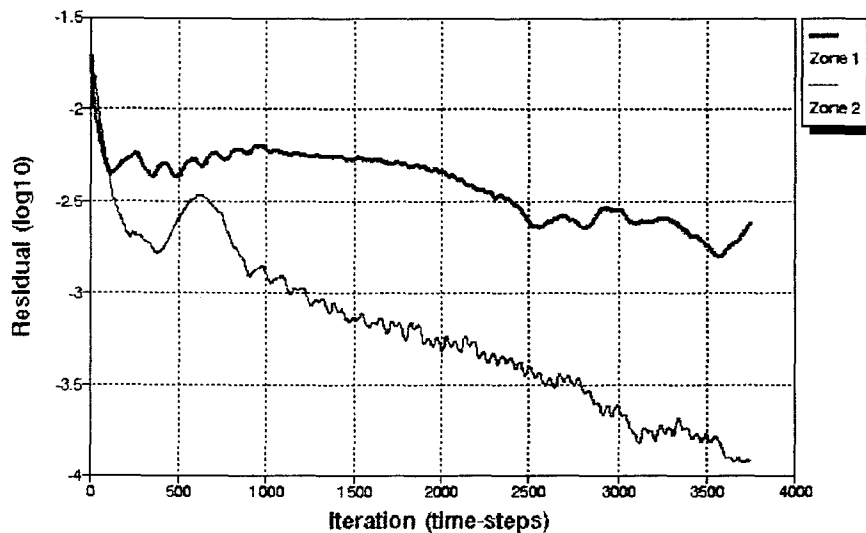
Convergence History for NACA0070
Navier-Stokes, AOA = 35 deg, Grid 50x40



(i)

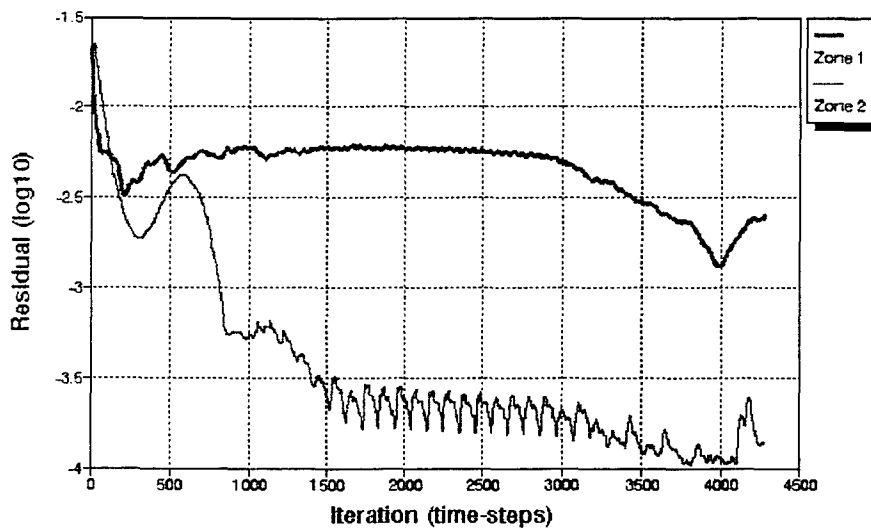
Figure 20 (continued). NACA0070 Viscous Solution - Convergence Histories
(h) AOA = 30° (i) AOA = 35°

Convergence History for NACA0070
Navier-Stokes, AOA = 40 deg, Grid 50x40



(j)

Convergence History for NACA0070
Navier-Stokes, AOA = 80 deg, Grid 50x40



(k)

Figure 20 (continued). NACA0070 Viscous Solution - Convergence Histories
(j) AOA = 40° (k) AOA = 80°

The residual decreases to a minimum value where it oscillates about an average value. For $\alpha=0^\circ$, the residual is on the order of 10^{-4} once again. As the angle of attack increases, it is interesting to note that the residual for zone 1 differs from zone 2. Zone 1, the top hemisphere, has a greater fluctuation in pressure forces than the bottom hemisphere, and as α increases, the difference in residual also increases. The reason for this variance can best be explained by examining the Mach contour plots, shown in Figure 21.

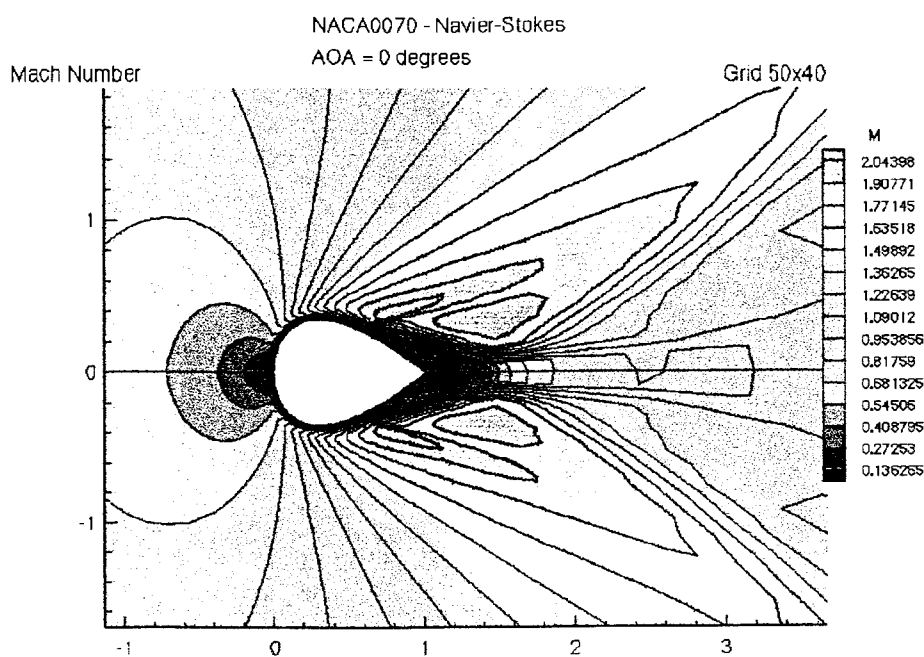
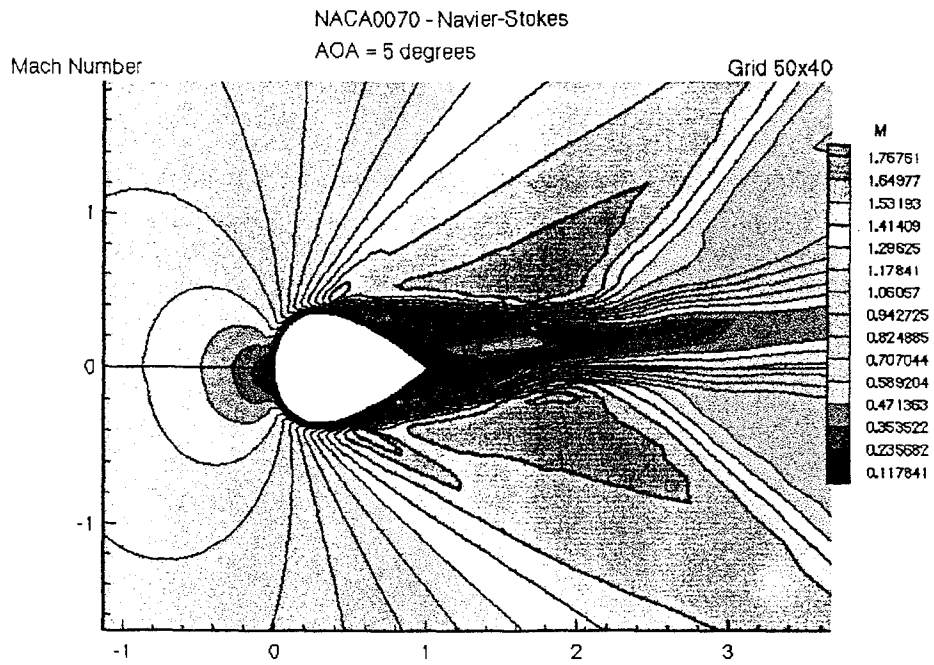
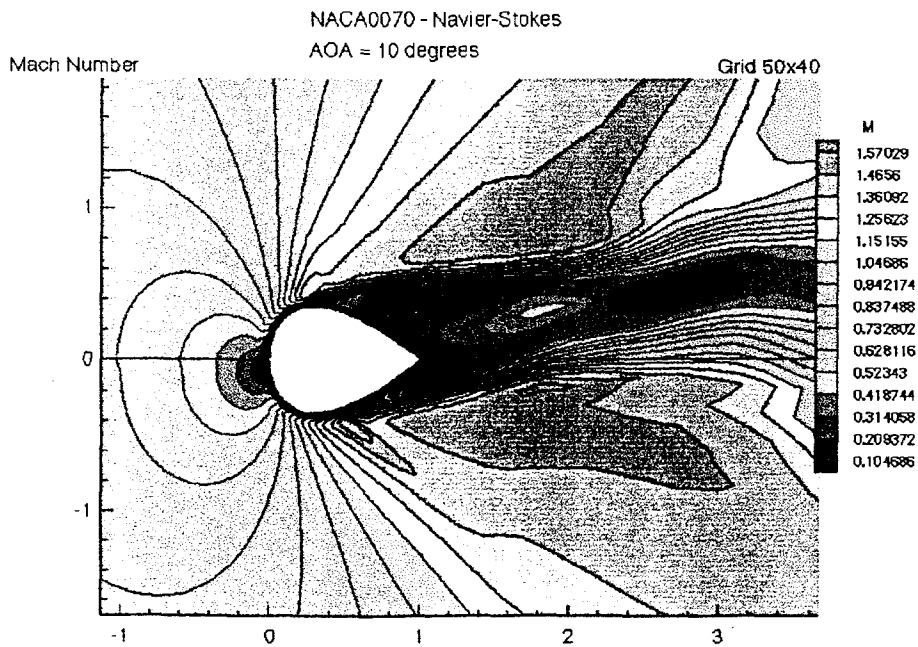


Figure 21. NACA0070 Viscous Solution - Mach Contour Plots
(a) AOA = 0°

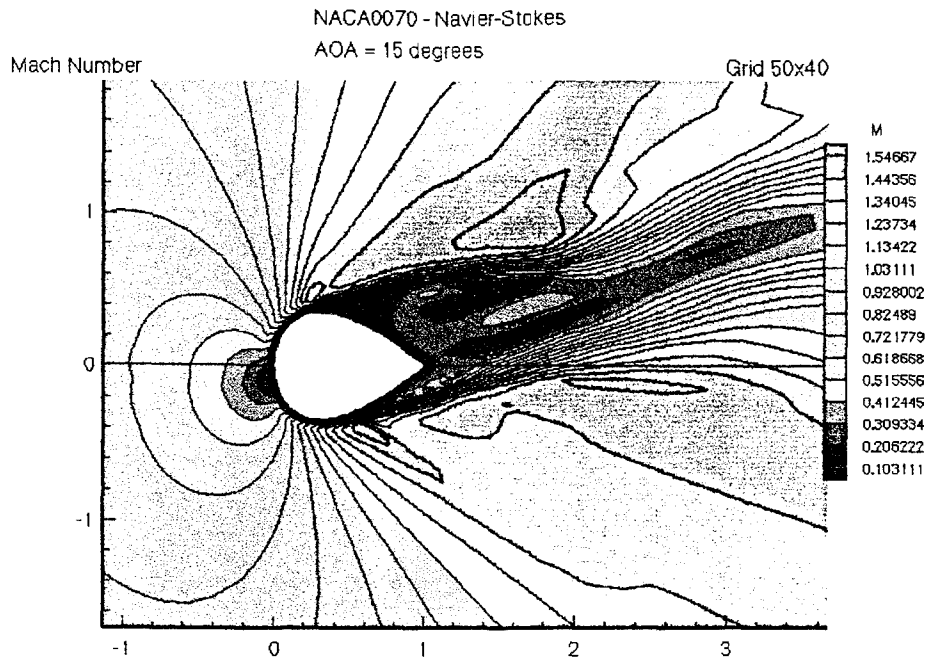


(b)

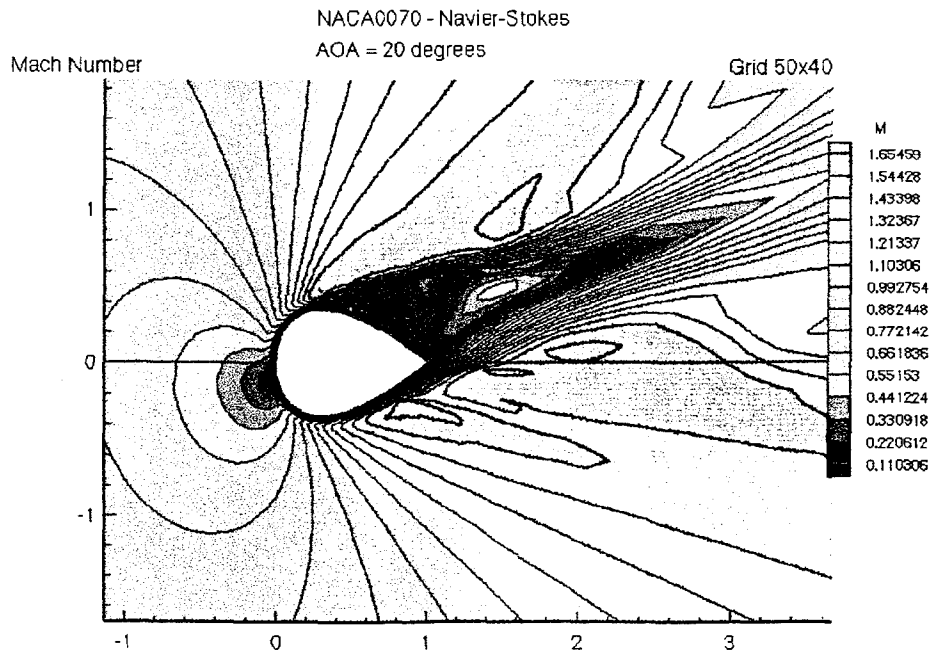


(c)

Figure 21 (continued). NACA0070 Viscous Solution - Mach Contour Plots
(b) AOA = 5° (c) AOA = 10°

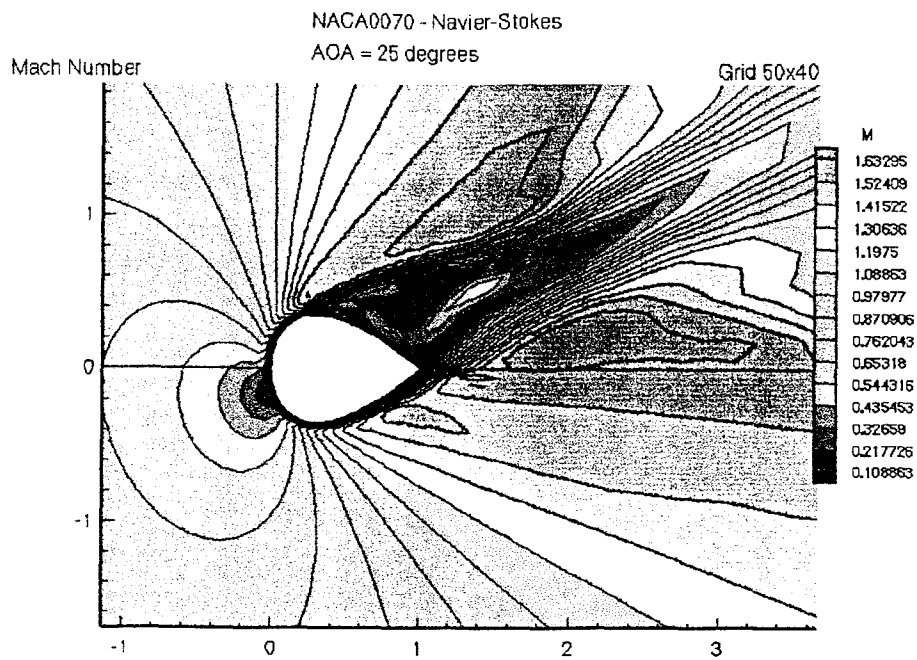


(d)

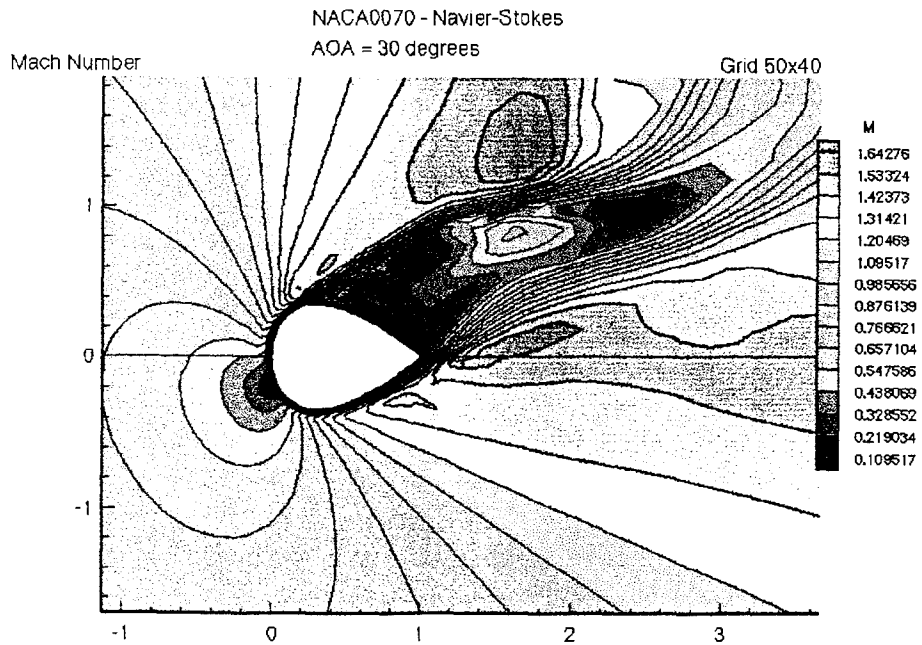


(e)

Figure 21 (continued). NACA0070 Viscous Solution - Mach Contour Plots
(d) AOA = 15° (e) AOA = 20°

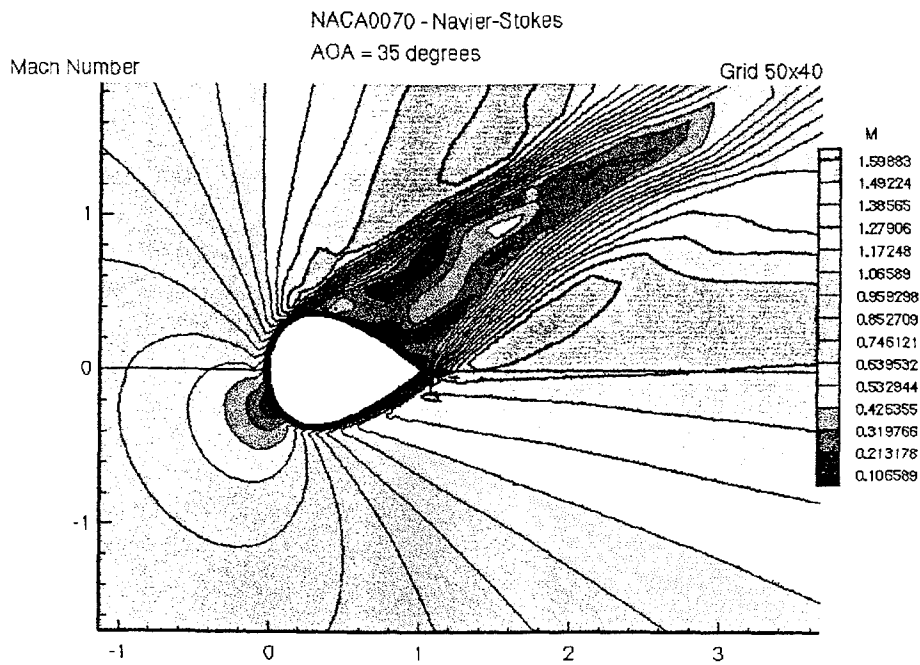


(f)

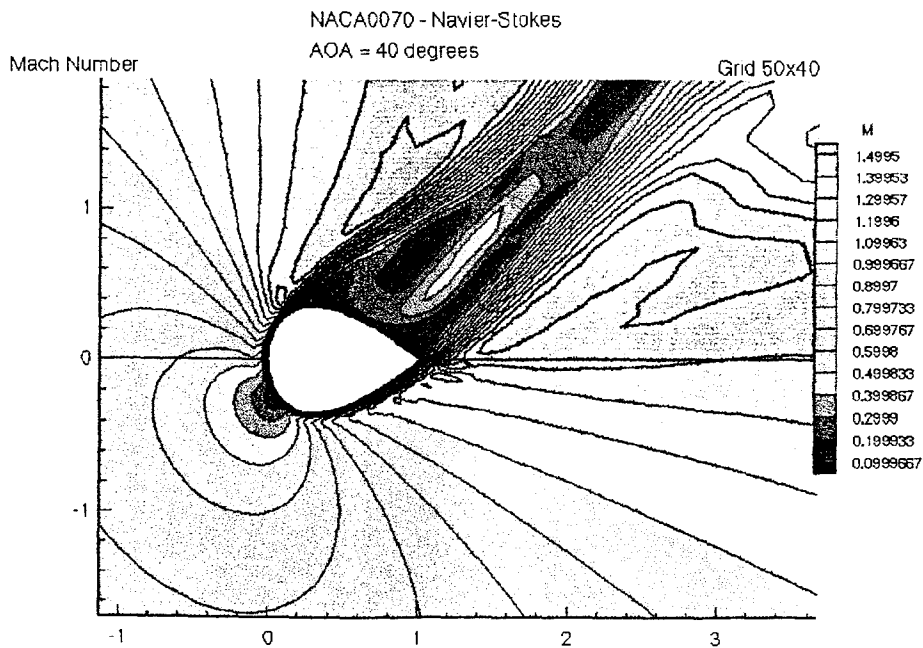


(g)

Figure 21 (continued). NACA0070 Viscous Solution - Mach Contour Plots
(f) AOA = 25° (g) AOA = 30°



(h)



(i)

Figure 21 (continued). NACA0070 Viscous Solution - Mach Contour Plots
(h) AOA = 35° (i) AOA = 40°

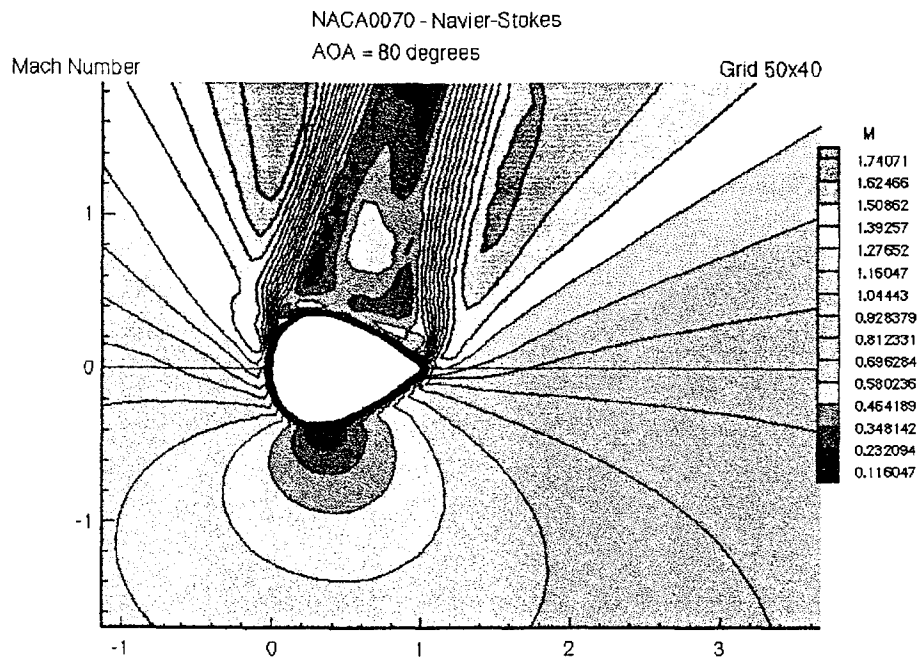
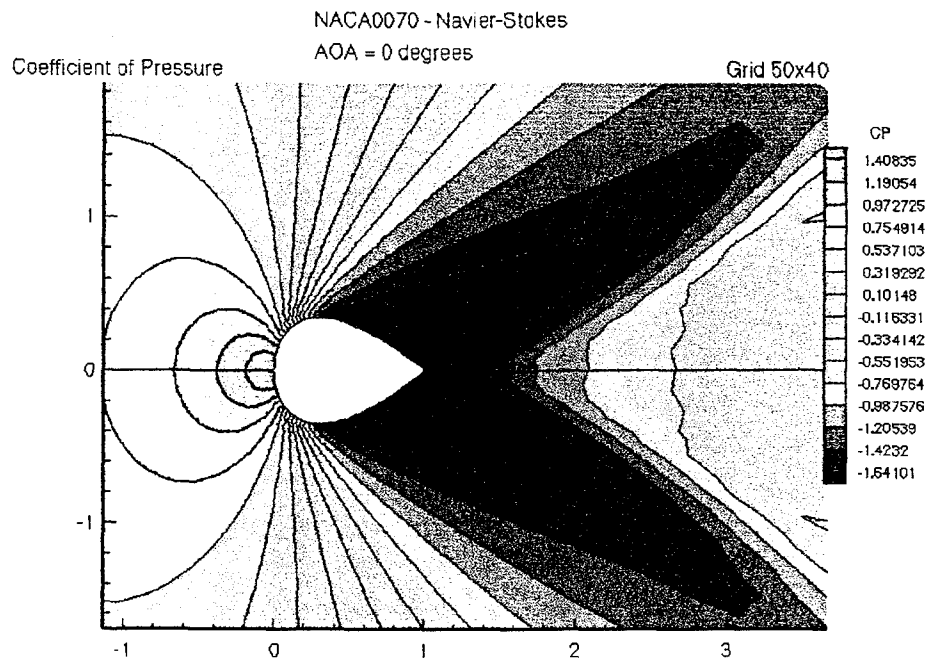


Figure 21 (continued). NACA0070 Viscous Solution - Mach Contour Plots
(j) AOA = 80°

The Mach lines at $\alpha=0^\circ$ show a symmetric flow about the cross-section, which is expected since the NACA0070 is a symmetric airfoil. However, at $\alpha=5^\circ$ the centerline, representing the boundary between zone 1 and zone 2 no longer doubles as a flow symmetry line. As the angle of attack increases, the flow pattern continues to rotate so that more of the wake, or irregular vortex flow, is located in zone 1, above the centerline. Therefore, a larger difference in pressure forces causes the residual to remain higher than in zone 2, where the flow is still mostly uniform as it contacts the lower surface of the airfoil. An additional ascertainment from these graphs is that the effects of the flow contacting the surface seem to be propagated further downstream as the angle of attack increases. The

explanation for this phenomenon is that a larger surface area is impacting the freestream flow conditions, thus causing a greater disturbance to the steady flow properties.

With the coefficient of pressure plots in Figure 22, this effect is also noted.



(a)

Figure 22. NACA0070 Viscous Solution - Coefficient of Pressure Contour Plots
(a) AOA = 0°

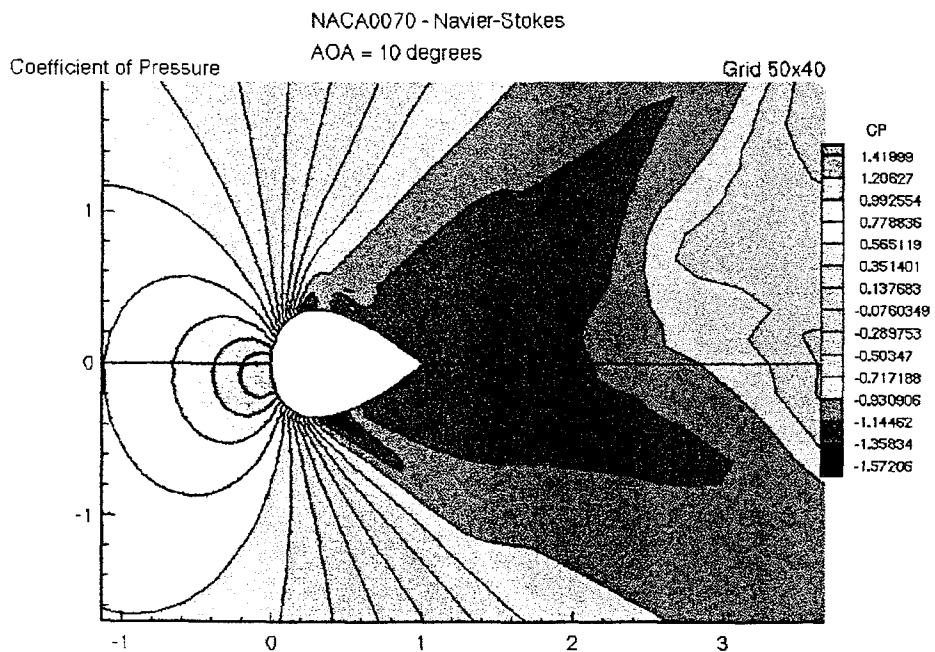
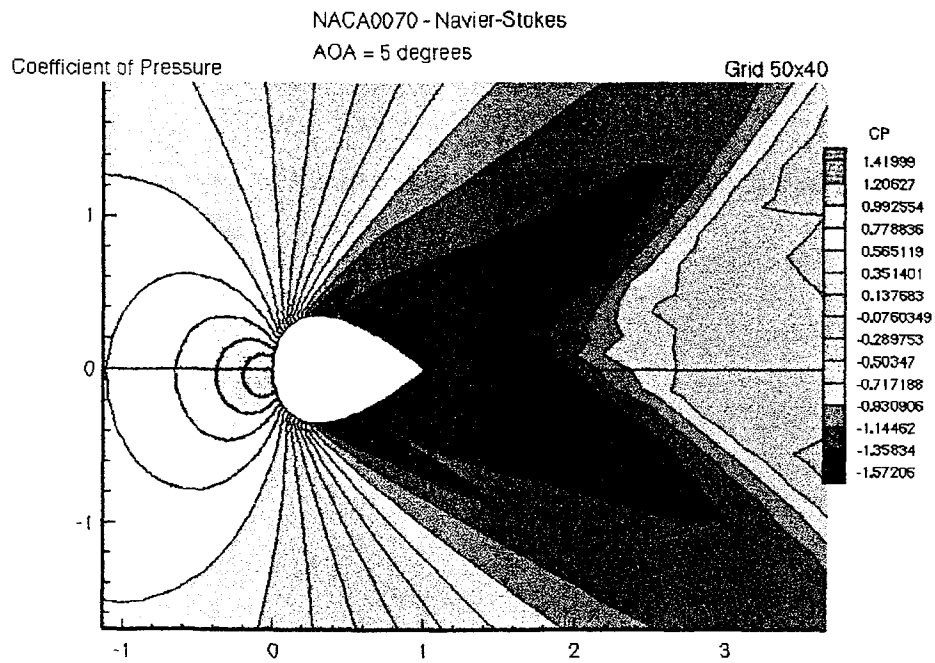
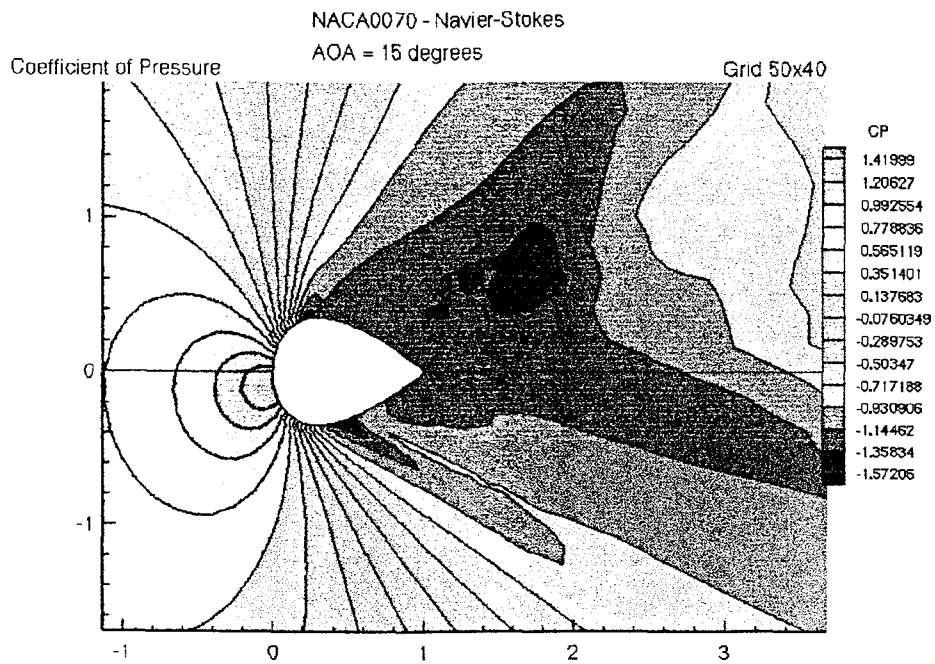
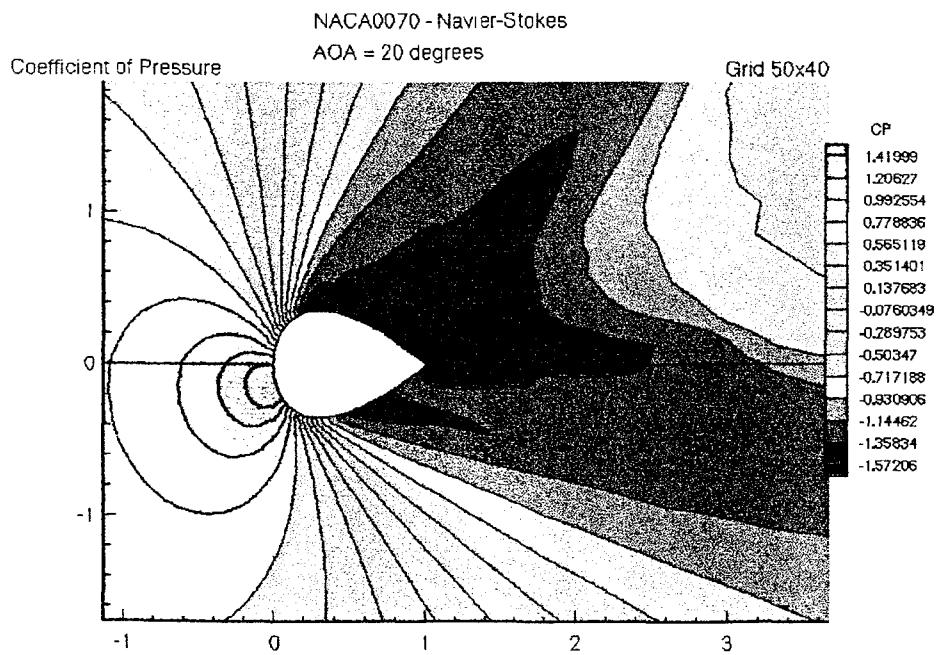


Figure 22 (continued). NACA0070 Viscous Solution -
Coefficient of Pressure Contour Plots (b) AOA = 5° (c) AOA = 10°

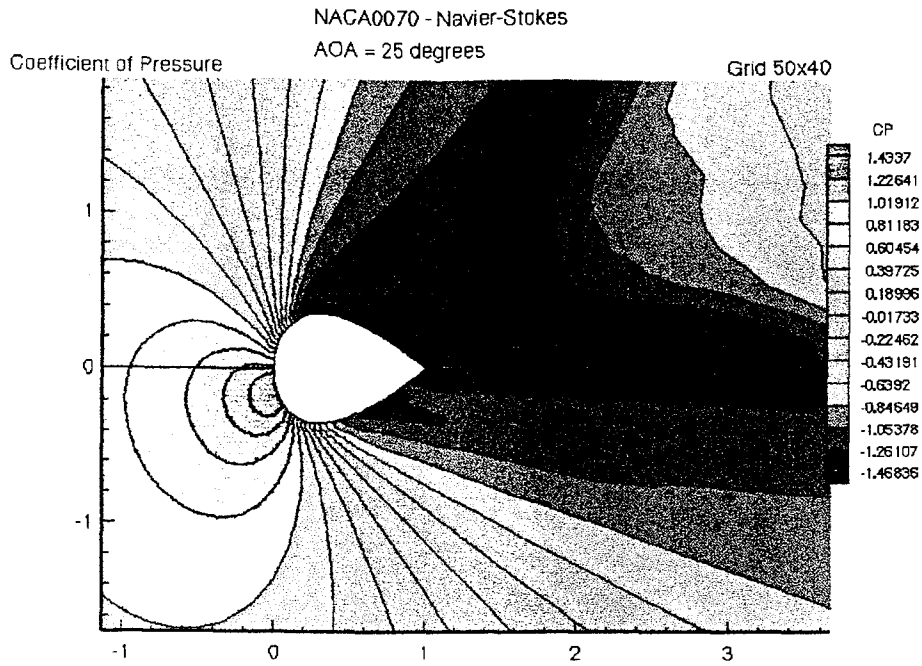


(d)

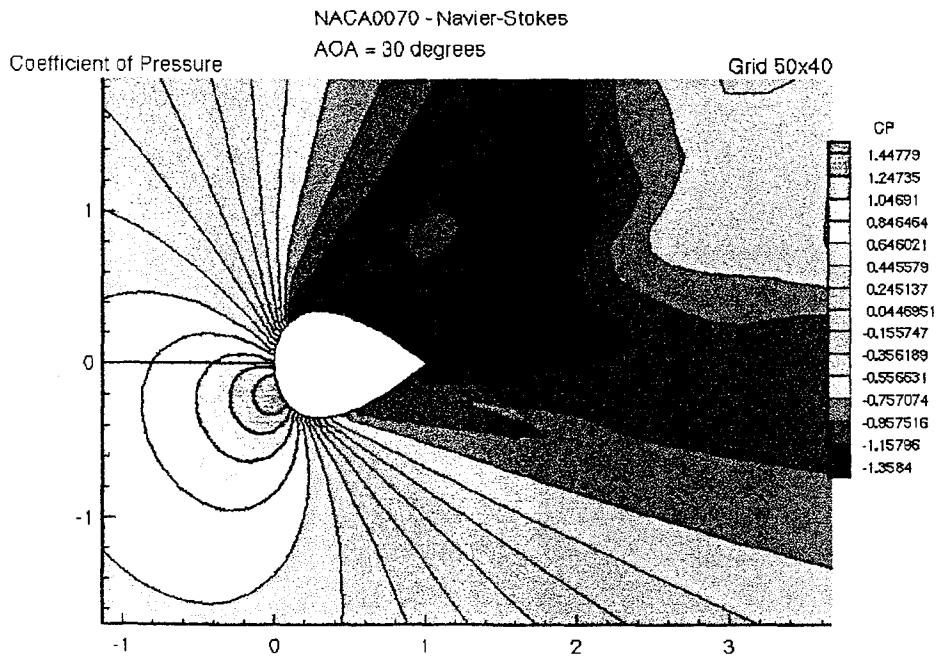


(e)

Figure 22 (continued). NACA0070 Viscous Solution -
Coefficient of Pressure Contour Plots (d) AOA = 15° (e) AOA = 20°

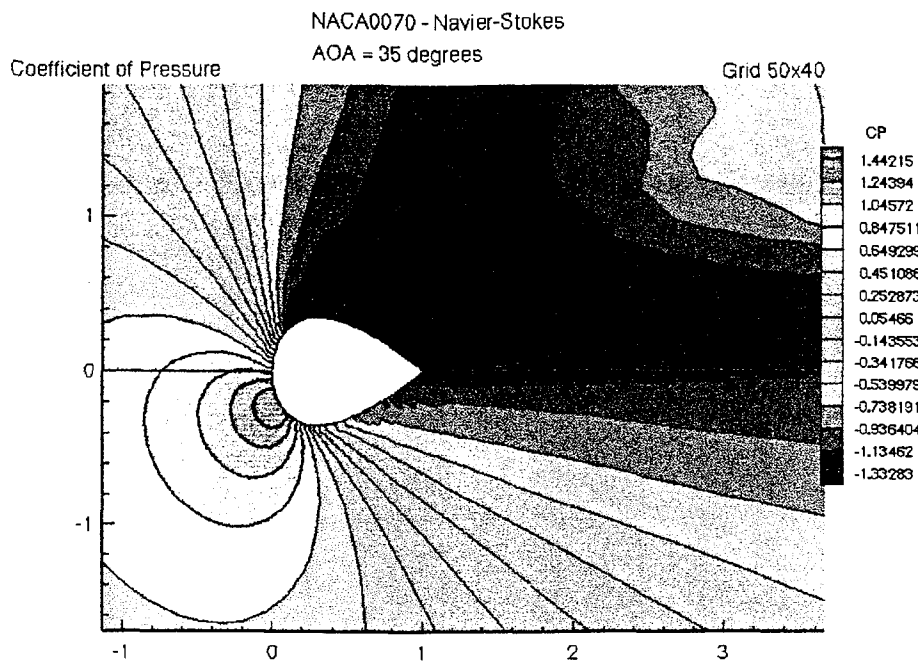


(f)

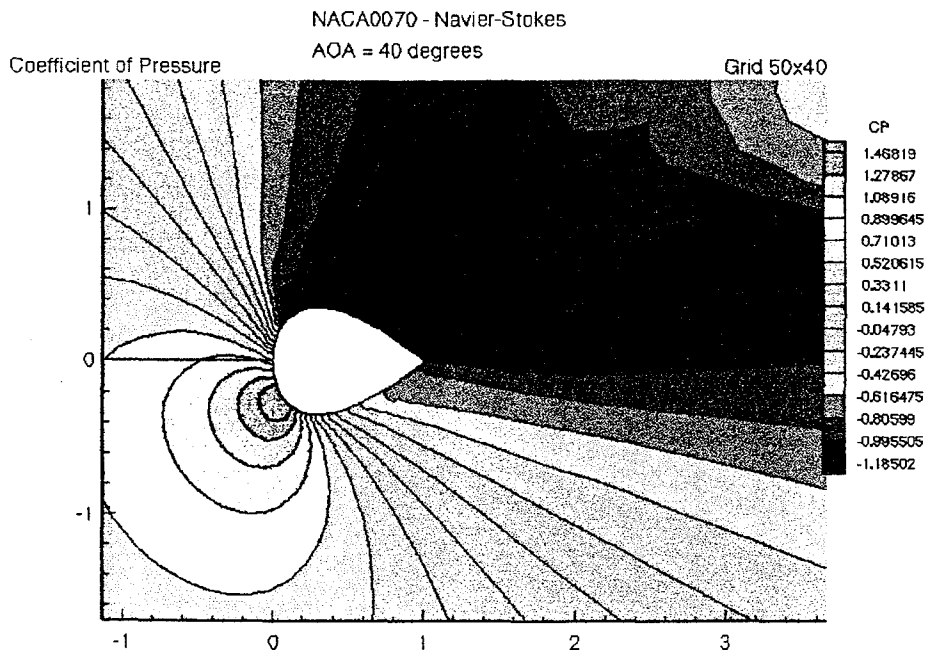


(g)

Figure 22 (continued). NACA0070 Viscous Solution -
Coefficient of Pressure Contour Plots (f) AOA = 25° (g) AOA = 30°

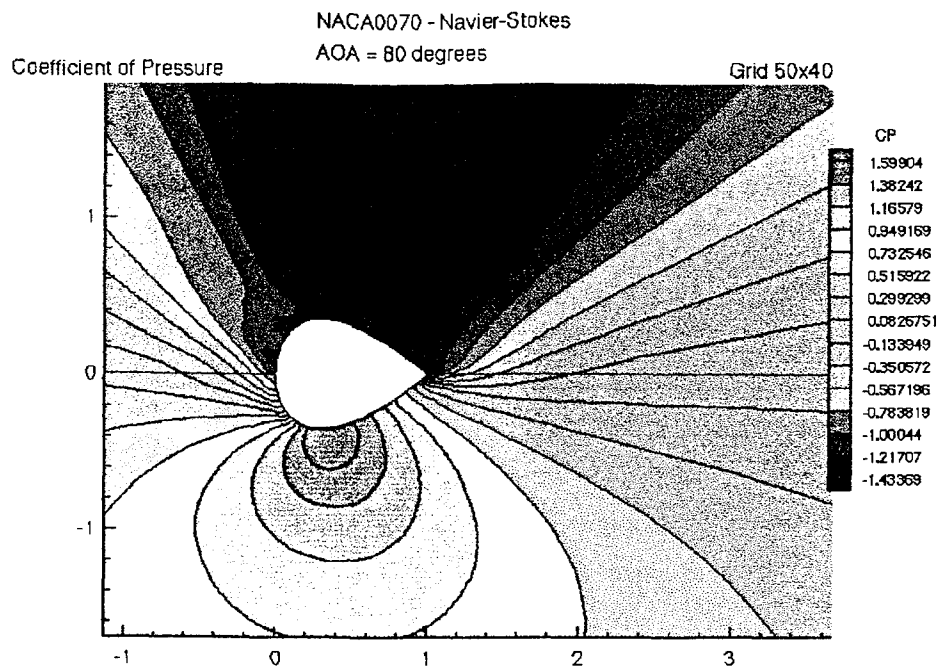


(h)



(i)

Figure 22 (continued). NACA0070 Viscous Solution -
Coefficient of Pressure Contour Plots (h) AOA = 35° (i) AOA = 40°



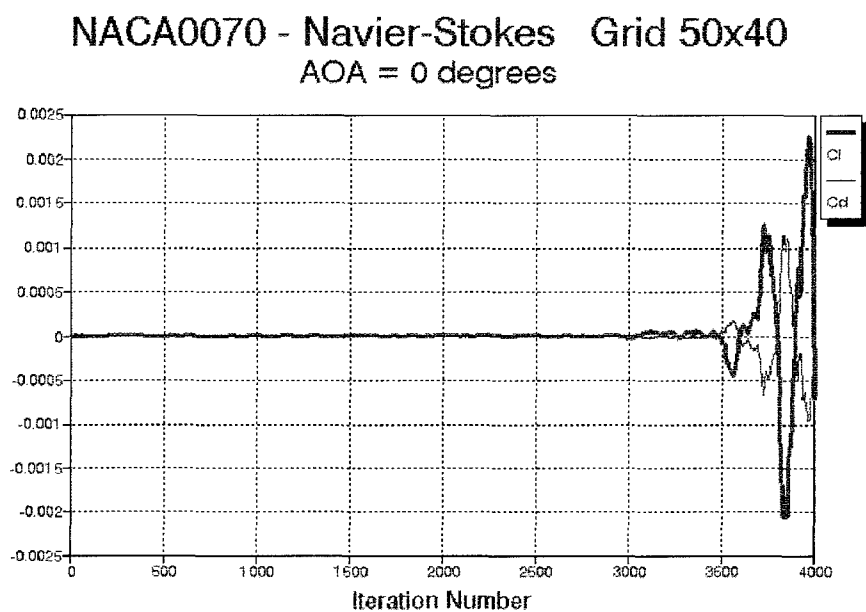
(j)

Figure 22 (continued). NACA0070 Viscous Solution -
Coefficient of Pressure Contour Plots (j) AOA = 80°

Furthermore, the reason for negative lift at positive angles of attack can be perceived. The pressure at freestream impact on the cross-section surface is high; however, a strong negative pressure coefficient is produced behind the shock. The area of negative pressure is due to separation of flow from the airfoil surface, and as α is initially increased, the wake region rotates to the top surface, and the lower surface has attached flow conditions. The attached flow produces a suction effect adding to the negative lift of the cross section. The balance between the high pressure at the nose, strongly attached flow on the lower surface, and separated flow on the upper surface causes the lift to vary with angle of attack, and the amount of negative pressure effecting the bottom surface decreases as α is

further increased. Thus, the positive and negative pressure effects on both surfaces reach equilibrium at approximately $\alpha=30^\circ$, and a c_l of zero is obtained.

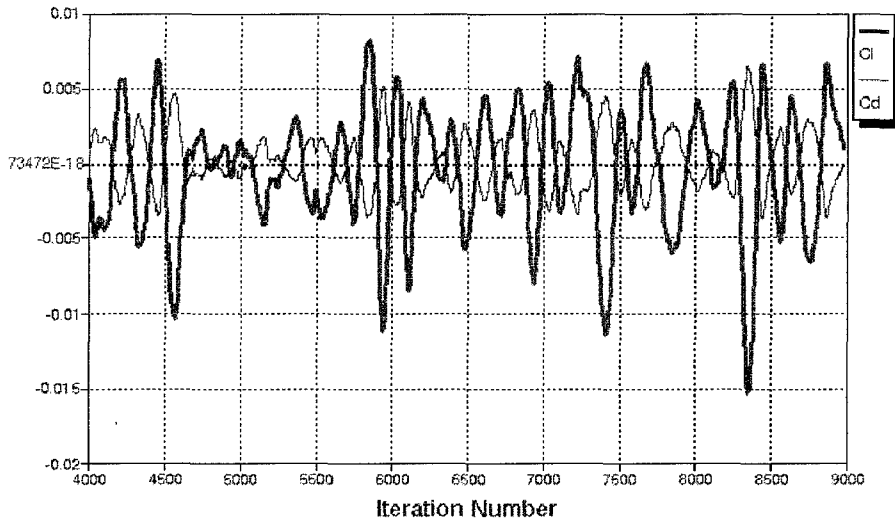
From the coefficients of lift and drag versus iteration graphs, see Figure 23, the same trend toward negative lift at $0^\circ < \alpha < 30^\circ$ is seen, as well as the same oscillation patterns as in the inviscid results.



(a)

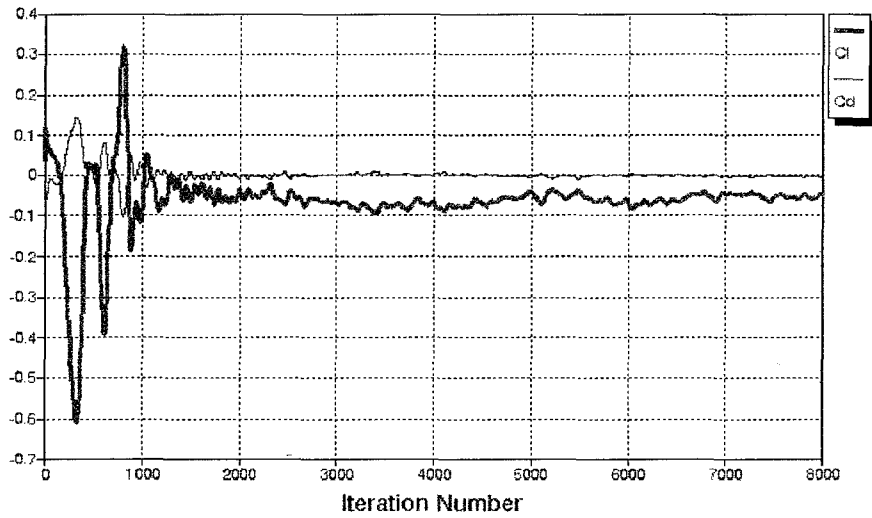
Figure 23. NACA0070 Viscous Solution -
Coefficients of Lift & Drag vs. Iteration Number Plots
(a) AOA = 0° , 0-4000 Iterations

NACA0070 - Navier-Stokes Grid 50x40
AOA = 0 degrees



(b)

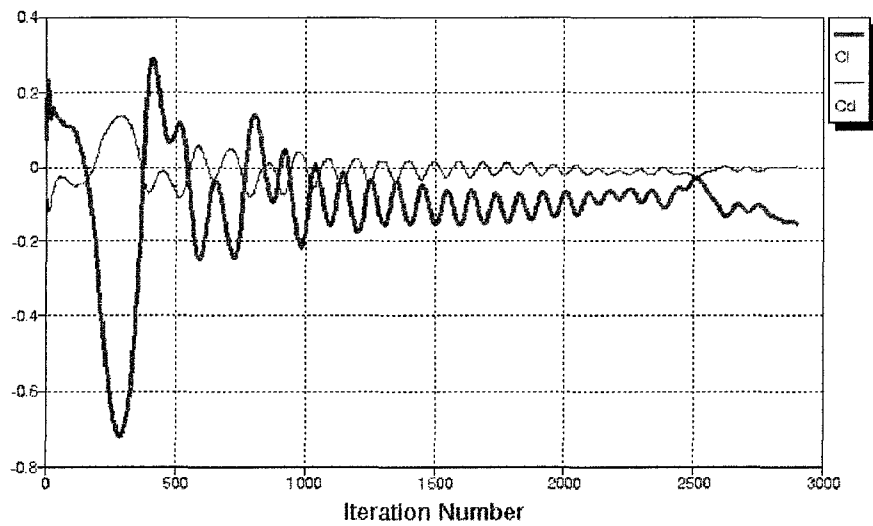
NACA0070 - Navier-Stokes Grid 50x40
AOA = 5 degrees



(c)

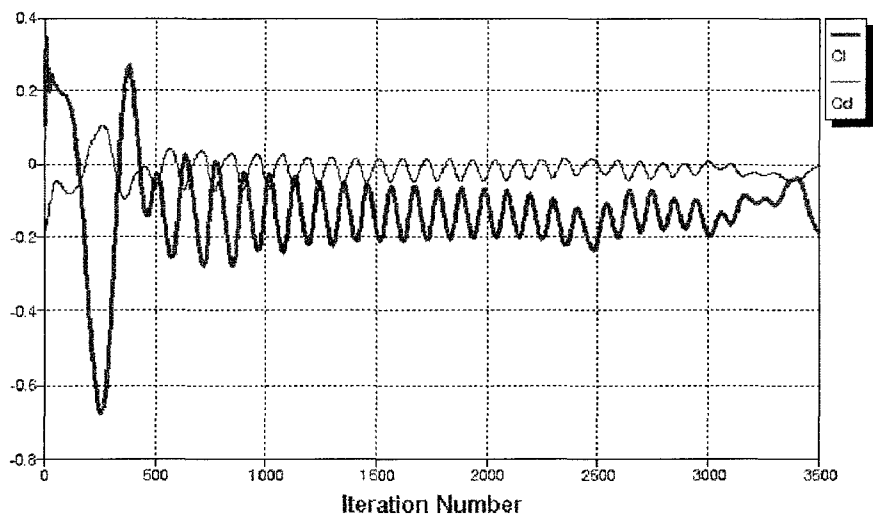
Figure 23 (continued). NACA0070 Viscous Solution -
Coefficients of Lift & Drag vs. Iteration Number Plots
(b) AOA = 0°, 4000-9000 Iterations (c) AOA = 5°

NACA0070 - Navier-Stokes Grid 50x40
AOA = 10 degrees



(d)

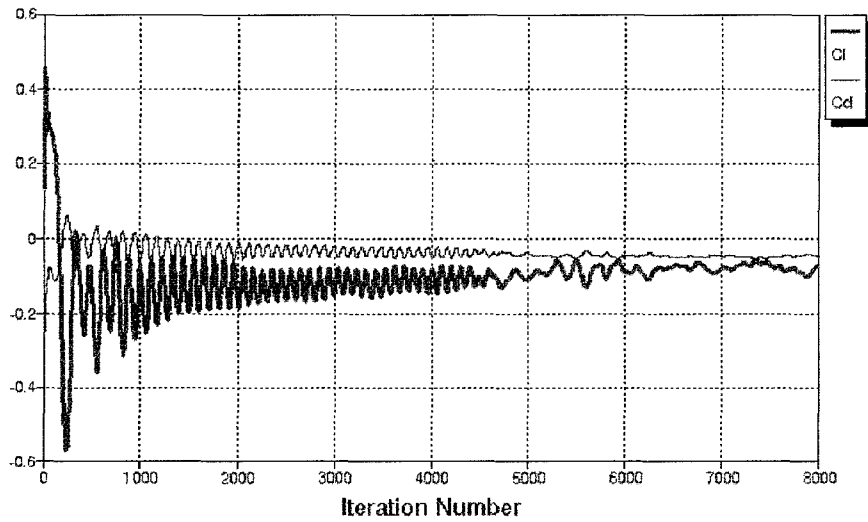
NACA0070 - Navier-Stokes Grid 50x40
AOA = 15 degrees



(e)

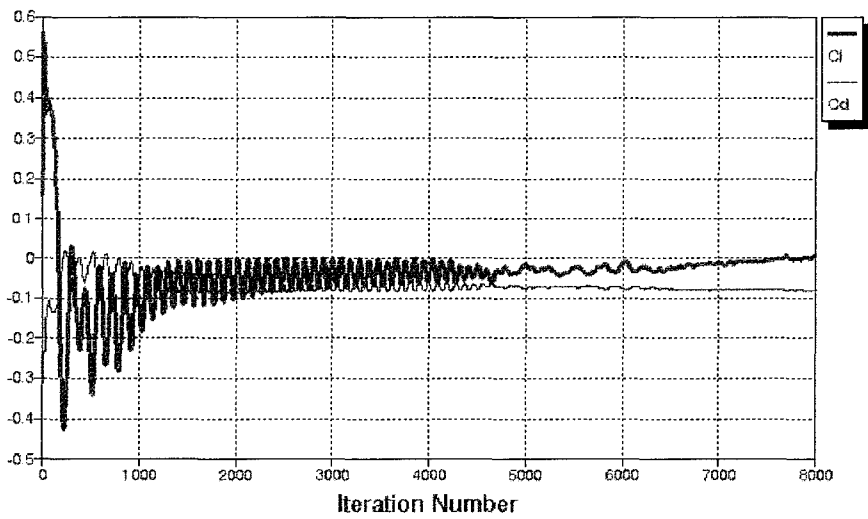
Figure 23 (continued). NACA0070 Viscous Solution -
Coefficients of Lift & Drag vs. Iteration Number Plots
(d) AOA = 10° (e) AOA = 15°

NACA0070 - Navier-Stokes Grid 50x40
AOA = 20 degrees



(f)

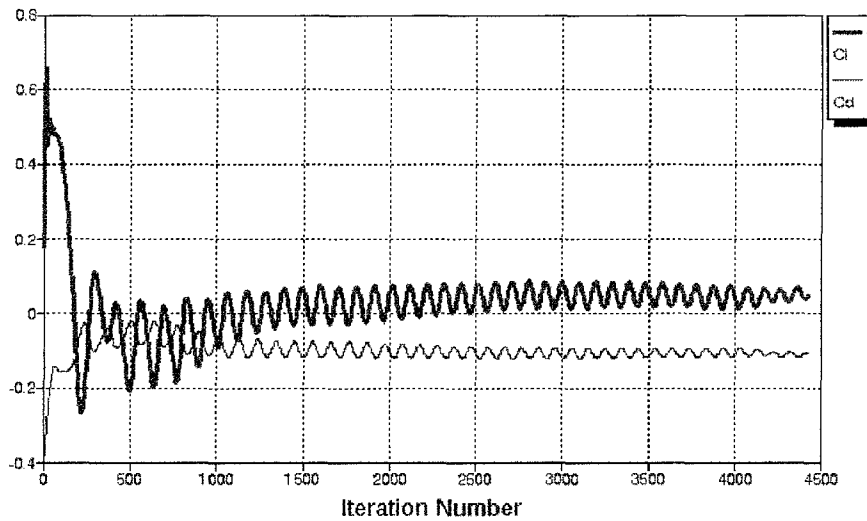
NACA0070 - Navier-Stokes Grid 50x40
AOA = 25 degrees



(g)

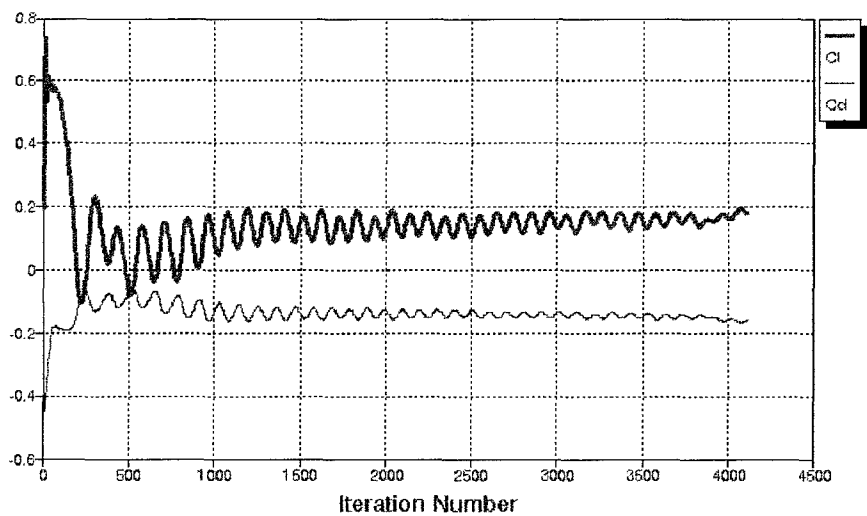
Figure 23 (continued). NACA0070 Viscous Solution -
Coefficients of Lift & Drag vs. Iteration Number Plots
(f) AOA = 20° (g) AOA = 25°

NACA0070 - Navier-Stokes Grid 50x40
AOA = 30 degrees



(h)

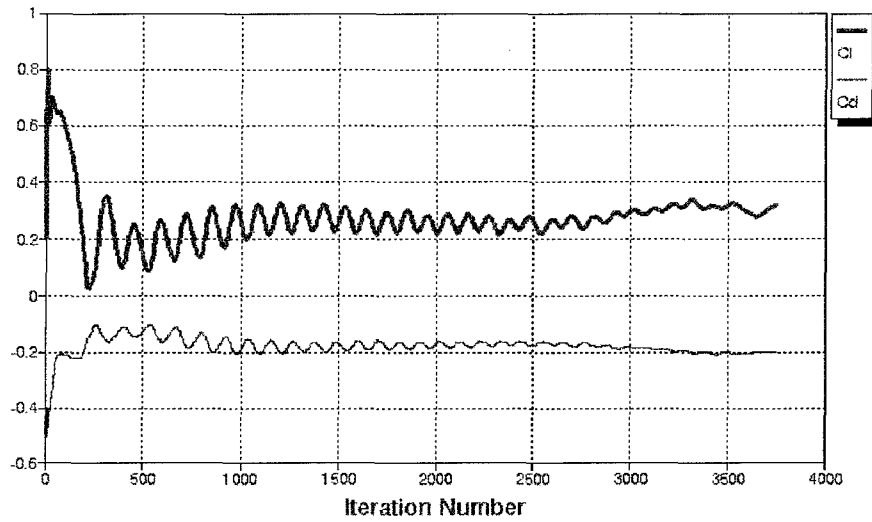
NACA0070 - Navier-Stokes Grid 50x40
AOA = 35 degrees



(i)

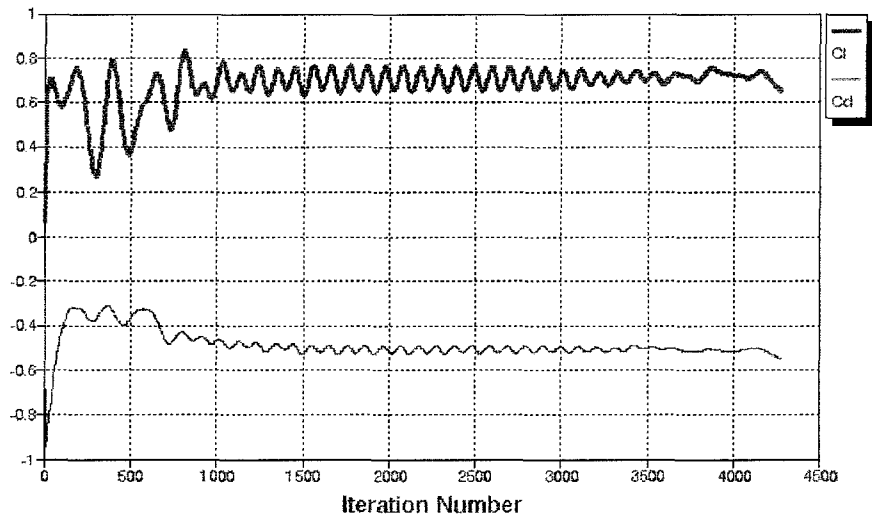
Figure 23 (continued). NACA0070 Viscous Solution -
Coefficients of Lift & Drag vs. Iteration Number Plots
(h) AOA = 30° (i) AOA = 35°

NACA0070 - Navier-Stokes Grid 50x40
AOA = 40 degrees



(j)

NACA0070 - Navier-Stokes Grid 50x40
AOA = 80 degrees



(k)

Figure 23 (continued). NACA0070 Viscous Solution -
Coefficients of Lift & Drag vs. Iteration Number Plots
(j) AOA = 40° (k) AOA = 80°

For each α , the oscillations seem to reach a steady average at approximately half of the total iterations. The ranges of c_ℓ and c_d also seem to remain consistent after these amounts. Notably, c_d does not vary as much as c_ℓ for a given α , and the overall trends in these values with respect to angle of attack can be seen in Figure 24.

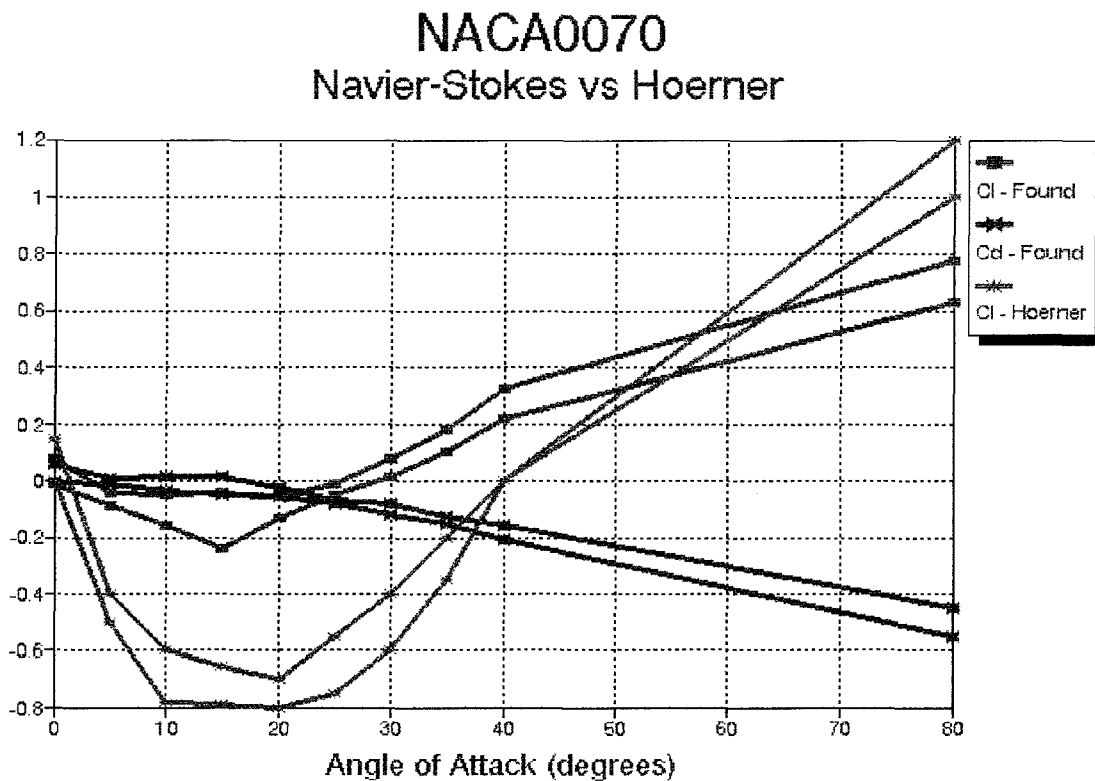


Figure 24. NACA0070 Calculated vs. Test Results

The ranges of c_ℓ and c_d from the ENS3DAE output is plotted versus Hoerner's test data for c_ℓ . The red lines with square data point markers bound the calculated coefficient of lift plots, while the blue line with "x" markers bound the minimum and maximum calculated drag coefficients. The Hoerner test data (Ref. 9) is shown by the green lines with

asterisks for markers. The output from this study matches the predicted trends of negative lift at small α and positive increasing lift after a certain α . Also, in both the predicted and calculated plots, there is an increase in the oscillating range as the average c_l for a specific α deviates from $c_l = 0$. Also, since the calculated lift and drag forces plotted in Figure 24 are as defined by Figure 5, with Hoerner's test data being based on the conventional definitions of lift and drag, the following relationship holds.

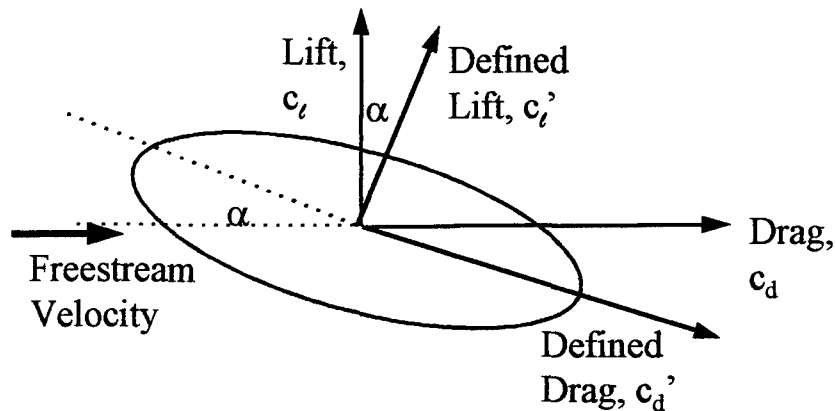


Figure 25. Relationship Between Conventional and Defined Lift and Drag Vectors

This geometry shown in Figure 25 yields

$$c_l = c_l' \cos \alpha - c_d' \cos(90^\circ - \alpha)$$

$$c_d = c_l' \cos(90^\circ - \alpha) + c_d' \cos \alpha$$

Therefore, by converting the calculated lift and drag coefficients to the conventional reference frame for lift and drag, the results become the curves shown in Figure 26.

NACA0070 - Navier-Stokes vs. Hoerner All Vectors Converted to Conventional

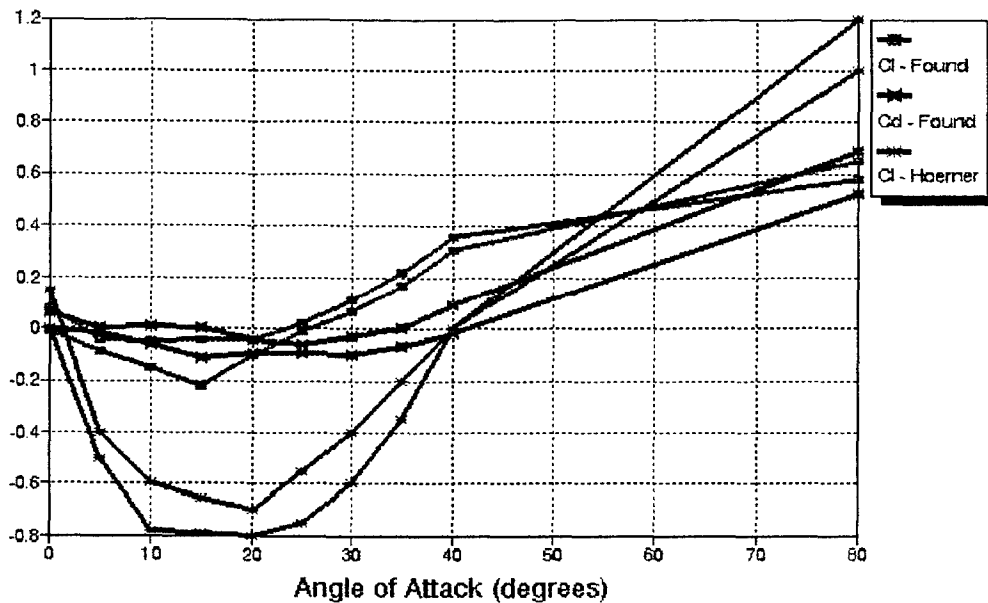


Figure 26. NACA0070 Calculated vs. Test Results in Conventional Vector Frame

The discrepancy in numerical values for c_l is due to Hoerner's test data being taken from a water tunnel test. Furthermore, no Mach number is specified in these tests, the only indicated value is that the Reynolds number is above the critical Reynolds number of 6×10^5 . To try to verify the test data, the Reynolds number for the calculated c_l was above this critical limit as well. Since the conditions of Hoerner's test could not be found, a conversion from the water tunnel output data to the viscous air flow computer results could not be made. However, the similar trend in c_l curve shapes is encouraging.

Refueling envelope

The next step in analyzing the NACA0070 cross-sectional boom shape was to find the possible refueling envelope size. This was accomplished by comparing the drag vs. Mach number relationship for each cross-section shape. These relationships are shown in Figure 27.

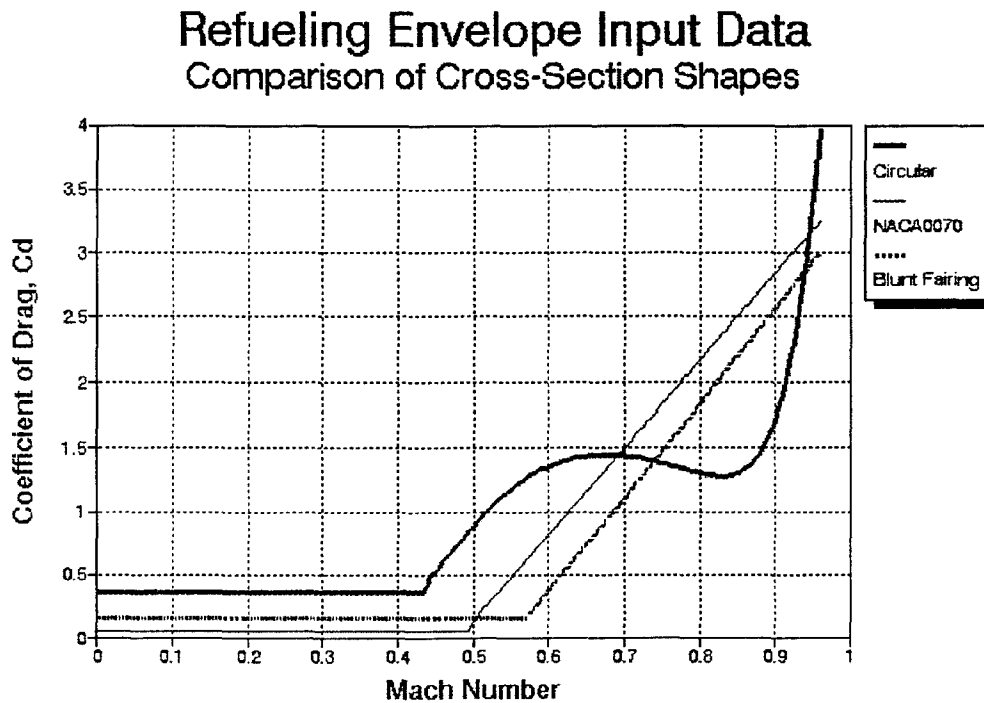


Figure 27. Coefficient of Drag vs. Mach Number Plots (Ref. 16)

In Figure 28, the flyable envelope for the current KC-135 boom cross-section (a circular cylinder), and the NACA0070 are compared.

KC-135 Flyable Envelope
Circular vs. NACA0070 Cross-Section
with All Limits

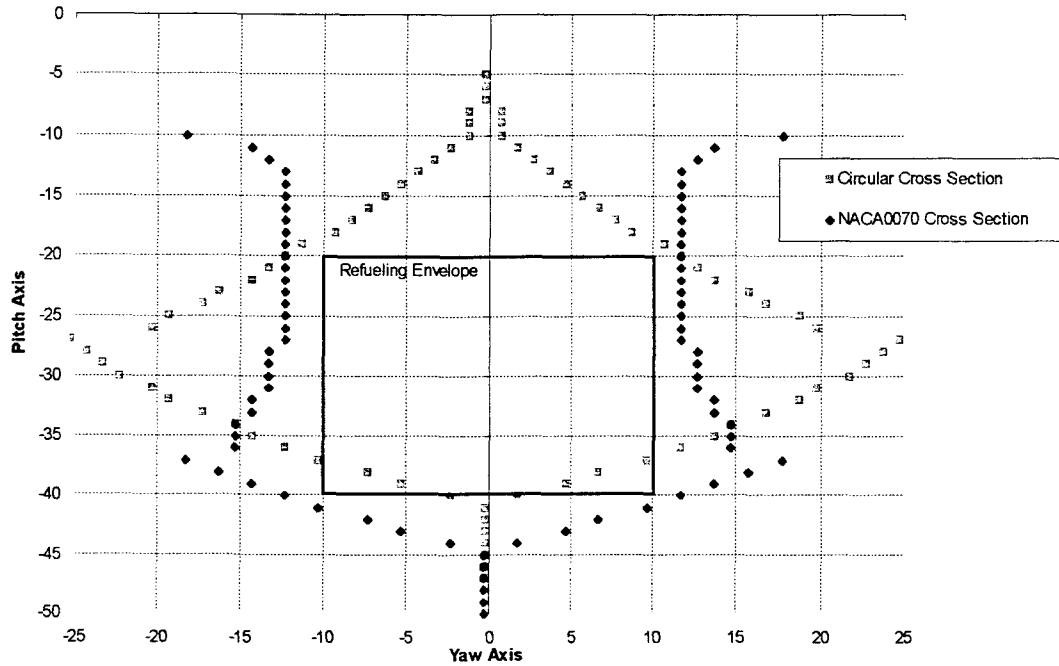


Figure 28. NACA0070 & Circular Flyable Envelopes

In Figure 28, the maximum angles for a boom with all the movement restrictions are found. Then, the limits are removed and the results on the flyable envelope are shown in Figure 29.

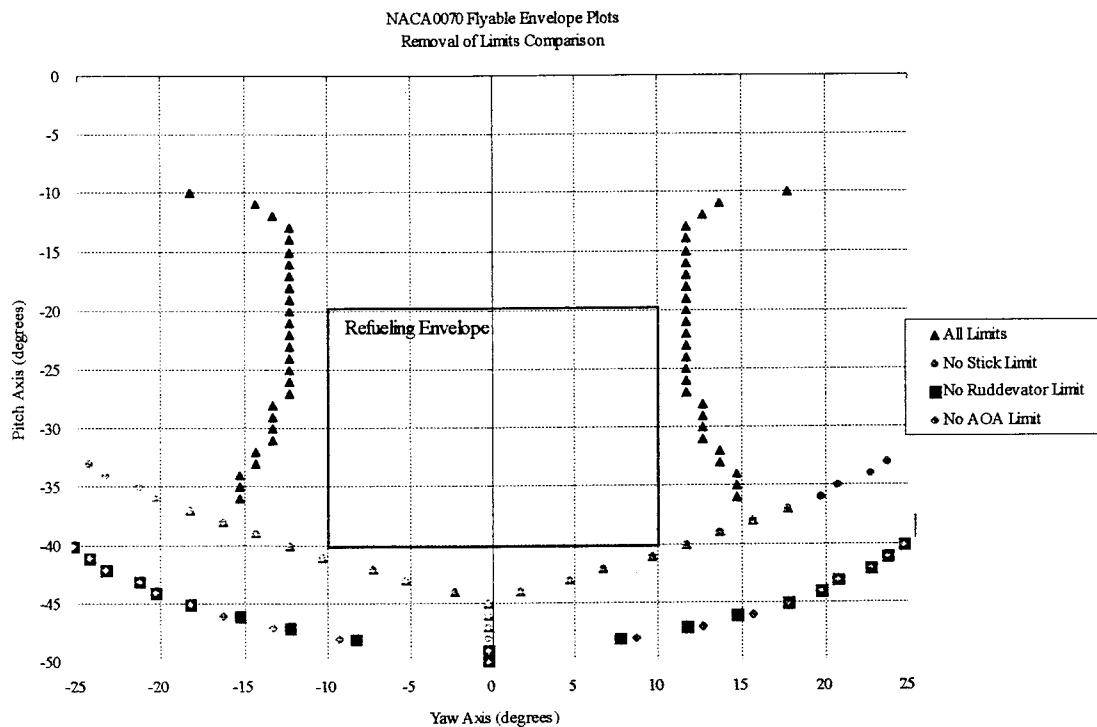
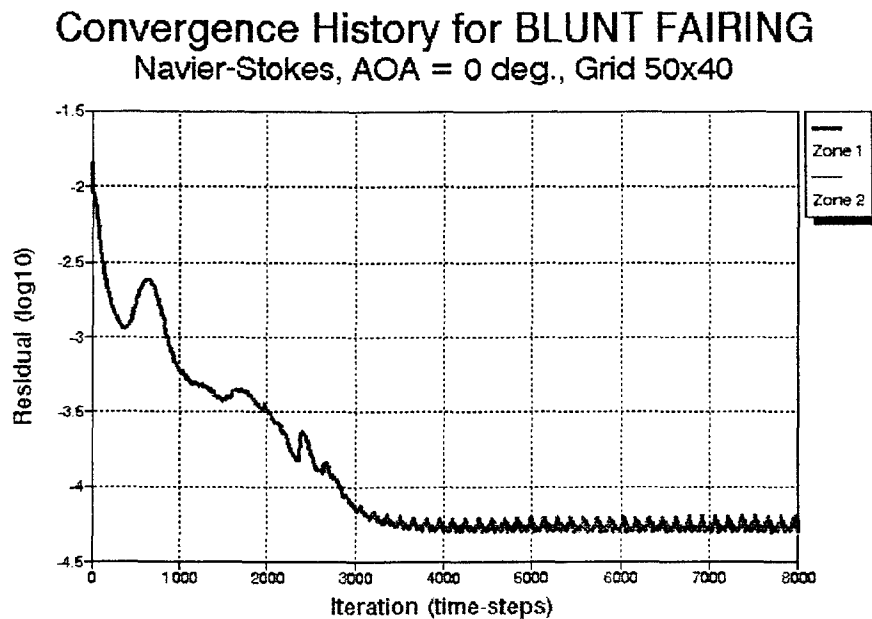


Figure 29. NACA0070 Flyable Envelope Plots

First, the stick limit was removed and the maximum angles were recalculated. This created a larger possible envelope, especially in the ψ rotation, and fully removed the maximum angle limitations from the current refueling envelope. The removal of the stick and rudder limits increased the refueling envelope size even more, this time mostly affecting the θ angle. Eliminating the angle of attack limit also further increased the possible envelope, but it was a minimal improvement from the removal of the rudder limit. Also, since the design changes necessary to remove the angle of attack limit are very complex, this modification is not justified. Therefore, the best improvements to the envelope size are an additional 5° for θ and ψ or an additional 10° in ψ and none in θ .

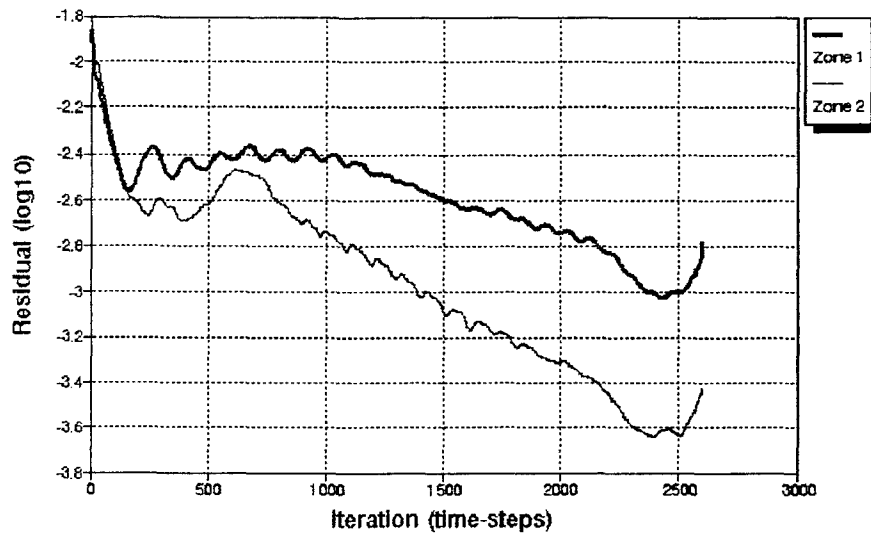
Since the NACA0070 shape gave some favorable results, a similar thick, blunt airfoil shape was investigated for comparable properties. The blunt fairing was chosen due to its similarity to the NACA0070 coefficient of drag versus Mach profile. By only changing the airfoil shape, using the same grid size and spacing, and using the same input data, the viscous flow results were acceptable when the convergence histories were considered, see Figure 30.



(a)

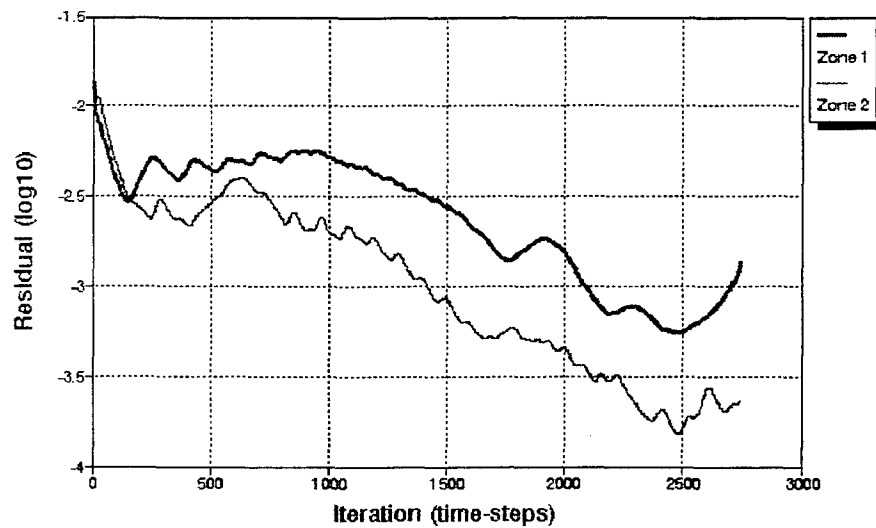
Figure 30. Blunt Fairing - Convergence Histories
(a) AOA = 0°

Convergence History for BLUNT FAIRING Navier-Stokes, AOA = 10 deg, Grid 50x40



(b)

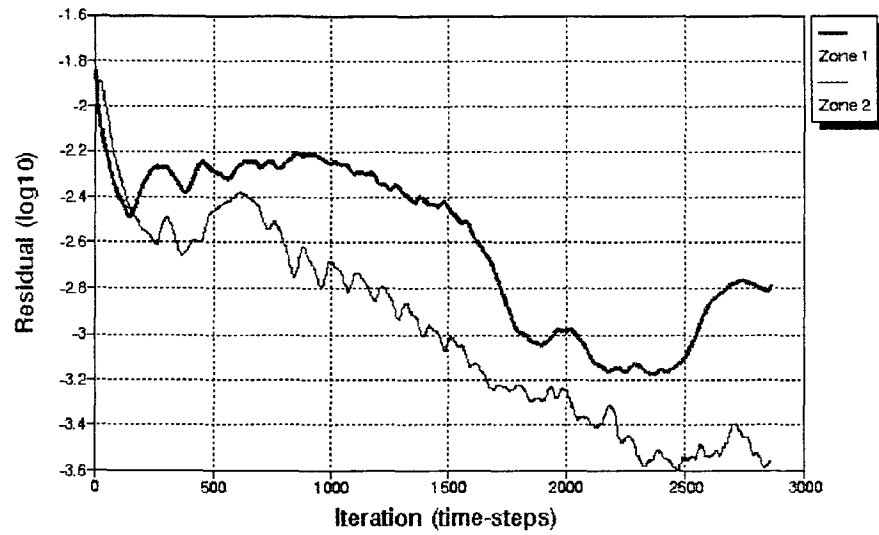
Convergence History for BLUNT FAIRING Navier-Stokes, AOA = 20 deg, Grid 50x40



(c)

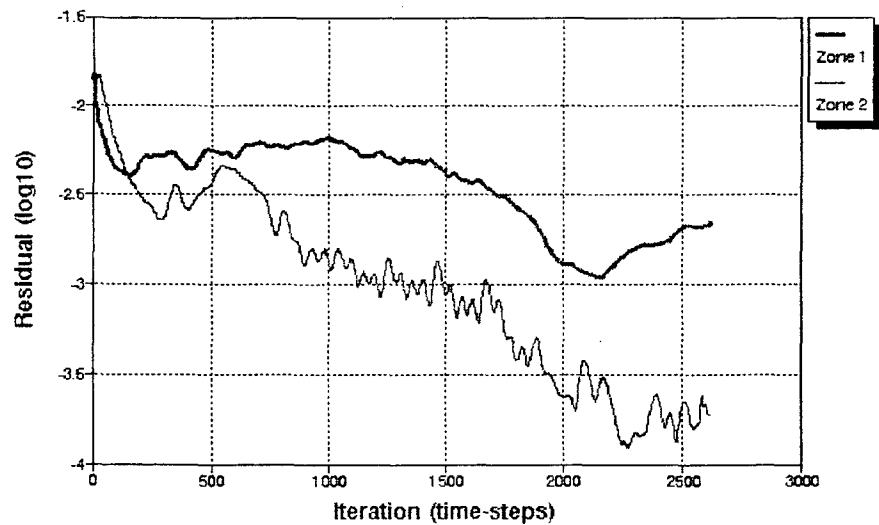
Figure 30 (continued). Blunt Fairing - Convergence Histories
(b) AOA = 10° (c) AOA = 20°

Convergence History for BLUNT FAIRING Navier-Stokes, AOA = 30 deg, Grid 50x40



(d)

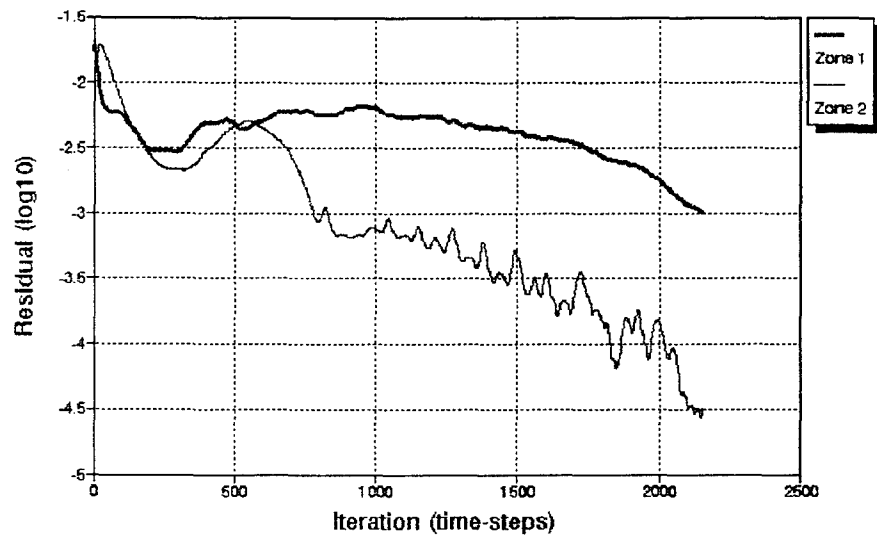
Convergence History for BLUNT FAIRING Navier-Stokes, AOA = 40 deg, Grid 50x40



(e)

Figure 30 (continued). Blunt Fairing - Convergence Histories
(d) AOA = 30° (e) AOA = 40°

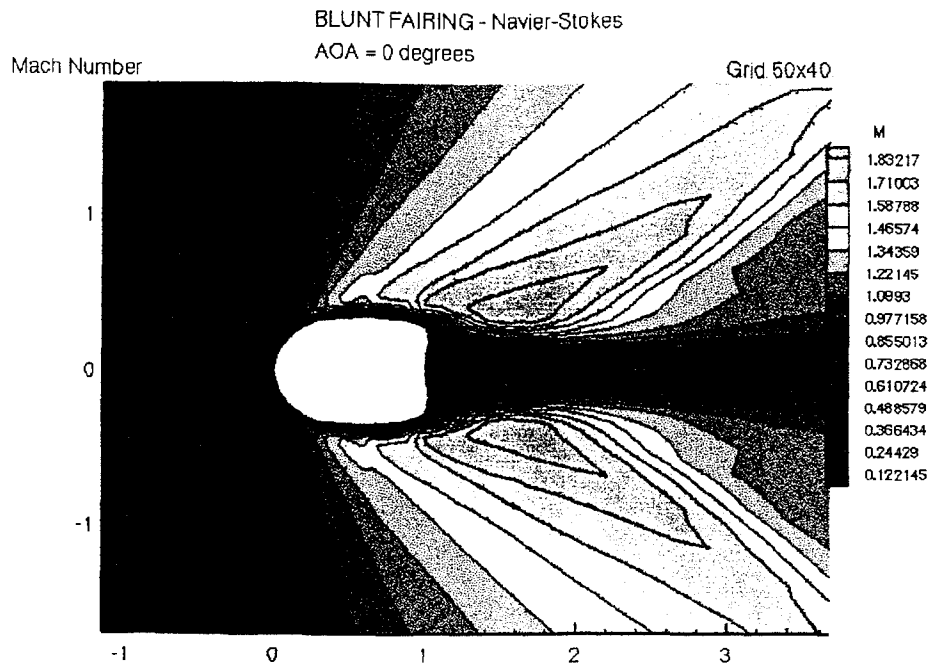
Convergence History for BLUNT FAIRING Navier-Stokes, AOA = 80 deg, Grid 50x40



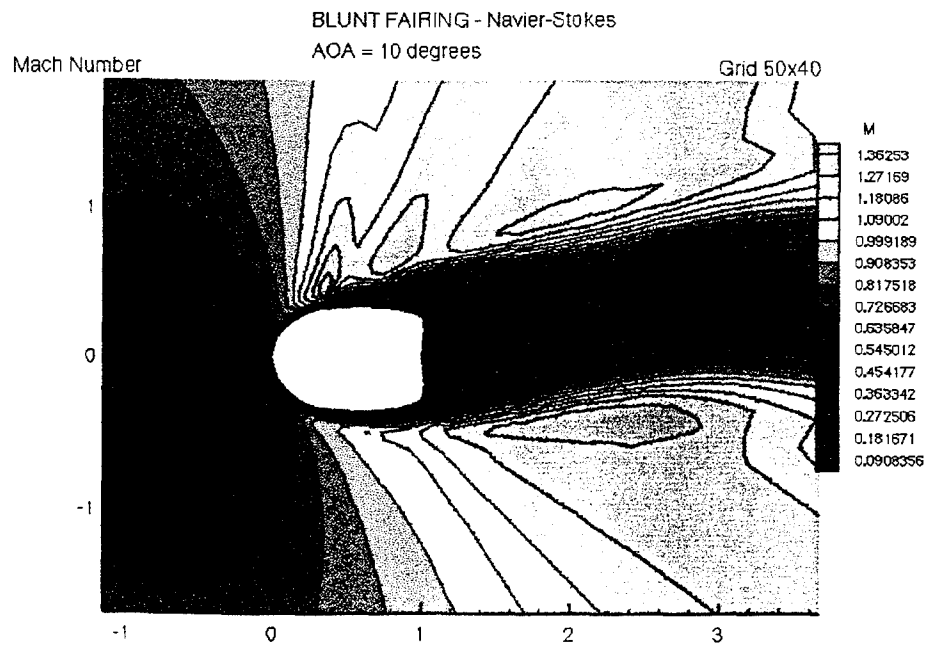
(f)

Figure 30 (continued). Blunt Fairing - Convergence Histories
(f) AOA = 80°

The residual once again decreased to an oscillatory wave, and zone 1 had a higher residual than zone 2 as angle of attack is increased. An analysis of the Mach contour plots in Figure 31 shows the same characteristic of separated flow behind a shock wave.

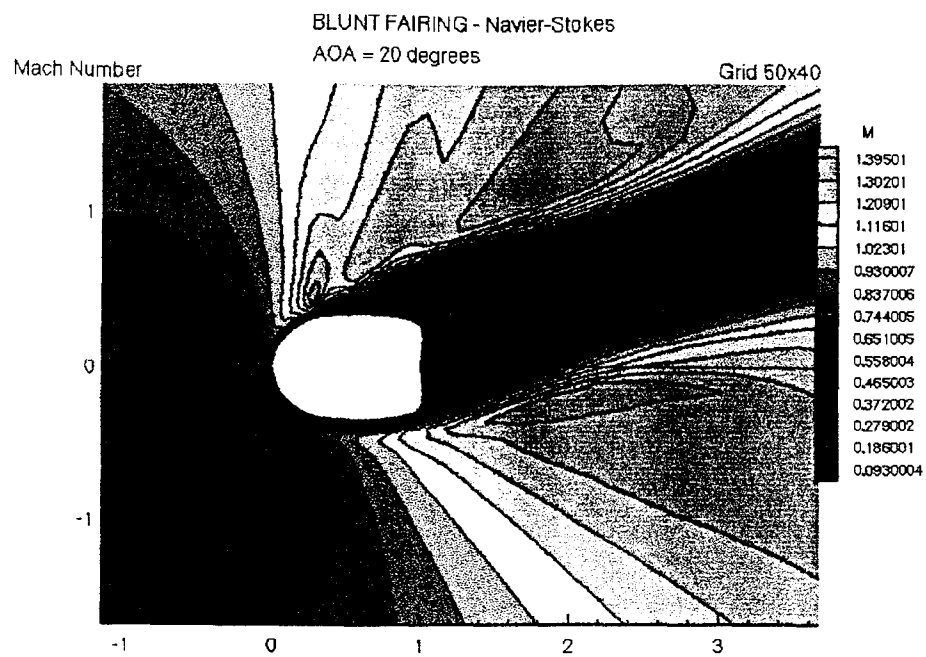


(a)

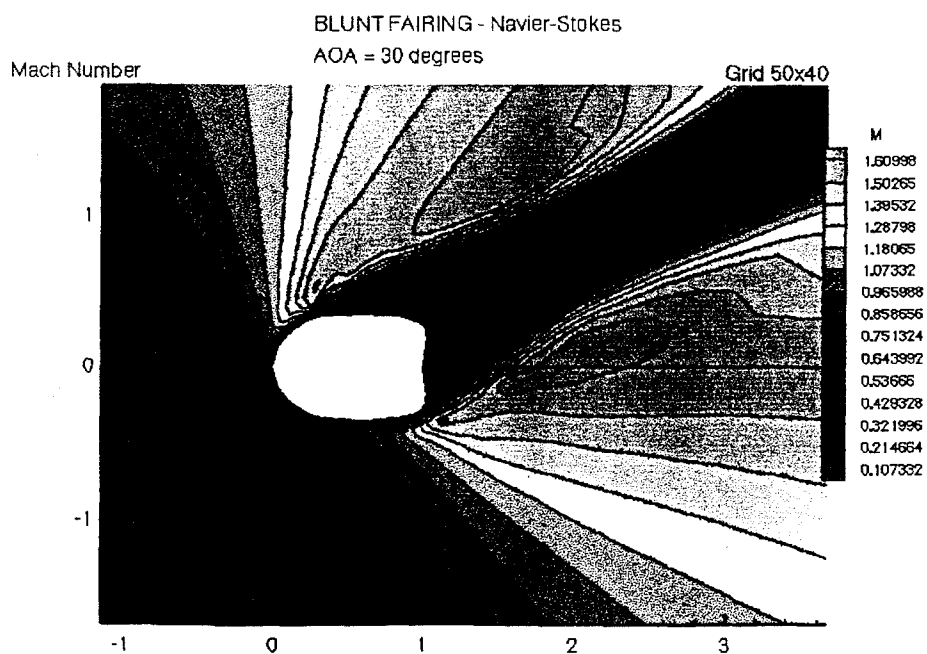


(b)

Figure 31. Blunt Fairing - Mach Contour Plots
(a) AOA = 0° (b) AOA = 10°

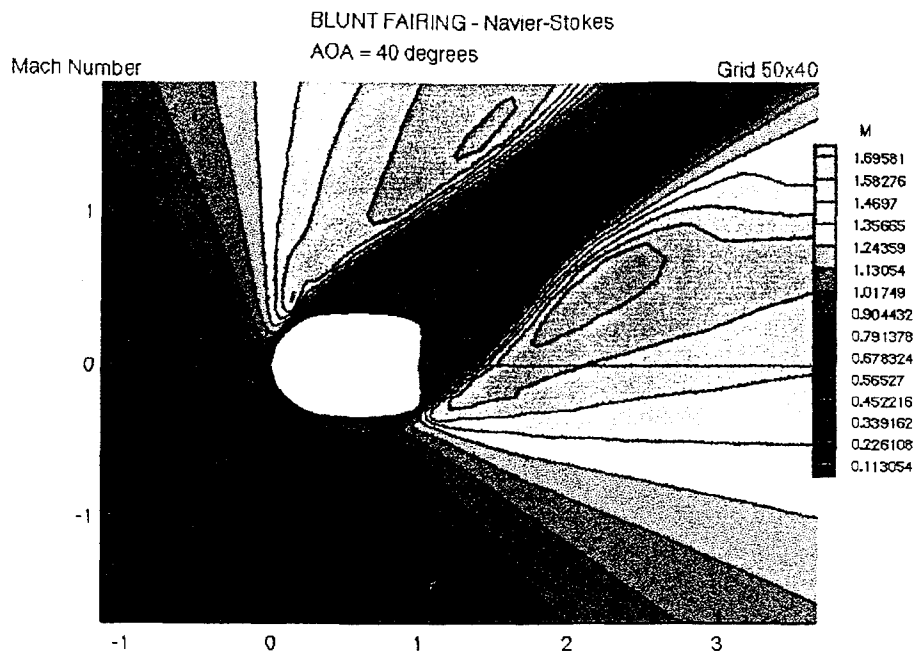


(c)

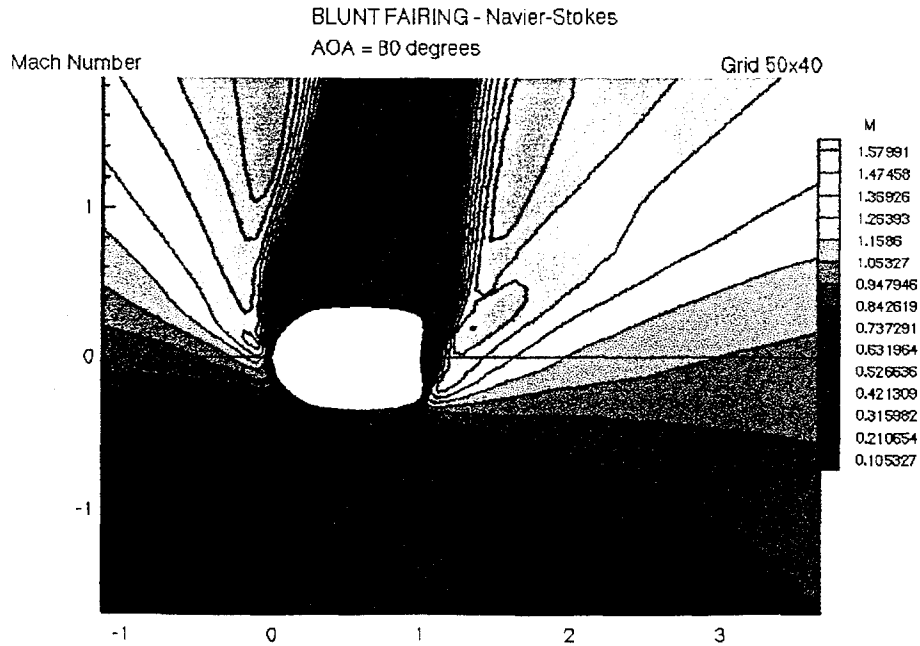


(d)

Figure 31 (continued). Blunt Fairing - Mach Contour Plots
(c) AOA = 20° (d) AOA = 30°



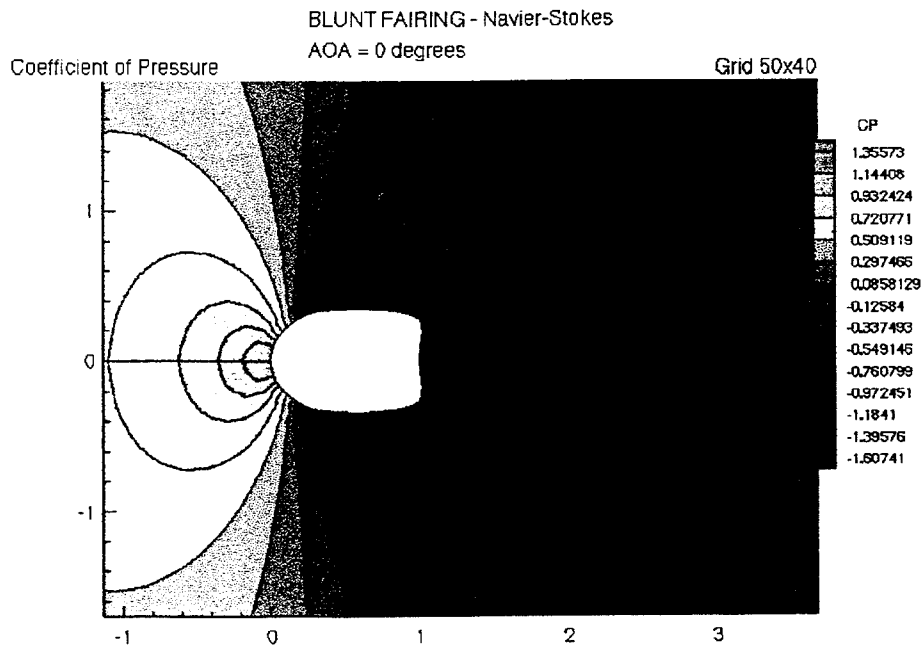
(e)



(f)

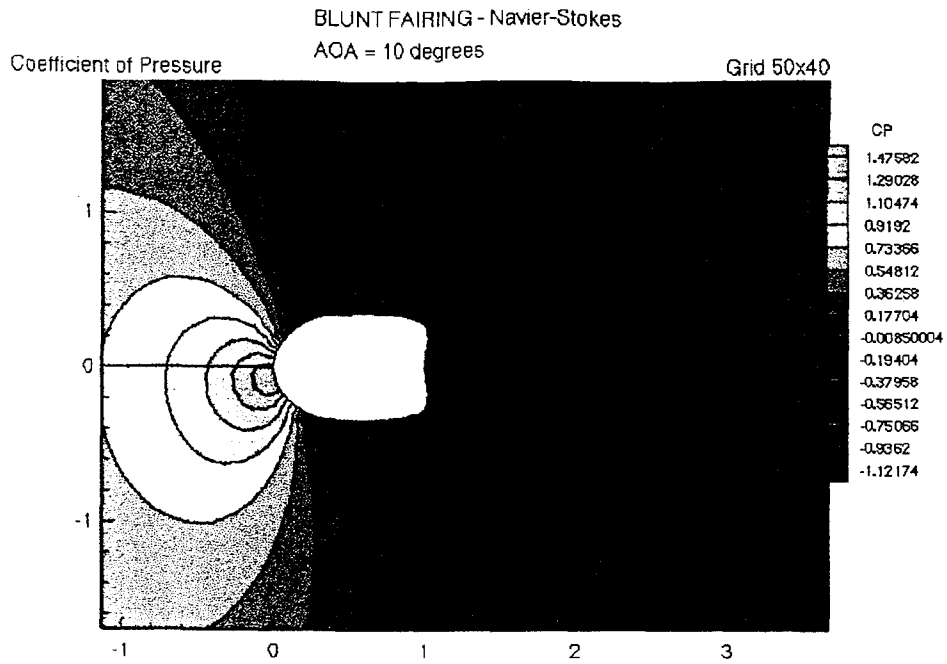
Figure 31 (continued). Blunt Fairing - Mach Contour Plots
e) AOA = 40° (f) AOA = 80°

However, the surface shape does not lend itself to the same strength of attached flow along the zone 2 boundary. Therefore, the coefficient of pressure contours, shown in Figure 32, display a negative pressure in the vortex flow, but along the surface, the strongest attached flow is along the top curved surface of the nose, thus creating positive lift.

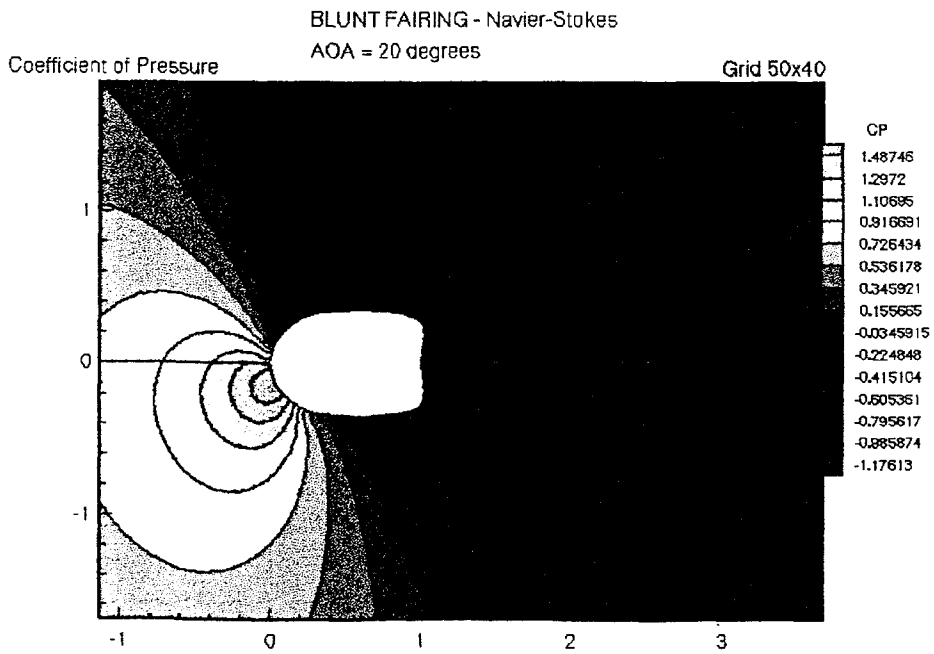


(a)

Figure 32. Blunt Fairing - Coefficient of Pressure Contour Plots
(a) AOA = 0°

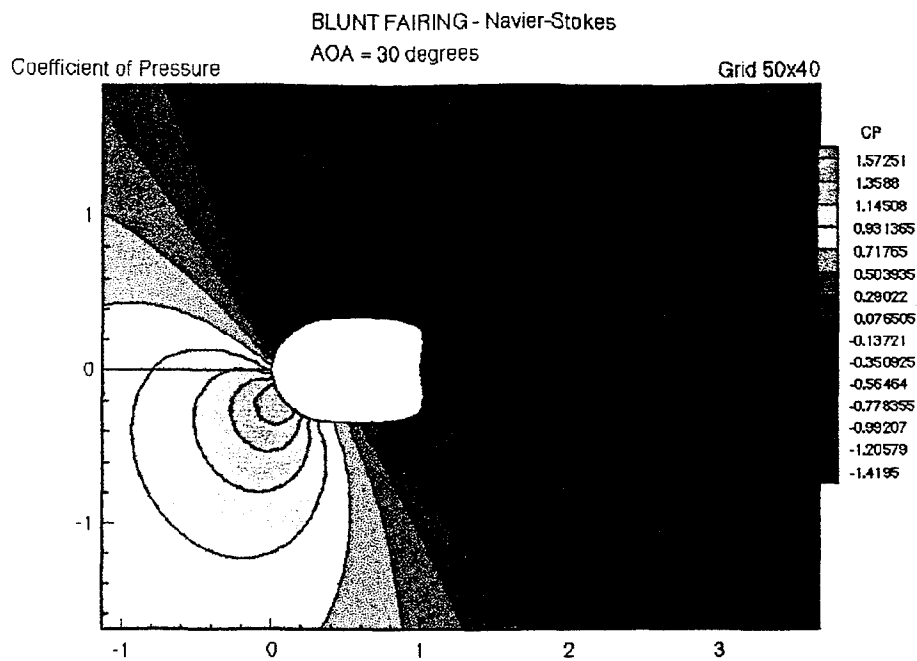


(b)

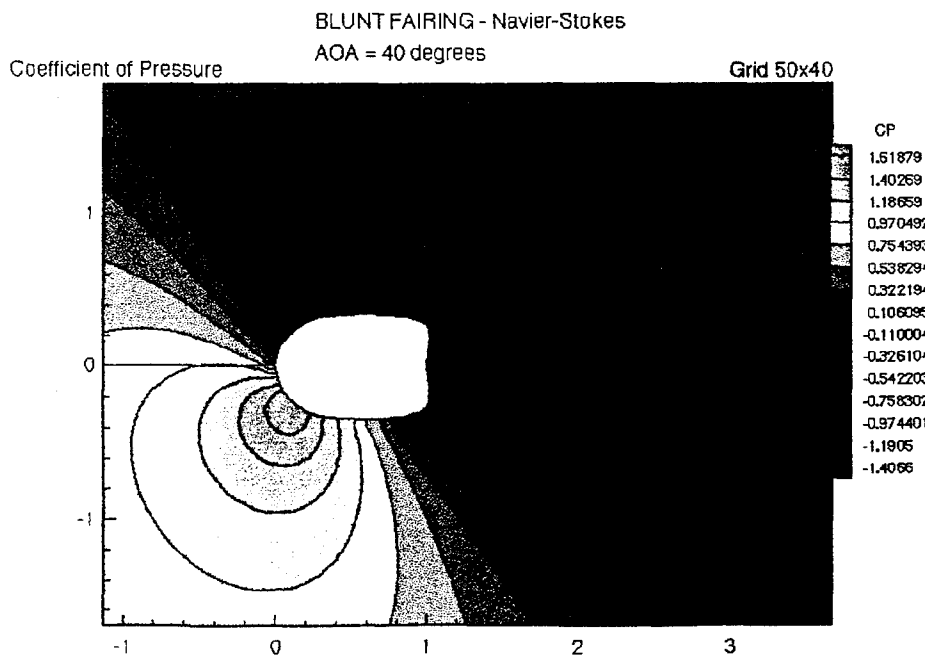


(c)

Figure 32 (continued). Blunt Fairing - Coefficient of Pressure Contour Plots
(b)AOA = 10° (c) AOA = 20°

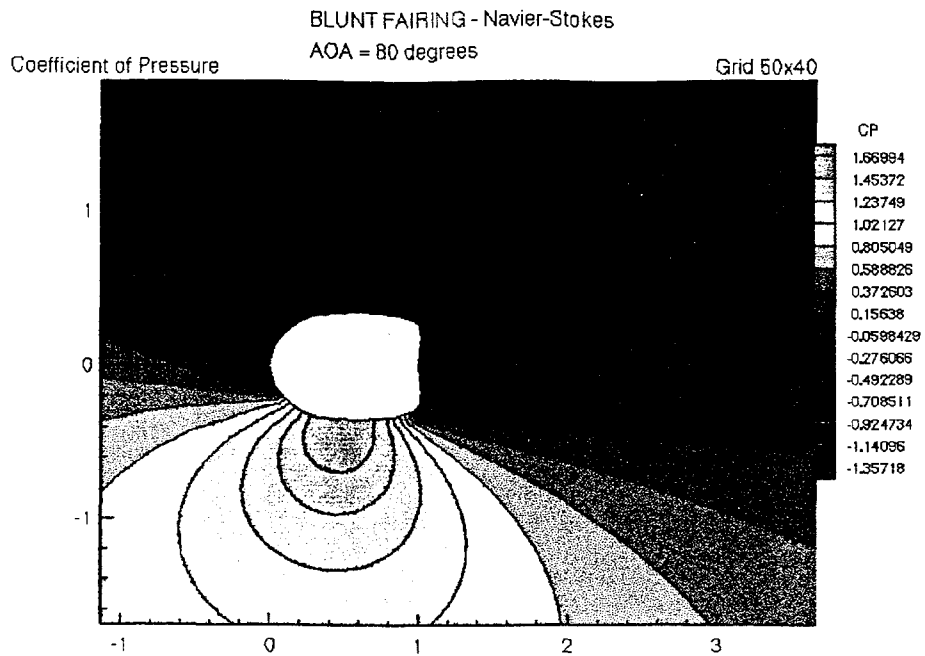


(d)



(e)

Figure 32 (continued). Blunt Fairing - Coefficient of Pressure Contour Plots
(d) AOA = 30° (e) AOA = 40°

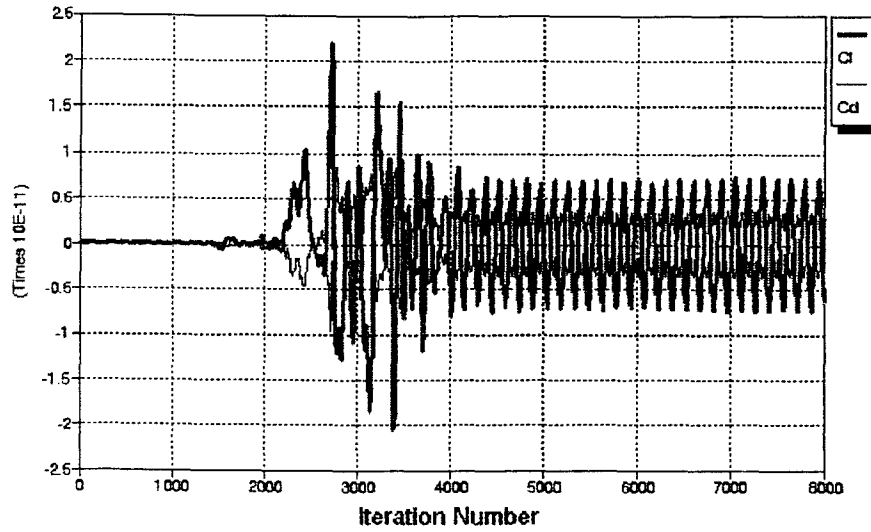


(f)

Figure 32 (continued). Blunt Fairing - Coefficient of Pressure Contour Plots
(f) AOA = 80°

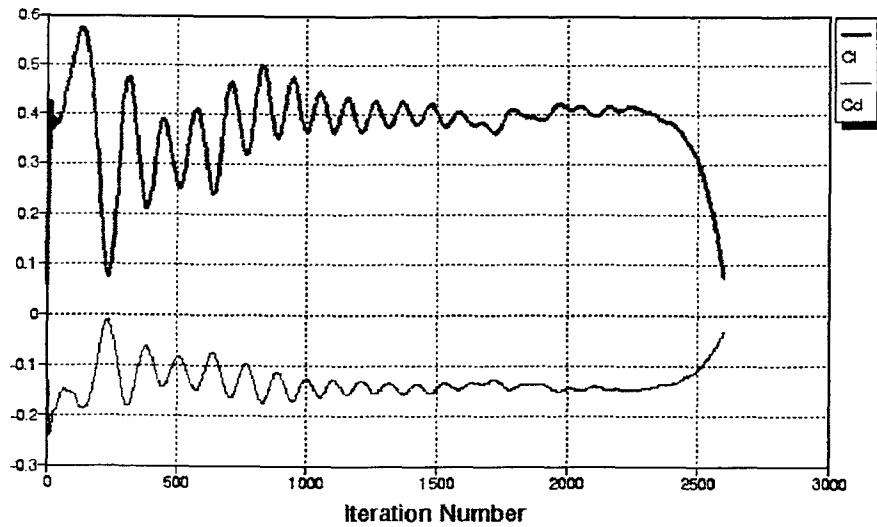
When the coefficients of lift and drag are plotted versus iteration number, as in Figure 33, the time dependent oscillations showing unsteady separated flow are present.

BLUNT FAIRING - Navier-Stokes
AOA = 0 degrees, Grid 50x40



(a)

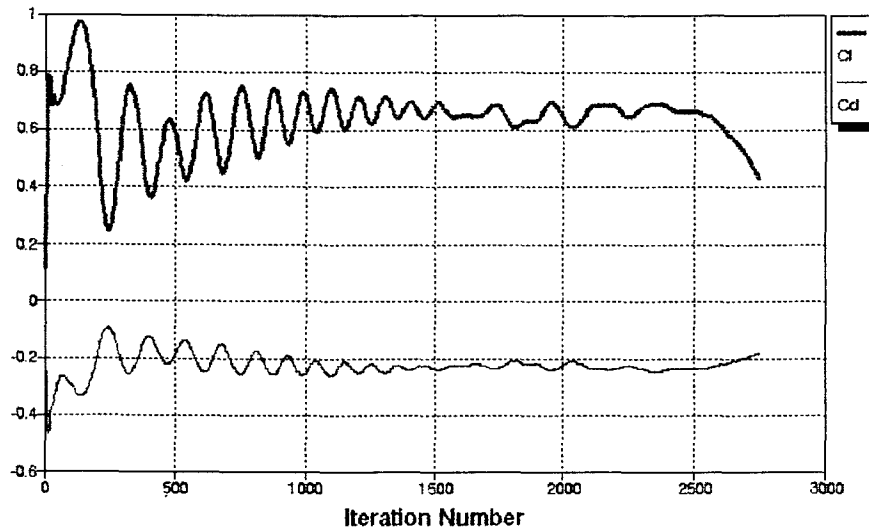
BLUNT FAIRING - Navier-Stokes
AOA = 10 degrees, Grid 50x40



(b)

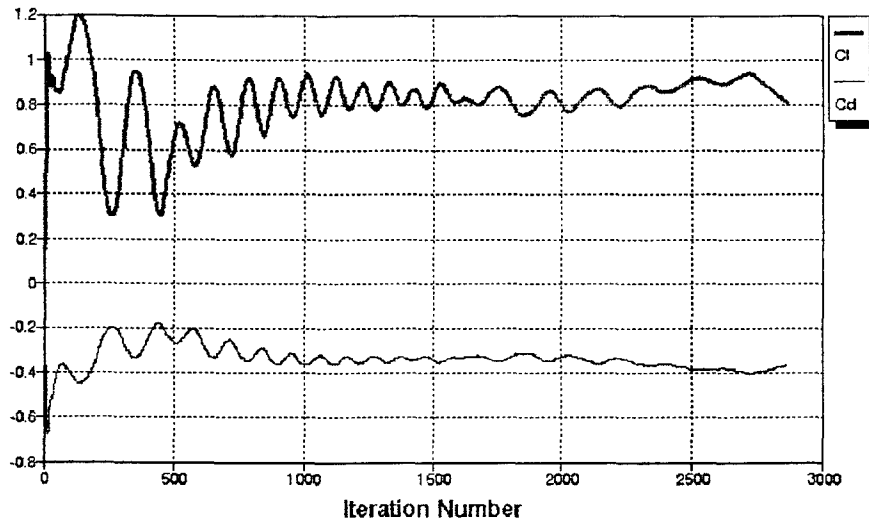
Figure 33. Blunt Fairing -
Coefficient of Lift & Drag vs. Iteration Number Plots
(a) AOA = 0° (b) AOA = 10°

BLUNT FAIRING - Navier-Stokes
AOA = 20 degrees, Grid 50x40



(c)

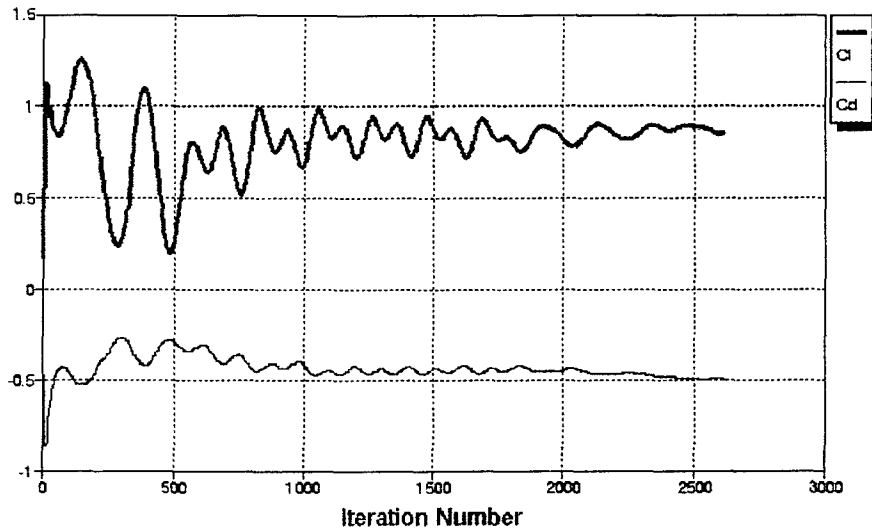
BLUNT FAIRING - Navier-Stokes
AOA = 30 degrees, Grid 50x40



(d)

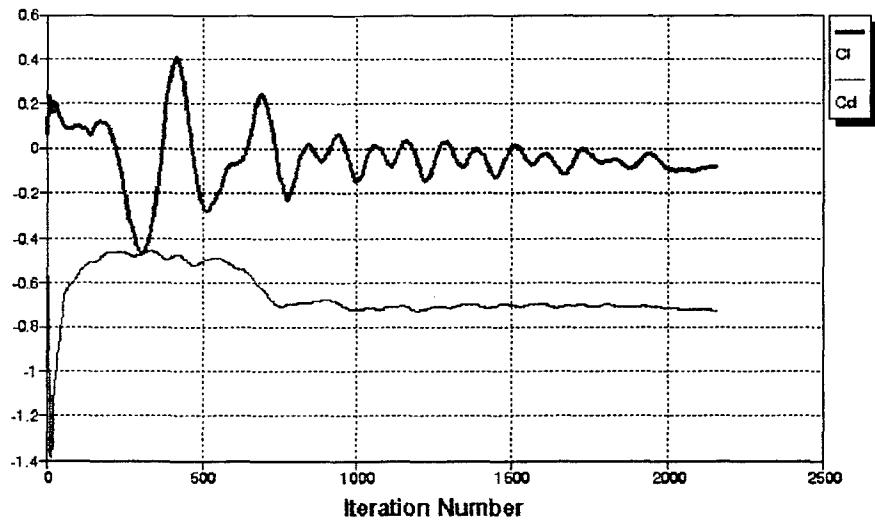
Figure 33 (continued). Blunt Fairing -
Coefficient of Lift & Drag vs. Iteration Number Plots
(c) AOA = 20° (d) AOA = 30°

BLUNT FAIRING - Navier-Stokes
AOA = 40 degrees, Grid 50x40



(e)

BLUNT FAIRING - Navier-Stokes
AOA = 80 degrees, Grid 50x40



(f)

Figure 33 (continued). Blunt Fairing -
Coefficient of Lift & Drag vs. Iteration Number Plots
(e) AOA = 40° (f) AOA = 80°

The same characteristics as for the NACA0070 are present. The c_l oscillations are larger than those for c_d , and the range is larger far from $c_l=0$. The overall c_l and c_d plotted versus angles of attack are presented in Figure 34.

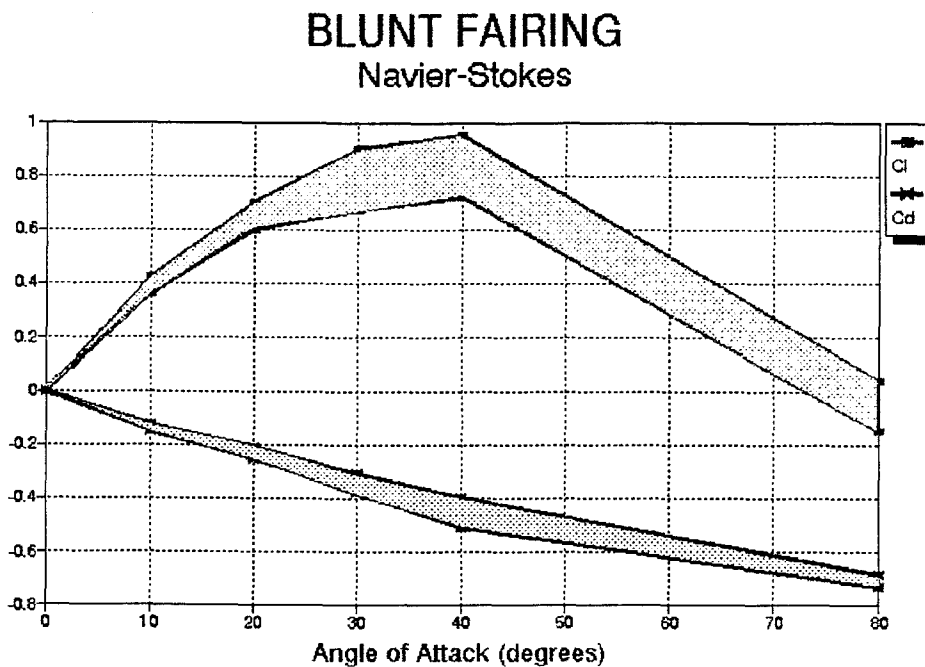


Figure 34. Blunt Fairing Calculated Results

Figure 34 once again uses the vector definitions as described in Figure 5. By using the same geometric relationships shown in Figure 25, the conventionally defined lift and drag curves are plotted in Figure 35.

BLUNT FAIRING - Navier-Stokes Conventional Vectors

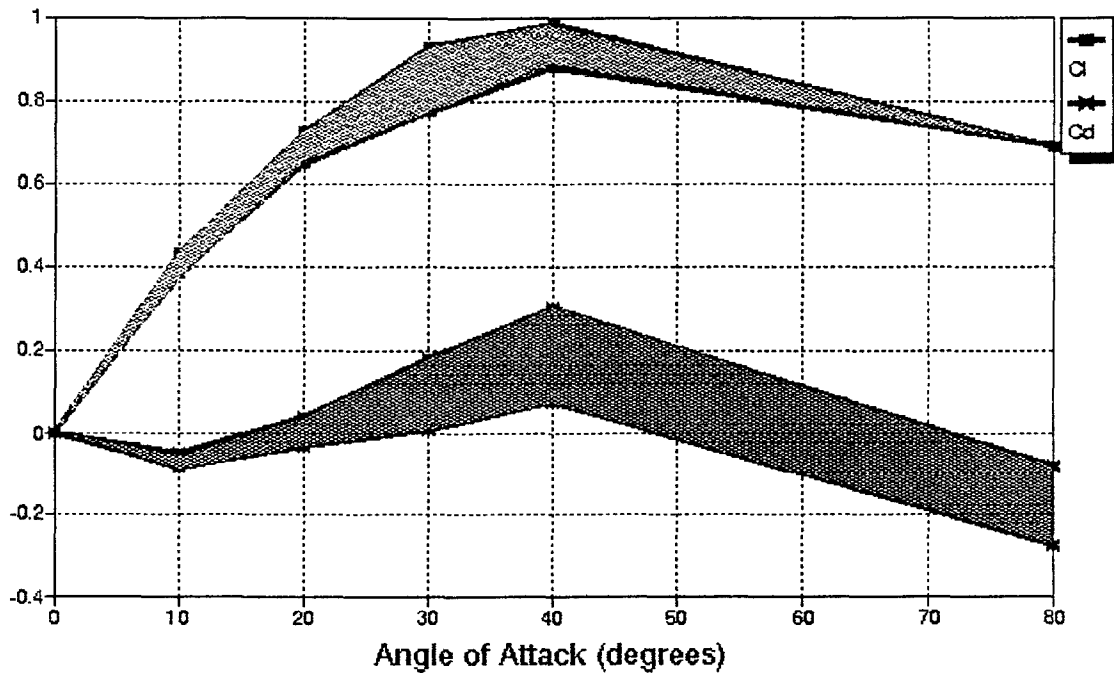


Figure 35. Blunt Fairing Calculated Results in Conventional Vector Frame

A band of possible values is available for each α , dependent on time and the nature of the separated vortex flow.

The blunt fairing also causes an increase in the refueling envelope when the drag versus Mach profile is input into the FORTRAN coding; the results are shown in Figure 36.

Blunt Fairing & NACA0070 Flyable Envelope Plots
All Limits

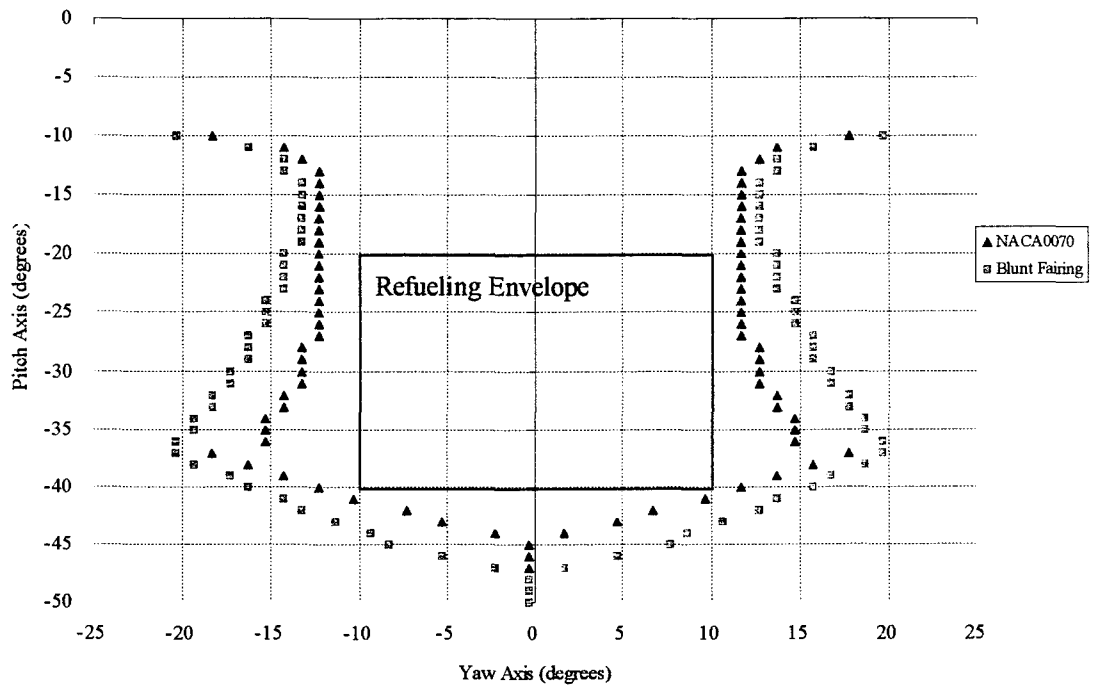


Figure 36. Blunt Fairing & NACA0070 Flyable Envelope Plots

When compared to the refueling envelopes produced by the NACA0070 cross-section, the blunt fairing is a better improvement to the boom structure. Figure 37 shows that, as with the NACA0070 cross section, the more limits that are removed, the larger the envelope size.

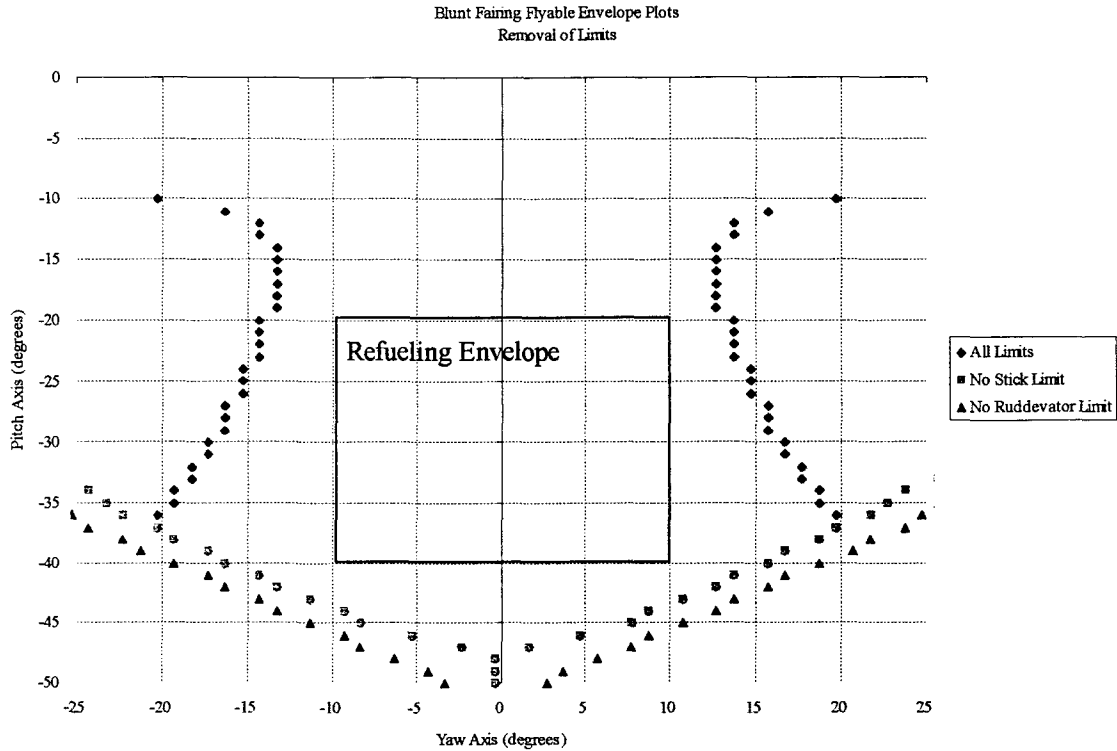
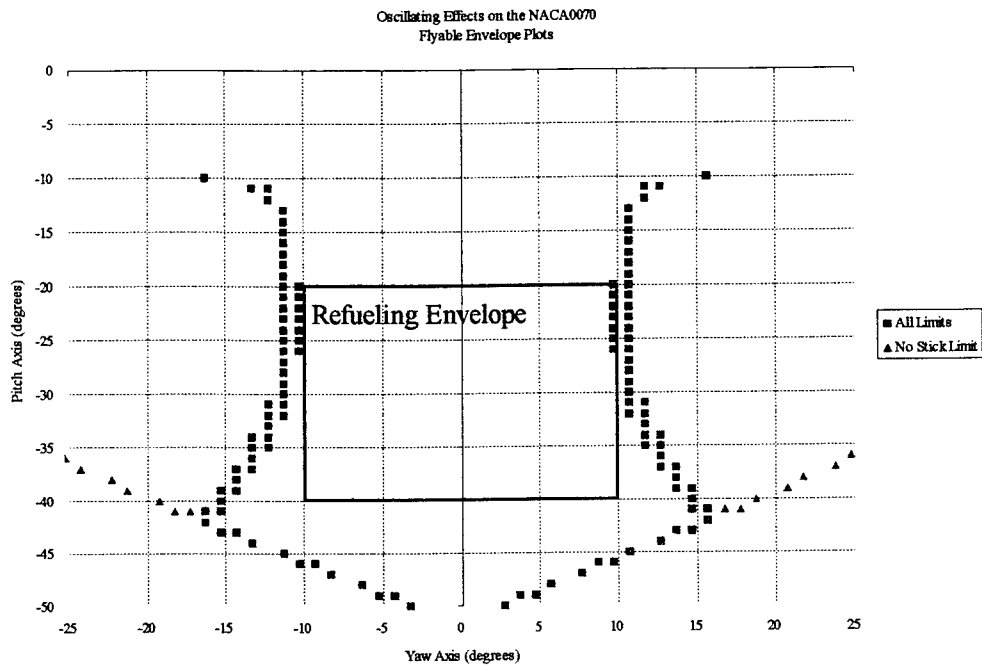


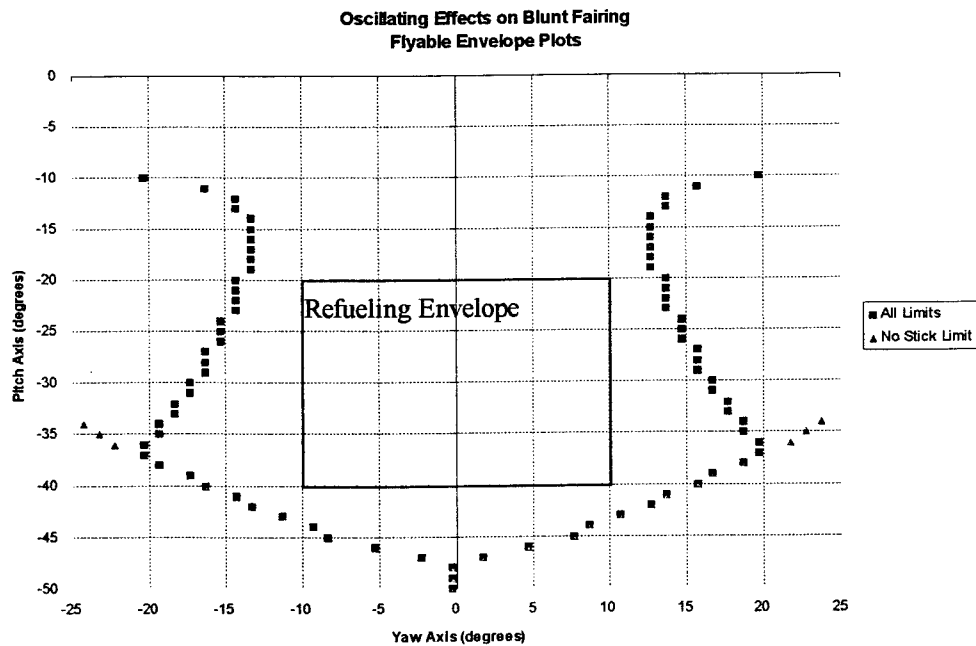
Figure 37. Blunt Fairing Flyable Envelope Plots

However, the most feasible limitation revisions are to the stick limit and the rudddevators. By redesigning the boom operator's control stick and increasing the rudddevator area by 20%, the flyable envelope marked by green triangles in Figure 37 is achieved. With this modification, the refueling envelope can be expanded by $\theta=3^\circ$ and $\psi=5^\circ$. This result is of practical significance since the current KC-135 refueling envelope is poorly designed due to the boom reaching its maximum angles within the envelope boundary (Ref. 16).

Another factor that needs to be considered is the effect of the oscillating coefficient values on the refueling envelope size. These effects are plotted in Figure 38.



(a)



(b)

Figure 38. Oscillating Effects on the Flyable Envelopes (a) NACA0070 (b) Blunt Fairing

By using the ENS3DAE drag coefficient output in the FORTRAN coding, an uncontrolled change in the refueling envelope occurs. On the NACA0070 cross-section, with all the limits intact, the maximum change is 1° , but with no stick limit present the boom can move as much as 3° without any operator input. However, for the blunt fairing cross-section there is no change in the envelope size due to oscillating drag since the time dependency at zero angle of attack produces a very narrow range. Thus, it can be seen that the amplitudes of the oscillations are what cause the envelope sizes to vary.

Oscillation Analysis

Since the oscillations do effect the refueling envelope parameters, a closer inspection of this phenomenon is warranted. By inspecting the NACA0070 coefficients of lift and drag with respect to the local time step (see Appendix B), the following relations were calculated (note that c_l and c_d always have the same frequency)

α (degrees)	c_l Amplitude	c_d Amplitude	Frequency (Hz)
0	0.011	0.005	0.43
5	0.025	0.0075	0.43
10	0.055	0.025	1.0
15	0.10	0.0325	1.0
20	0.035	0.015	0.63
25	0.02	0.0075	0.8
30	0.035	0.02	1.1
35	0.04	0.0125	1.05
40	0.055	0.025	1.0
80	0.075	0.05	0.8

Table 3. NACA0070 Frequency and Amplitude Tabulation

From this chart, it can be found that the average frequency of oscillation is 0.734 Hertz, which means the boom is expected to vibrate every 1.36 seconds. It is important to mention that at small angles of attack, i.e., $\alpha < 10^\circ$, the frequency of oscillation is considerably smaller, and therefore the boom operator can correct for this twisting about the yaw axis caused by unsteady flow.

A comparable analysis was conducted for the blunt fairing cross-section data (see Appendix C). The results are compiled as follows

α (degrees)	c_l Amplitude	c_d Amplitude	Frequency (Hz)
0	7.8×10^{-12}	3.8×10^{-12}	0.48
10	0.03	0.0125	0.67
20	0.05	0.02	0.56
30	0.113	0.035	0.44
40	0.115	0.055	0.5
80	0.095	0.02	0.64

Table 4. Blunt Fairing Frequency and Amplitude Tabulation

These computations show that the blunt fairing has an average oscillation frequency of 0.55 hertz, hence an expected movement every 1.8 seconds. This would appear to indicate that the blunt fairing cross-section corresponds to an easier to control boom cross-section, but the amplitudes of the oscillations are also a factor. The NACA0070 has a smaller range of oscillations in both the c_l and c_d , on average. Thus, there are drawbacks and advantages to both configurations depending on the desired aerodynamic characteristics. If the KC-135 root pivot is also modified to model the KC-10 rolling boom pivot, then the analysis becomes simpler as the only case that needs to be optimized is for a zero degree angle of attack cross-section. Another benefit of the blunt fairing cross-section is larger frequency, since the operator has an increased possibility of overcorrecting for the oscillation. Additionally, the receiving aircraft experiences a time delay between the boom movement and the effect on its flight pattern.

Furthermore, it is doubtful that the boom structure experiences any damaging fatigue or stress from oscillations as large as 1-2 seconds, so human error due to over-correction is the greatest determining factor for minimizing any desired performance discontinuities.

Conclusions

Through the use of a computer simulation model, the trends of Hoerner's test data for a cross-sectional NACA0070 shape were verified. It is important to note that the magnitudes produced by the model simulation were smaller than those predicted by Hoerner's water tests. The negative lift for small angles of attack can be applied usefully to the KC-135 boom structure in order to decrease the necessary input for a desired movement. Also, the existence of time dependent oscillations were validated.

These oscillations were also present in the case of a blunt fairing cross-section. In order to help choose the optimal boom cross-sectional shape, the differences in refueling envelope sizes were examined. The envelope size was found to be maximized by removing as many limits as possible, the most feasible being the stick limit. Therefore, the largest improvement in defining the refueling envelope size was created by removing the boom operator's control stick limit and changing the boom cross-section to a blunt fairing shape.

Next, the effect of the unsteady, separated flow oscillations on the refueling envelope was analyzed. From the computer data output, it was found that the fluctuating aerodynamic properties result in no perceptible envelope change for the blunt fairing, but a noticeable change by angles of up to 3° for the NACA0070.

Since the oscillations were shown to have a result on the actual operating envelope, the frequencies and amplitudes of both drag and lift coefficients versus angles of attack for the blunt fairing and NACA0070 were presented in Tables 3 and 4. Inspection

of these figures leads to the conclusion that the blunt fairing is a better cross-sectional shape for the KC-135 boom due to its negative lift qualities, increase in refueling envelope size, and discountable oscillation frequencies and amplitudes.

V. Recommendations for Further Study

In order to best optimize a change in the aerodynamic shape of the KC-135 boom, other blunt body cross-sections should be analyzed. Cross-sectional shapes that optimize the lift and drag vector effects on the size of the flyable envelope should be studied.

Possible shapes to examine are a variety of thick, symmetric airfoils, such as the NACA0050 through NACA0090.

Also, the computer simulation presented in this report should be repeated using a wind tunnel test. Therefore the discrepancies between Hoerner's test data and the results found in this thesis could be further evaluated. The actual magnitude of negative lift could thus be verified, as well as at what angles of attack this phenomena occurs.

Before implementation of the suggested boom modifications, a more complicated computer model should be accomplished. In order to obtain more complete and fully developed flow quantities, a turbulent model of the cross-sections can be accomplished by using ENS3DAE. The use of a panel code should also be used to model the fuselage effect on the boom aerodynamics, since it is doubtful that this phenomenon can be neglected.

The ENS3DAE code is also capable of performing dynamic analysis. A simulation should be run that investigates the boom response to the time dependent oscillations as the boom angle of attack is changed.

Bibliography

1. Abbott, Ira H. and Albert E. Von Doenhoff. Theory of Wing Sections. New York: Dover Publications, Inc., 1959.
2. Anderson, John D., Jr. Introduction to Flight. New York: McGraw-Hill Book Company, 1989.
3. Campbell, Terry G., Capt. et al. "System Study of the KC-135 Aerial Refueling System." Air Force Institute of Technology: AFIT/GSE/ENY/89D-01, December 1989.
4. Carter, Thomas J., III, Capt. "Dynamic Characteristics of Aerial Refueling Systems." Air Force Institute of Technology: AFIT/GAE/AA/82D-4, December 1982.
5. Cobb, Marck R., Maj. "Aerial Refueling: The Need for a Multipoint, Dual-System Capability." Maxwell AFB, Alabama: Air University Press, July 1987.
6. Congress of the United States. "Modernizing the Aerial Tanker Fleet: Prospects for Capacity, Timing, and Cost." Washington, DC: Congressional Budget Office, September 1985.
7. Flight Loads Prediction Methods for Aircraft: Volume III. Wright-Patterson AFB, OH: Wright Laboratory, August 1993.
8. Hoerner, Sighard F. Fluid-Dynamic Drag. Midland Park, NJ: Hoerner, 1965.
9. Hoerner, Sighard F. and Henry V. Borst. Fluid-Dynamic Lift. Brick Town, NJ: Hoerner Fluid Dynamics, 1975.
10. Hoffmann, Klaus A. and Steve T. Chiang. Computational Fluid Dynamics for Engineers - Volume I. Wichita, KS: Engineering Education System™, 1993.
11. Jeffreys, Richard T., Capt. and Maj. Carver L. Sears. "A Logistics Support Cost Analysis of the Advanced Aerial Refueling Boom." Air Force Institute of Technology: GSM/SM/76S-13, September 1976.
12. Maiersperger, Walter P., Lt. Col. "General Design Aspects of Flight Refueling." Aeronautical Engineering Review. March, 1954, p.52-61.
13. The Matheson Unabridged Gas Data Book. New York: Matheson Gas Products, 1974.

14. Moulden, T. H. Fundamentals of Transonic Flow. New York: John Wiley & Sons, Inc., 1984.
15. Ropelewski, Robert R. "KC-10 Readied for Delivery to USAF." *Aviation Week & Space Technology*. March 2, 1961, p. 43-44.
16. Spenny, C. H. "Boom Refueling envelope Expansion for Aerial Refueling with the KC-135 Tanker." *Proceedings of the AIAA/AHS/ASEE 2nd Aerospace Design Conference*, Paper No. AIAA93-1167, February 1993.

Appendix A: Input File for ENS3DAE

A copy of the input file for a viscous run of ENS3DAE using a 50 x 40 x 5 O-grid configuration.

```

$FLWCND   XMFS=2*0.8,
          PITCH=40.0,
          GAMMA=1.4,
          PR=.737,
          YAW=0.0,
          REY=2*8.7382E05,
          KVIS=2,
          CSUTH=0.4906997,

$SEND
$NUMCND   ITTOTAL=8000,
          ITMAX=1,
          CFL(1)=1.0,1.0,1.0,1.0,1.0,
          ITCFL(1)=100000,200000,300000,400000,
          EI(1)=5*4.0,
          XK2(1)=5*0.25,
          XK4(1)=5*0.004,
          ITDAMP(1)=100000,200000,300000,400000,

$SEND
$NUMOPT   KRSTRT=0,
          KTSTEP=2,
          NTCALC=1,
          KTARE=1,
          KCONVC=0,
          MJACOB=0,
          NGRID=1,
          KCORE=1,
          KSPEC=0,
          KBEXT=3,
          KBPEXT=3,
          KOEXT=2,
          KIEXT=2,
          IORD(1)=0,IORD(2)=0,IORD(3)=0,
          KCFEXT=3,
          KSPEXT=1,

$SEND
$PRTOPT   NCORRECT=1,
          NITPRNT=1000,
          LPRINT=1,
          NDUMP=20*0,
          DITER=0,
          NINTPR=100,
          NITFPR=1000,
          NITOPR=1,
          IPRINT(1,1)=24*0,61*0,35*0,
          JPRINT(1,1)=0,4*0,0,7*0,0,5*0,0,12*0,
          KPRINT(1,1)=49*0,0,
          IPRINT(1,2)=24*0,61*0,35*0,
          JPRINT(1,2)=0,4*0,0,7*0,0,5*0,0,12*0,
          KPRINT(1,2)=0,49*0,

$SEND
$STRBOPT  KTURB=0,
          TCONST=26.0,0.4,5.5,0.3,0.25,0.0168,1.6,0.0,0.0,0.0,
          PRT=0.90,

```

```

                NTBCALC=10,
$SEND
$AEROEL
                WAREA=1.0,
                XMOM=0.25,
$SEND
*B.C.'S FOR 2 BLOCK O-GRID FOR NACA0070 AIRFOIL
*
BLOCK #1 AIRFOIL TOP GRID
*IMAX JMAX KMAX
  50 40 5
FACE.1...JS...JE...KS...KE..NBC I=1 PLANE
  1 1 1 5 2
  2 39 1 1 2
  2 39 2 4 3
  2 39 5 5 2
  40 40 1 1 2
  40 40 2 4 6
  40 40 5 5 2
FACE.2...JS...JE...KS...KE..NBC I=IMAX PLANE
  1 1 1 5 2
  2 39 1 1 2
  2 39 2 4 3
  2 39 5 5 2
  40 40 1 1 2
  40 40 2 4 6
  40 40 5 5 2
FACE.3...IS...IE...KS...KE..NBC J=1 PLANE
  1 50 1 5 2
FACE.4...IS...IE...KS...KE..NBC J=JMAX PLANE
  1 50 1 1 2
  1 50 2 4 6
  1 50 5 5 2
FACE.5...IS...IE...JS...JE..NBC K=1 PLANE
  1 50 1 40 1
FACE.6...IS...IE...JS...JE..NBC K=KMAX PLANE
  1 50 1 40 1
*
*B.C.'S FOR 2 BLOCK O-GRID FOR NACA0070 AIRFOIL
*
BLOCK #2 AIRFOIL BOTTOM GRID
*IMAX JMAX KMAX
  50 40 5
FACE.1...JS...JE...KS...KE..NBC I=1 PLANE
  1 1 1 5 2
  2 39 1 1 2
  2 39 2 4 3
  2 39 5 5 2
  40 40 1 1 2
  40 40 2 4 6
  40 40 5 5 2
FACE.2...JS...JE...KS...KE..NBC I=IMAX PLANE
  1 1 1 5 2

```

```

2 39 1 1 2
2 39 2 4 3
2 39 5 5 2
40 40 1 1 2
40 40 2 4 6
40 40 5 5 2
FACE.3...IS...IE...KS...KE..NBC J=1 PLANE
1 50 1 5 2
FACE.4...IS...IE...KS...KE..NBC J=JMAX PLANE
1 50 1 1 2
1 50 2 4 6
1 50 5 5 2
FACE.5...IS...IE...JS...JE..NBC K=1 PLANE
1 50 1 40 1
FACE.6...IS...IE...JS...JE..NBC K=KMAX PLANE
1 50 1 40 1
*
INTERFACES
*ZONE1 PLANE1  INS INE  INS INE ZONE2 PLANE2  INS INE  INS INE
1 I= 1 J= 1 40 K= 1 5  2 I=50 J= 1 40 K= 1 5
1 I= 50 J= 1 40 K= 1 5  2 I= 1 J= 1 40 K= 1 5
*TURBULENCE
*TZONE TPLANE  INS INE  INS INE TYPE OSTOP XTRANS
* 1 K= 32 I= 1 25 J= 1 24  1 0 0.0
* 1 K= 32 I= 26 84 J= 1 24  2 10 0.0
* 1 K= 32 I= 85 120 J= 1 24  3 10 0.0
* 1 K= 32 I= 1 120 J= 25 32  1 10 0.0
*
* 2 K= 1 I= 1 25 J= 1 24  1 0 0.0
* 2 K= 1 I= 26 84 J= 1 24  2 10 0.0
* 2 K= 1 I= 85 120 J= 1 24  3 10 0.0
* 2 K= 1 I= 1 120 J= 25 32  1 10 0.0
FORCES
COMPONENT WING
* NZ IS IE JS JE KS KE NORM
1 1 50 1 1 1 5 -1.0
2 50 1 1 1 1 5 1.0
UNSTEADY
* NZ IS IE ISKIP JS JE JSKIP KS KE KSKIP
1 1 50 1 1 1 1 3 3 1
2 2 50 1 1 1 1 3 3 1
END OF SOLVER INPUT
BEGIN PROBLEM DEFINITION
TITLE:NACA0070 SOLUTION
STATIC RIGID
END OF PROBLEM

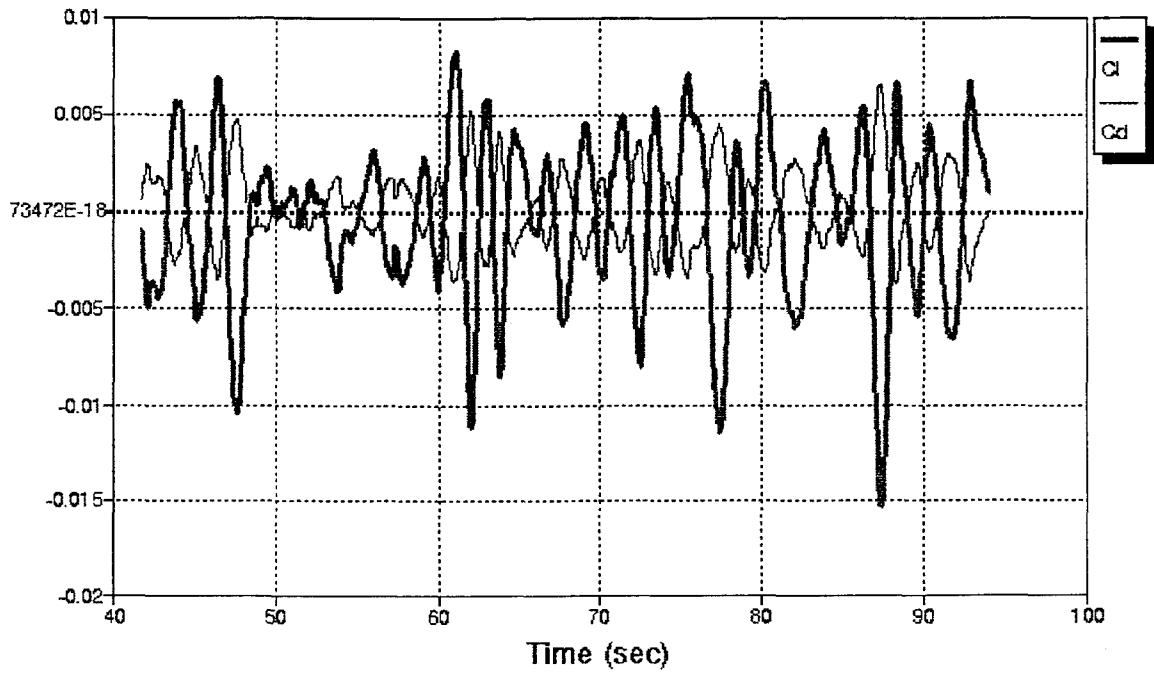
```

Appendix B: NACA0070 Coefficients of Lift and Drag vs. Time Plots

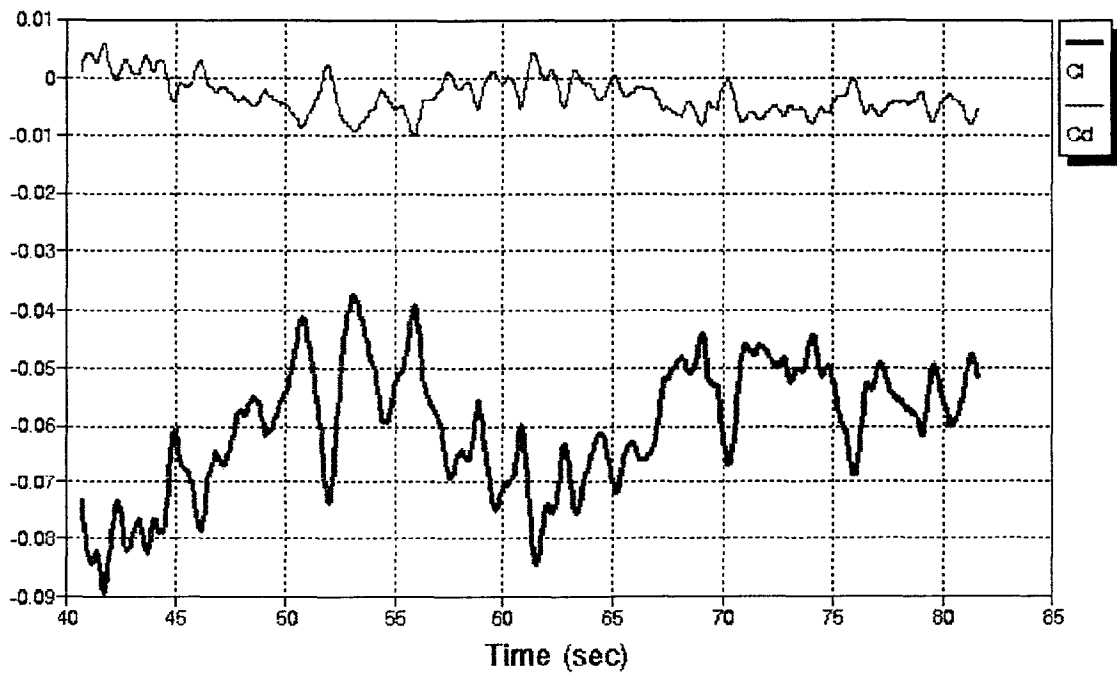
The Navier-Stokes equations solution to the NACA0070 cross-section using a 50 x 40 grid showing lift and drag coefficients vs. time step for angles of attack 0, 5, 10, 15, 20, 25, 30, 35, 40 and 80 degrees.

NACA0070 - Navier-Stokes Grid 50x40

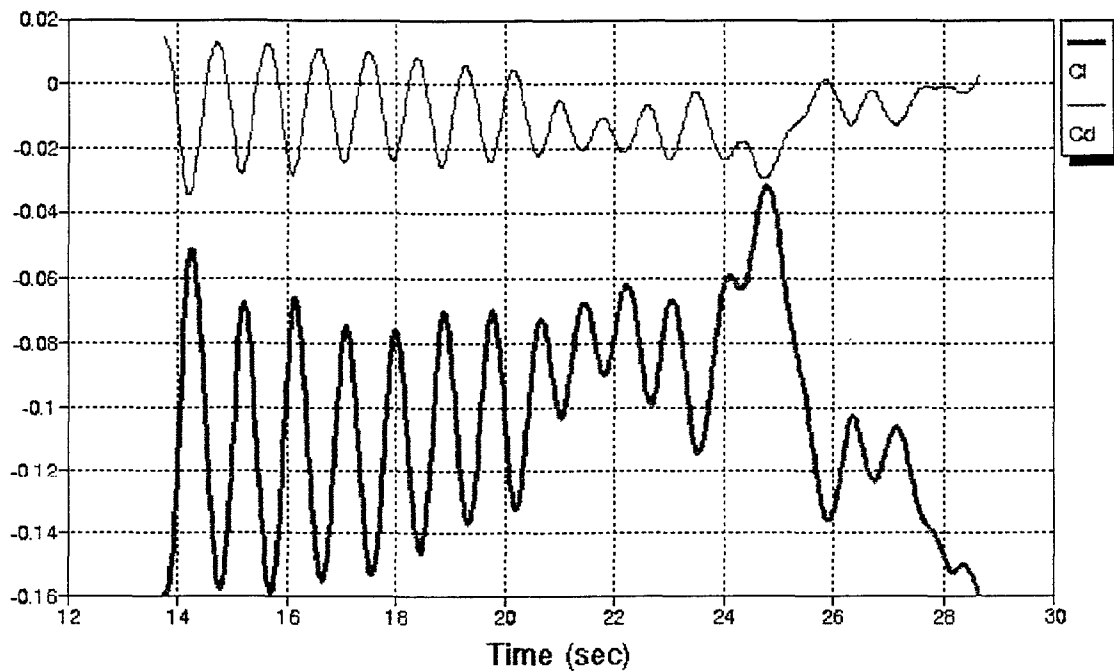
AOA = 0 degrees



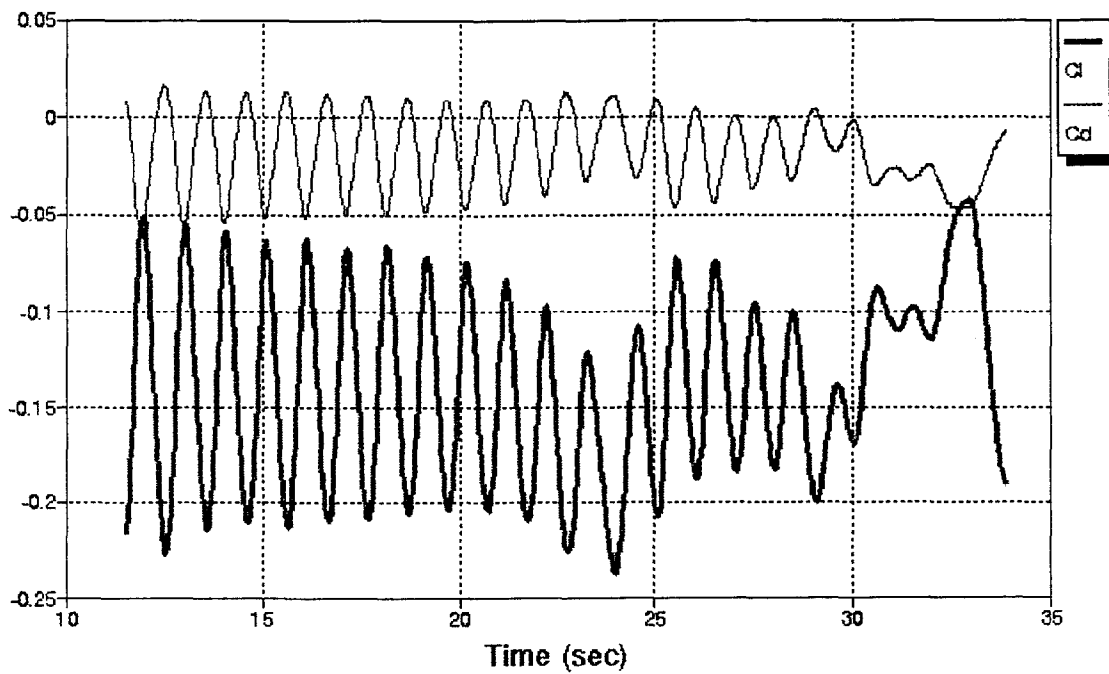
NACA0070 - Navier-Stokes Grid 50x40
AOA = 5 degrees



NACA0070 - Navier-Stokes Grid 50x40
AOA = 10 degrees

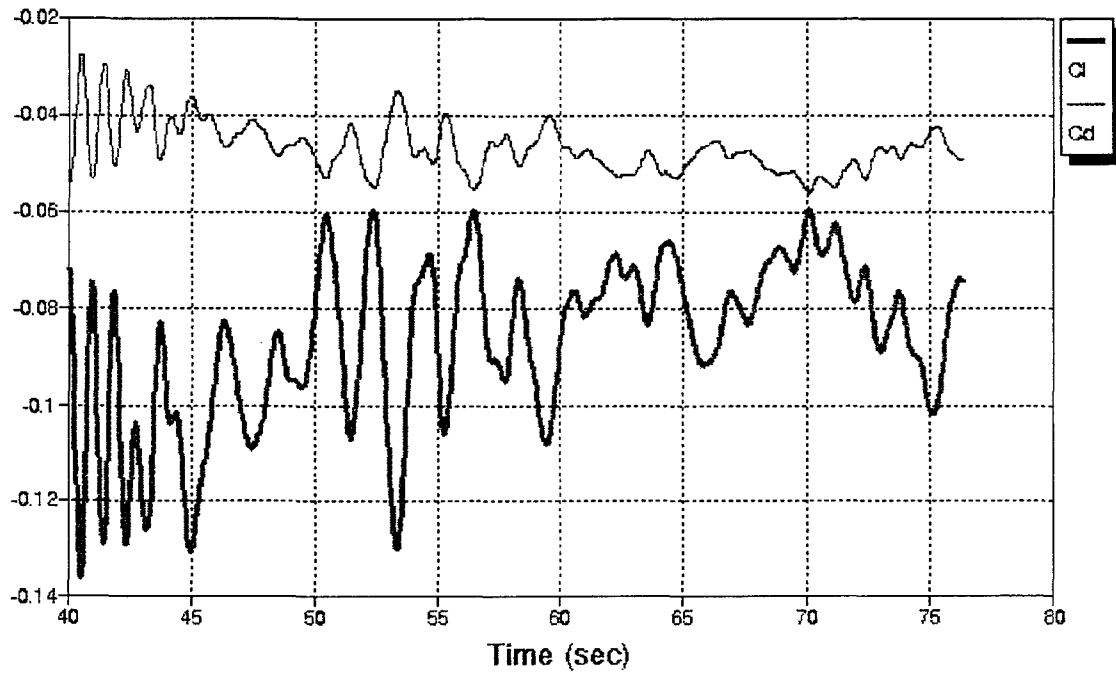


NACA0070 - Navier-Stokes Grid 50x40 AOA = 15 degrees

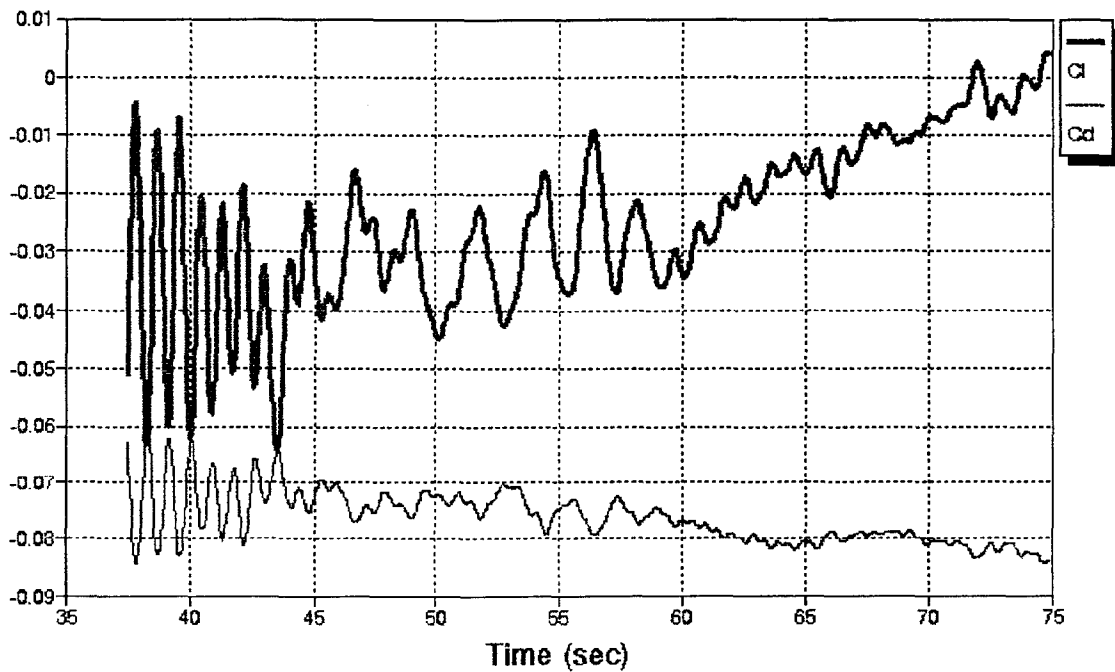


NACA0070 - Navier-Stokes Grid 50x40

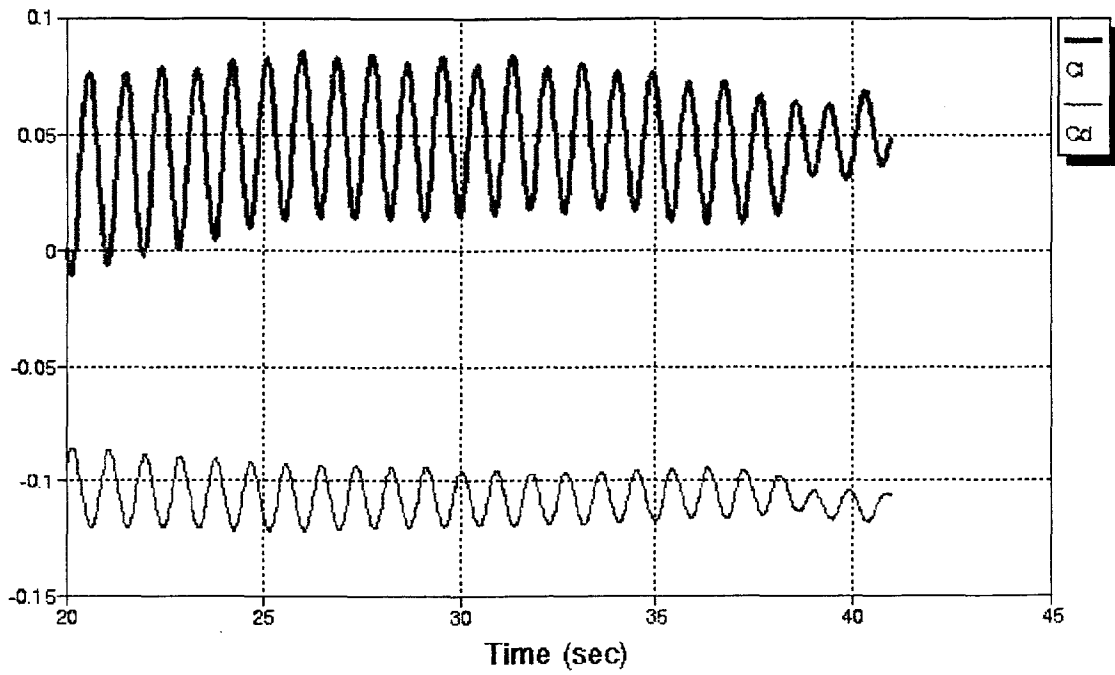
AOA = 20 degrees



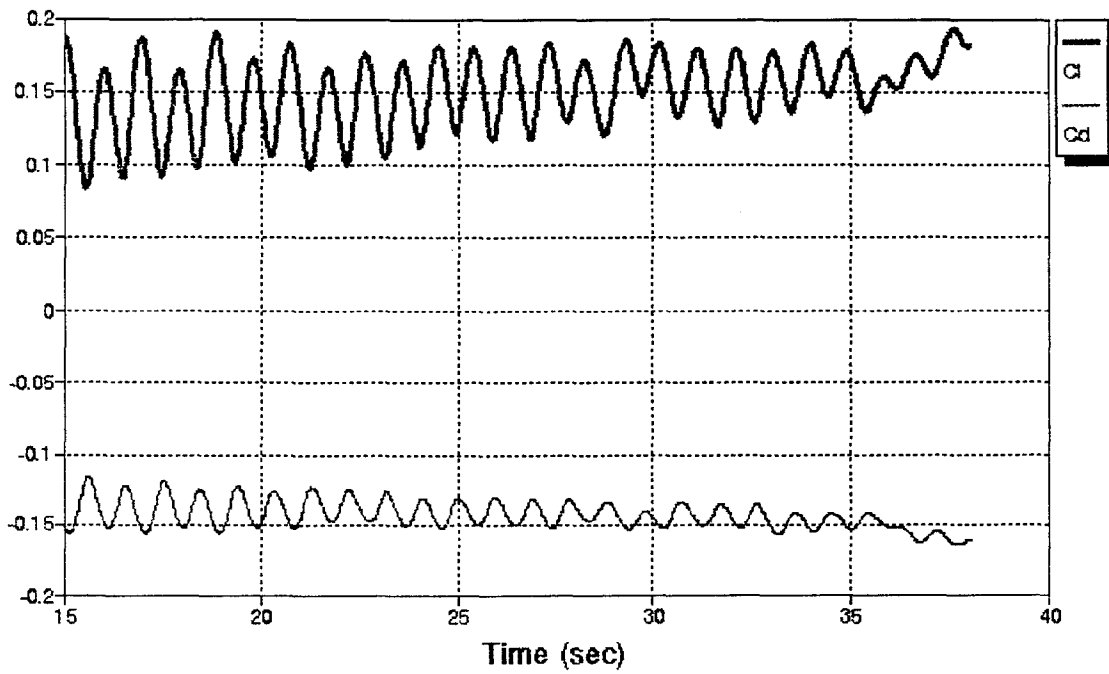
NACA0070 - Navier-Stokes Grid 50x40
AOA = 25 degrees



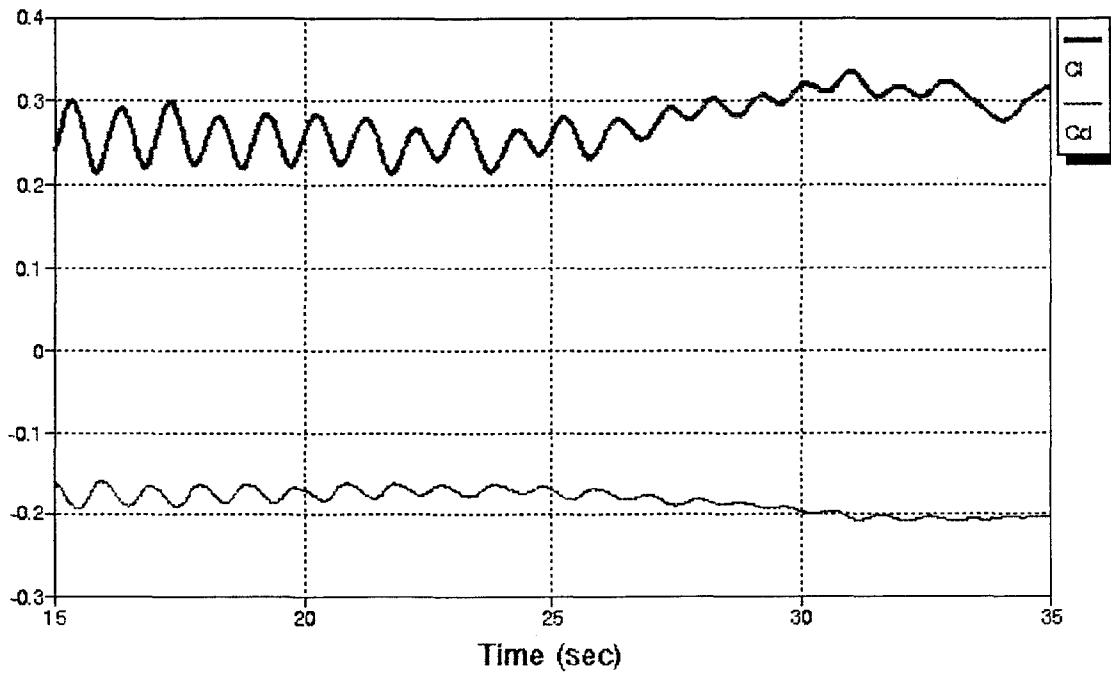
NACA0070 - Navier-Stokes Grid 50x40
AOA = 30 degrees



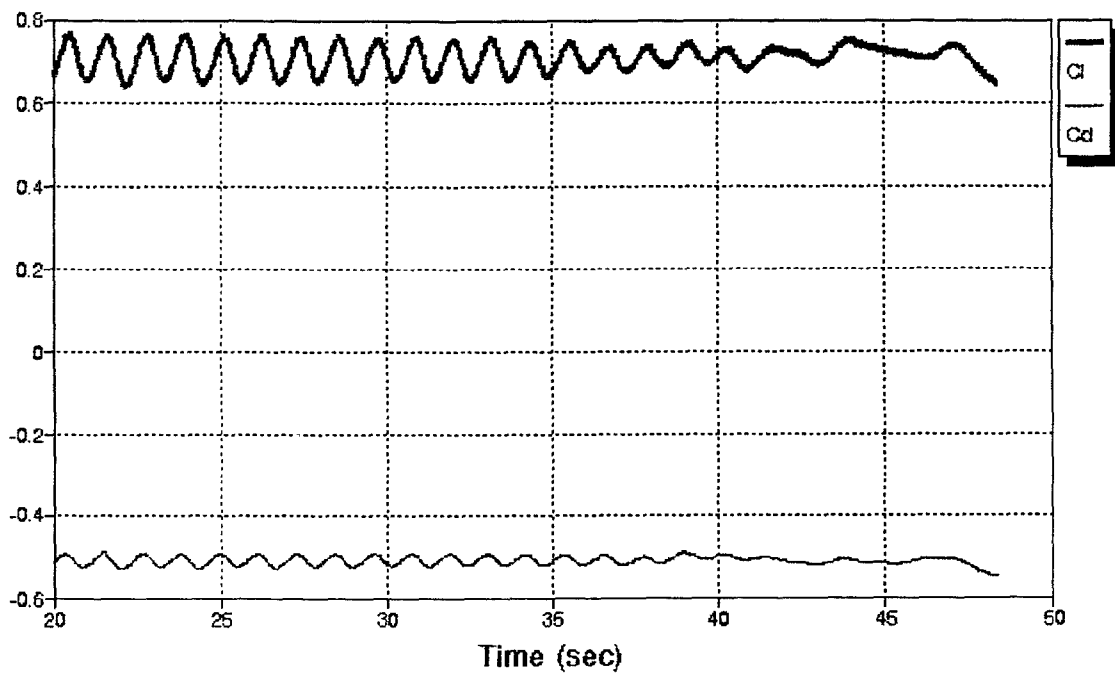
NACA0070 - Navier-Stokes Grid 50x40
AOA = 35 degrees



NACA0070 - Navier-Stokes Grid 50x40
AOA = 40 degrees



NACA0070 - Navier-Stokes Grid 50x40
AOA = 80 degrees

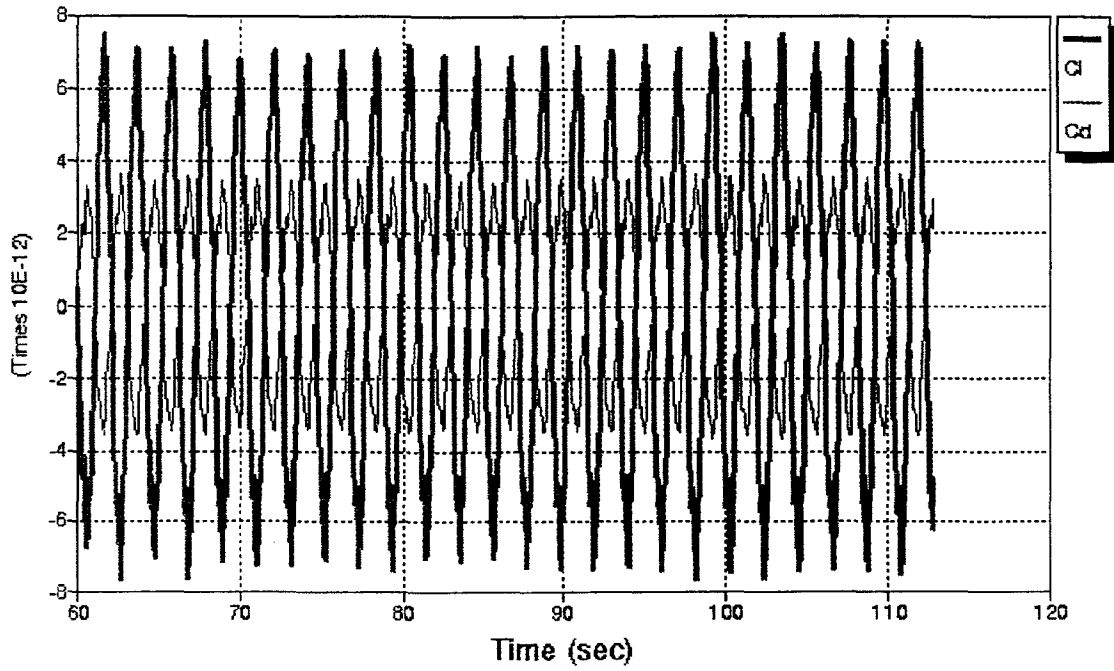


Appendix C: Blunt Fairing Coefficients of Lift and Drag vs. Time Plots

The Navier-Stokes equations solution to the blunt fairing cross-section using a 50 x 40 grid showing lift and drag coefficients vs. time step for angles of attack 0, 10, 20, 30, 40 and 80 degrees.

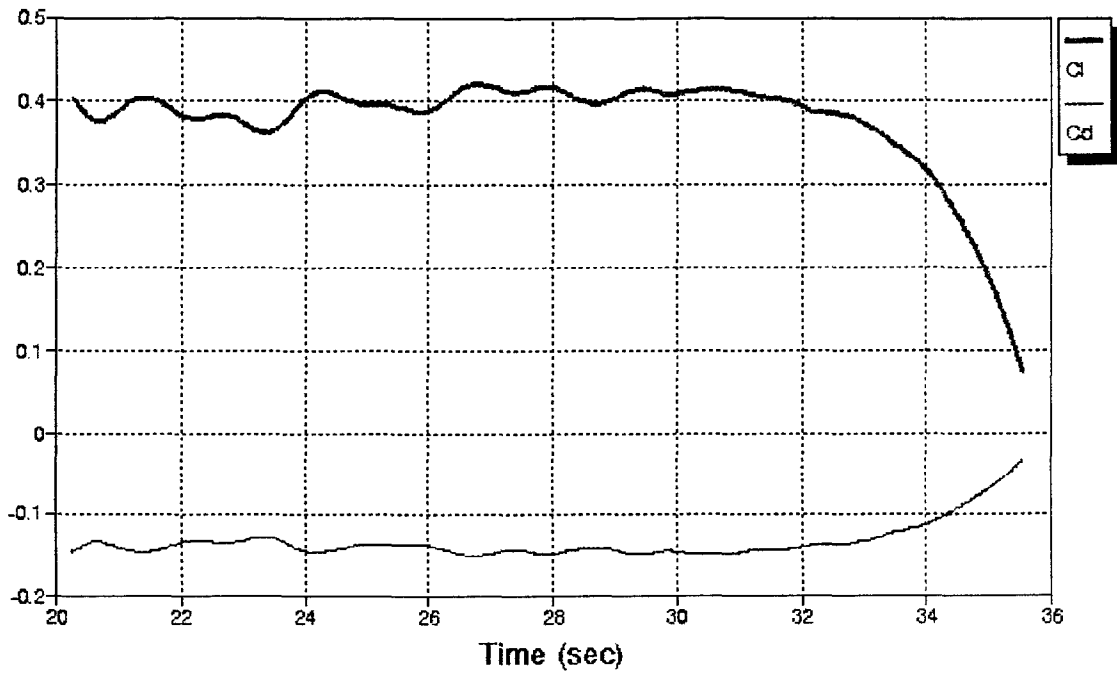
BLUNT FAIRING - Navier-Stokes

AOA = 0 degrees, Grid 50x40



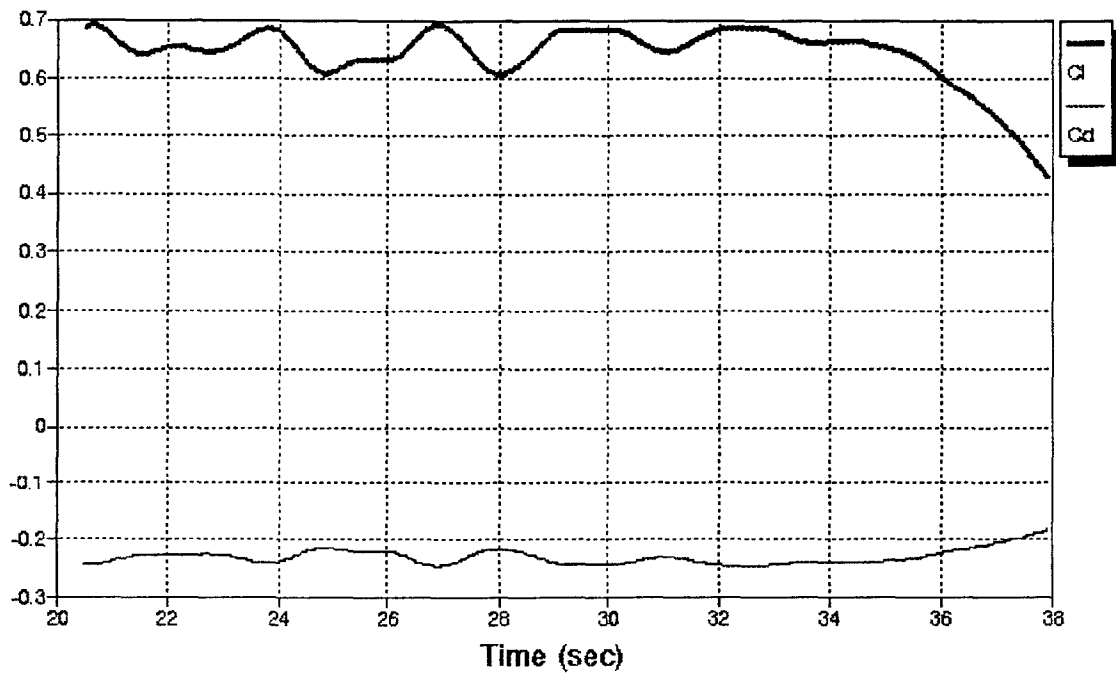
BLUNT FAIRING - Navier-Stokes

AOA = 10 degrees, Grid 50x40



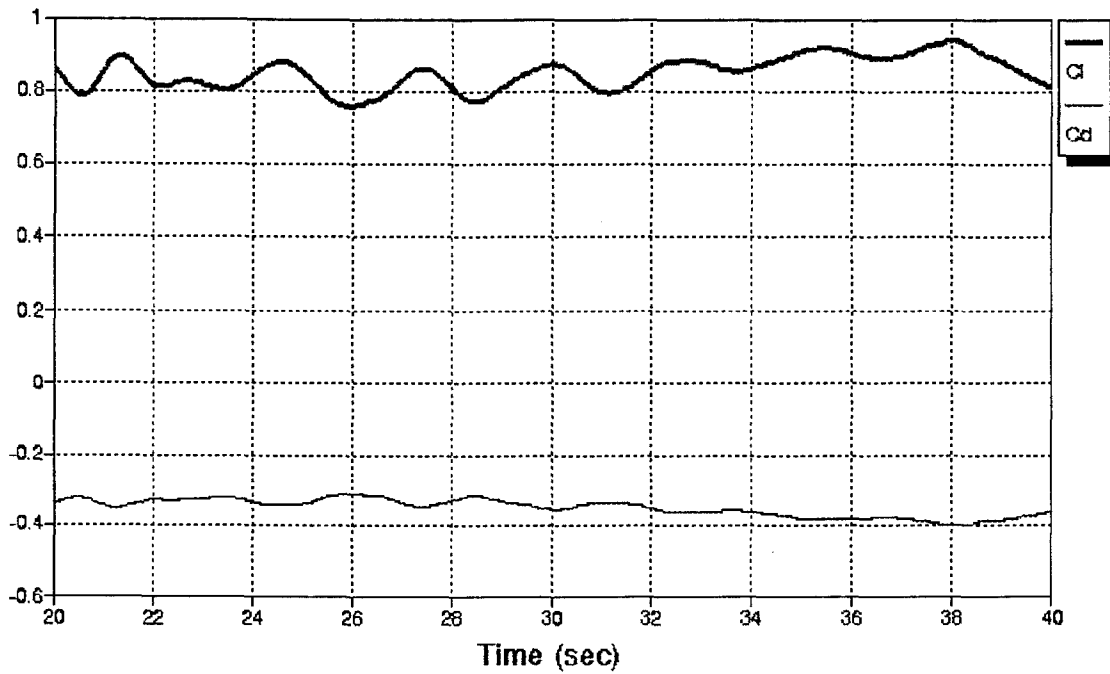
BLUNT FAIRING - Navier-Stokes

AOA = 20 degrees, Grid 50x40



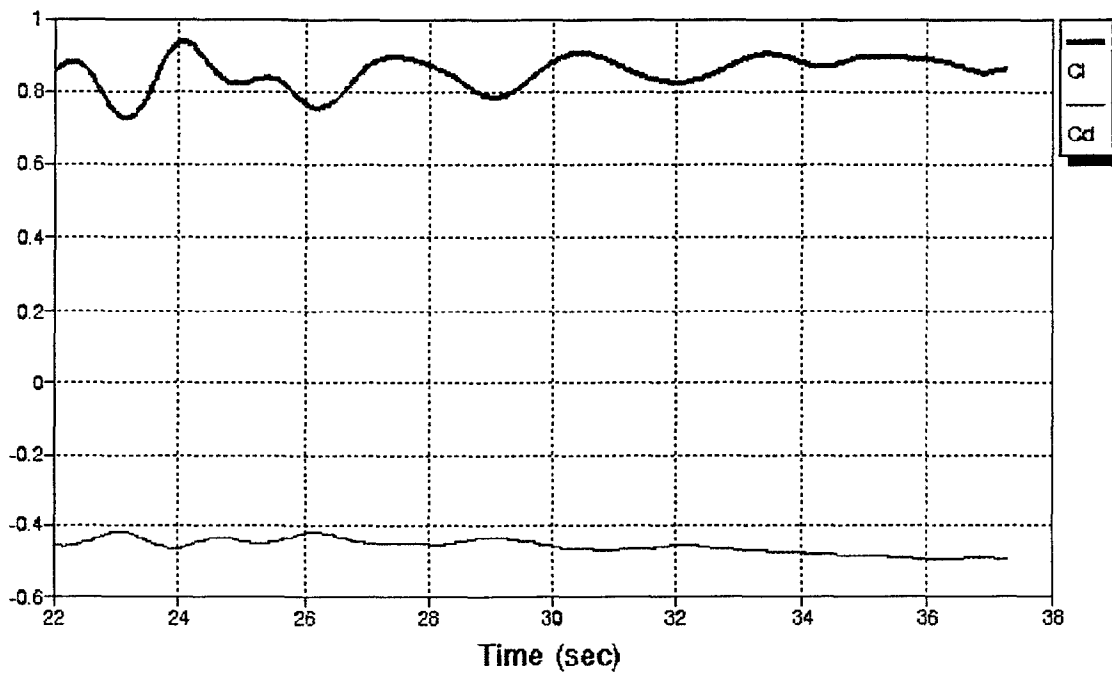
BLUNT FAIRING - Navier-Stokes

AOA = 30 degrees, Grid 50x40



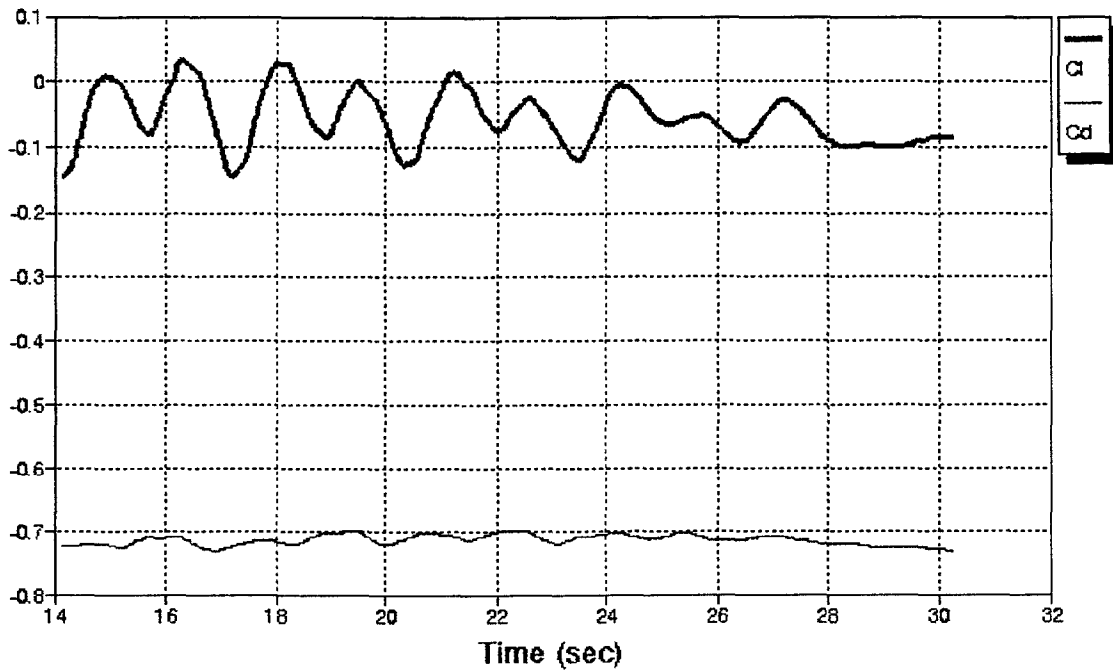
BLUNT FAIRING - Navier-Stokes

AOA = 40 degrees, Grid 50x40



BLUNT FAIRING - Navier-Stokes

AOA = 80 degrees, Grid 50x40



REPORT DOCUMENTATION PAGE

Form Approved
OMB No. 0704-0188

Public reporting burden for this collection of information is estimated to average 1 hour per response, including the time for reviewing instructions, searching existing data sources, gathering and maintaining the data needed, and completing and reviewing the collection of information. Send comments regarding this burden estimate or any other aspect of this collection of information, including suggestions for reducing this burden, to Washington Headquarters Services, Directorate for Information Operations and Reports, 1215 Jefferson Davis Highway, Suite 1204, Arlington, VA 22202-4302, and to the Office of Management and Budget, Paperwork Reduction Project (0704-0188), Washington, DC 20503.

1. AGENCY USE ONLY (Leave blank)		2. REPORT DATE December 1995	3. REPORT TYPE AND DATES COVERED Master's Thesis	
4. TITLE AND SUBTITLE Investigation of Aerodynamic Alterations for Improving the KC-135 Boom Performance During Aerial Refueling			5. FUNDING NUMBERS	
6. AUTHOR(S) Debra A. Nawrocki, 2nd Lt, USAF				
7. PERFORMING ORGANIZATION NAME(S) AND ADDRESS(ES) Air Force Institute of Technology, WPAFB OH 45433-6583			8. PERFORMING ORGANIZATION REPORT NUMBER AFIT/GAE/ENY/95D-17	
9. SPONSORING/MONITORING AGENCY NAME(S) AND ADDRESS(ES)			10. SPONSORING/MONITORING AGENCY REPORT NUMBER	
11. SUPPLEMENTARY NOTES				
12a. DISTRIBUTION / AVAILABILITY STATEMENT Approved for Public Release; Distribution Unlimited			12b. DISTRIBUTION CODE	
13. ABSTRACT (Maximum 200 words) This study investigated the eligibility of the KC-135 air refueling boom for improved capabilities in the areas of control and performance. By using a thick airfoil cross-section for the boom tube, rather than the current circular cross-section, the ability to increase the lift characteristics was verified. Prior compiled test data was used for comparison against analytical computer solutions. The possibility and effects of control frequency oscillations were also examined due to the unstable nature of the flow at test conditions. Additionally, the effect of other cross-section shapes, such as the blunt fairing, on the size of the flyable envelope for the trailing aircraft was investigated by using FORTRAN coding. Results show that the KC-135 air refueling boom can be modified for better lift and performance envelope capabilities.				
14. SUBJECT TERMS KC-135, Air Refueling, Tanker Aircraft, Euler Solutions, Navier-Stokes Solutions, Time Dependent Oscillations			15. NUMBER OF PAGES 139	
			16. PRICE CODE	
17. SECURITY CLASSIFICATION OF REPORT UNCLASSIFIED	18. SECURITY CLASSIFICATION OF THIS PAGE UNCLASSIFIED	19. SECURITY CLASSIFICATION OF ABSTRACT UNCLASSIFIED	20. LIMITATION OF ABSTRACT UL	